Statistical physics of fracture, friction, and earthquakes

Hikaru Kawamura[*]

Department of Earth & Space Science, Osaka University, Osaka, Japan

Takahiro Hatano[†] and Naoyuki Kato[‡]

Earthquake Research Institute, University of Tokyo, Japan

Soumyajyoti Biswas[§] and Bikas K. Chakrabarti[||]

Theoretical Condensed Matter Physics Division and Centre for Applied Mathematics and Computational Science, Saha Institute of Nuclear Physics, 1/AF Bidhan Nagar, Kolkata 700064, India

(published 18 May 2012)

The present status of research and understanding regarding the dynamics and the statistical properties of earthquakes is reviewed, mainly from a statistical physical viewpoint. Emphasis is put both on the physics of friction and fracture, which provides a microscopic basis for our understanding of an earthquake instability, and on the statistical physical modelling of earthquakes, which provides macroscopic aspects of such phenomena. Recent numerical results from several representative models are reviewed, with attention to both their critical and their characteristic properties. Some of the relevant notions and related issues are highlighted, including the origin of power laws often observed in statistical properties of earthquakes, apparently contrasting features of characteristic earthquakes or asperities, the nature of precursory phenomena and nucleation processes, and the origin of slow earthquakes, etc.American Physical Society

CONTENTS

[*]kawamura@ess.sci.osaka-u.ac.jp
[†]hatano@eri.u-tokyo.ac.jp
[‡]nkato@eri.u-tokyo.ac.jp
[§]soumyajyoti.biswas@saha.ac.in
[||]bikask.chakrabarti@saha.ac.in

I. INTRODUCTION

Earthquakes are large-scale mechanical failure phenomena, which still defy our complete understanding. In this century, we have already experienced two gigantic earthquakes: the 2004 Sumatra-Andaman earthquake (M9.1) and the 2011 East Japan earthquake (M9.0). Given the disastrous nature of the phenomena, the understanding and forecasting of earthquakes remains the most important issue in physics and geoscience (Carlson, Langer and Shaw, 1994; Rundle, Turcotte and Klein, 2000; Scholz, 2002; Rundle *et al.*, 2003; Bhattacharyya and Chakrabarti, 2006; Burridge, 2006; De Rubies *et al.*, 2006; Ben-Zion, 2008; Kanamori, 2009; Daub and Carlson, 2010). Although there is some recent progress in our understanding of the basic physics of fracture and friction, it is still at a primitive stage (Marone, 1998; Scholz, 1998; Scholz, 2002; Dieterich, 2009; Tullis, 2009; Daub and Carlson, 2010). Furthermore, our lack of a proper understanding of the dynamics of earthquakes poses an outstanding challenge to both physicists and seismologists.

While earthquakes are obviously complex phenomena, certain empirical laws are known concerning their statistical properties, e.g., the Gutenberg-Richter (GR) law for the magnitude distribution of earthquakes, and the Omori law for the time evolution of the frequency of aftershocks (Scholz, 2002; Rundle *et al.*, 2003; Turcotte, Shcherbakov, and Rundle, 2009). The GR law states that the frequency of earthquakes with energy (seismic moment) E decays with E, obeying a power law, i.e., proportionally to $E^{-(1+B)} = E^{-(1+[2/3]b)}$ where B and $b = \frac{3}{2}B$ are appropriate exponents, whereas the Omori law states that the frequency of aftershocks decays with the time elapsed after the mainshock, also obeying a power law. These laws, both of which are power laws possessing a scale invariance, are basically of statistical nature, becoming evident only after examination of a large number of events. Although it is extremely difficult to give a definitive prediction for each individual earthquake event, clear regularity often shows up when one measures the statistical aspects of an ensemble of many earthquake events. This observation motivates the statistical physical study of earthquakes for the following two reasons: First, a law appearing after averaging over many events is exactly the subject of statistical physics. Second, power laws or scale invariance have been a central subject of statistical physics for years in the context of critical phenomena. Indeed, Bak and collaborators proposed the concept of ``self-organized criticality'' (SOC) (Bak, Tang, and Wiesenfeld, 1987). According to this view, the Earth's crust is always in a critical state which is self-generated dynamically (Turcotte, 1997; Hergarten, 2002; Turcotte, Shcherbakov, and Rundle, 2009; Pradhan, Hansen, and Chakrabarti, 2010). It is possible that the idea of SOC might give an explanation of the scale-invariant power law behaviors frequently observed in earthquakes, including the GR law and the Omori law. However, one should bear in mind that real earthquakes often exhibit apparently contradictory features, i.e., the features

represented by ``characteristic earthquakes,'' where an earthquake is regarded as possessing a characteristic energy or time scale (Scholz, 2002; Turcotte, Shcherbakov, and Rundle, 2009).

Earthquakes also possess strong relevance to material science. It is now established that earthquakes can be regarded as a stick-slip frictional instability of a preexisting fault, and statistical properties of earthquakes are governed by the physical law of rock friction (Marone, 1998; Scholz, 1998; Scholz, 2002, Dieterich, 2009; Tullis, 2009). The physical law describing rock friction or fracture is often called the ``constitutive law.'' As most of the major earthquakes are caused by the rubbing of faults, such friction laws give the microscopic basis for analyzing the dynamics of earthquakes. One might naturally ask how the statistical properties of earthquakes depend on the material properties characterizing earthquake faults, e.g., the elastic properties of the crust or the frictional properties of the fault. Answering such questions would give us valuable information in understanding the nature of earthquakes.

In spite of some recent progress, we still do not have precise knowledge of the constitutive law characterizing the stick-slip dynamics of earthquake faults. In fact, the law of rock friction is often quite complicated, depending not just on the velocity or the displacement, but on the previous history and the ``state'' of the contact surface, etc. The rate-and-state friction (RSF) law is currently the standard friction law in the field of tectonophysics. Although the RSF law was formulated empirically three decades ago to account for certain aspects of rock friction experiments (Dieterich, 1979; Ruina, 1983), the underlying physics was not known until very recently. While the RSF law shows qualitatively good agreement with numerous experiments, it is good only at aseismic slip velocities (slower than mm/s).

Among some progress made recently in the study of friction processes, the most fascinating findings might be the rich variety of mechanochemical phenomena that come into play at seismic slip velocities. Other important progress might be the understanding of the friction law of granular matter. This is also an important point in understanding the friction law of faults, as they consist of fine powder from rocks that were ground up by the fault motion of the past. Investigation of friction phenomena at seismic slip velocities is now a frontier in tectonophysics. The RSF law no longer applies to this regime, where many mechanochemical phenomena have been observed in experiments. The most obvious examples are melting due to frictional heat, thermal decomposition of calcite, silica-gel lubrication, etc. There are no friction laws that can describe such a varied class of phenomena, which significantly affect the nature of sliding friction. In this article, we review recent developments concerning the basic physics of friction and fracture.

Statistical physical study of earthquakes is usually based on models of various levels of simplification. There are several advantages in employing simplified models in the study of earthquakes. First, it is straightforward in a model study to control various material parameters as input parameters. A systematic field study of the material-parameter dependence of real earthquakes meets serious difficulties, because it is difficult to control, or even get

precise knowledge of, various material parameters characterizing real earthquake faults. Second, since an earthquake is a large-scale natural phenomenon, it is intrinsically not "reproducible." Furthermore, large earthquakes are rare, say, once in hundreds of years for a given fault. If some observations are made for a given large event, it is often extremely difficult to determine how universal they are and to put reliable error bars on the obtained data. In a model, on the other hand, it is often quite possible to put reliable error bars on the data under well-controlled conditions, say, by performing extensive computer simulations. An obvious disadvantage of a model study is that the model is not reality, and one has to be careful in elucidating what aspects of reality are taken into account or discarded in the model under study.

While numerous earthquake models of various levels of simplifications have been studied in the past, one may classify them roughly into two categories: The first one is of the type possessing an equation of motion describing its dynamics where the constitutive relation can be incorporated as a form of "force." The so-called spring-block or Burridge-Knopoff (BK) model, which is a discretized model consisting of an assembly of blocks coupled via elastic springs, belongs to this category (Burridge and Knopoff, 1967). Continuum models also belong to this category (Tse and Rice, 1986; Rice, 1993). The second category encompasses further simplified statistical physical models, the coupled-lattice models, most of which were originally introduced as a model of SOC. This category includes the so-called Olami-Feder-Christensen (OFC) model (Olami, Feder, and Christensen, 1992), the fiber-bundle model (Pradhan, Hansen, and Chakrabarti, 2010), and the two-fractal-overlap model (Chakrabarti and Stinchcombe, 1999; Bhattacharyya, 2005; Bhattacharya *et al.*, 2009). These models possess extremely simplified evolution rules, instead of realistic dynamics and constitutive relations. Yet one expects that this simplicity enables one to perform exact or precise analysis, which might be useful in extracting essential qualitative features of the phenomena.

It often happens in practice that, even when the adopted model appears simple, it is still nontrivial to reveal its statistical properties. Then the strategy in examining the model properties is often to perform numerical computer simulations on the model, together with the analytical treatment. In this article, we review recent developments concerning the properties of these models mainly studied in statistical physics.

Earthquake forecast is the ultimate goal of any earthquake study. An important ingredient playing a central role there might be various kinds of precursory phenomena. We touch upon the following two types of precursory phenomenon in this article: The first type is a possible change in statistical properties of earthquakes which might occur prior to the mainshocks. The form of certain spatiotemporal correlations of earthquakes might change due to the proximity effect of the upcoming mainshock. For example, it has been pointed out that the power-law exponent describing the GR law might change before the mainshock, or a doughnutlike quiescence phenomenon might occur around the hypocenter of the upcoming mainshock. The second type of precursory phenomenon is a possible nucleation process which might occur preceding mainshocks (Dieterich, 2009). Namely, prior to the seismic rupture of a mainshock, the fault might exhibit a slow rupture process localized to a compact "seed" area, with its rupture velocity orders of magnitude lower than the seismic-wave velocity. The fault spends a very long time in this nucleation process, and then at some stage exhibits a rapid acceleration process accompanied by an expansion of the rupture zone, before getting into the final seismic rupture of the mainshock. These possible precursory phenomena preceding mainshocks are of paramount importance in their own right as well as in possible connection to an earthquake forecast. We note that a similar nucleation process is ubiquitously observed in various types of failure process in material science and engineering.

The purpose of the present article is to help researchers link different branches of earthquake studies. First, we wish to link the basic physics of friction and fracture underlying earthquake phenomena to macroscopic properties of earthquakes considered as large-scale dynamical instabilities. These two features should be inter-related as an "input versus output" or "microscopic versus macroscopic" relation, but the true connection is nontrivial and still remains largely unexplored. It is crucially important in understanding earthquakes to develop appropriate constitutive laws describing earthquake instabilityies and to make a link between such constitutive relations and the macroscopic properties of earthquakes. Second, we want to promote an interaction between statistical physicists and seismologists. We believe that the cooperation of scientists in these two areas would be very effective, and in some sense, indispensable in our proper understanding of earthquakes.

Recently, there has been some progress made by statistical physicists in characterizing the statistical aspects of earthquake phenomena. These efforts are of course based on established literature in seismology and the physics of fracture and friction. Also, there has been considerable fusion and migration of scientists and established knowledge bases between physics and seismology. In this article, we review the present state of our understanding regarding the dynamics of earthquakes and the statistical physical modeling of such phenomena, starting with fracture and friction.

The article is organized as follows. In Sec. II, we deal with the basic physics of fracture and friction. After reviewing the classic Griffith theory of fracture in Sec. II.A, we discuss the extreme nature of failure statistics in Sec. II.B and then briefly discuss a theory of fracture as a dynamical phase transition in Sec. II.C. The rate- and state-dependent friction law is reviewed in Sec. II.D, while the recent development beyond the RSF law is discussed in Sec. II.E. Section II.F is devoted to some microscopic statistical mechanical theories of friction. In Sec. III, we deal with statistical properties of a model of our first type which includes the spring-block Burridge-Knopoff model (Sec. III.A) and the continuum model (Sec. III.B). In Sec. III.A, we examine statistical properties of earthquakes, including precursory phenomena, with emphasis on both their critical and characteristic properties, while, in Sec. III.B, we mainly examine characteristic properties of earthquakes, includig slow earthquakes, and various slip behaviors. Implications of RSF laws for earthquake physics are also discussed in Sec. III.B. In Sec. IV, we deal with statistical properties of our second type of model, which includes the OFC model (Sec. IV.A), the fiber-bundle model

(Sec. IV.B), and the two fractal overlap model (Sec. IV.C). We also provide a Glossary of some interdisciplinary terms as the Appendix.

II. FRACTURE AND FRICTION

A. Griffith energy balance and brittle fracture strength of solids

In a solid, stress (σ) and strain (S) bear a linear relation in the Hookean region (small stress). Nonlinearity appears with further increase of stress, which finally ends in fracture or failure of the solid. In brittle solids, failure occurs immediately after the linear region. Hence, linear elastic theory can be applied to study this essentially nonlinear and irreversible phenomenon.

The failure process has strong dependence on, among other things, the disorder properties of the material (Caldarelli, Castellano, and Petri, 1999). Often, stress becomes concentrated around the disorder (Lawn, 1993; Petri *et al.*, 1994; Chakrabarti and Benguigui, 1997) where microcracks are formed. The stress values at the notches and corners of the microcracks can be several times higher than the applied stress. Therefore, the scaling properties of disorder play an important role in the breakdown properties of solids. Although the disorder properties tell us about the location of instabilities, they do not tell us about when a microcrack propagates. For that detail, an energy balance study is needed.

Griffith in 1920, equating the released elastic energy (in an elastic continuum) with the energy of the surface newly created (as the crack grows), arrived at a quantitative criterion for the equilibrium extension of the microcrack already present within a stressed material (Bergman and Stroud, 1992). The following analysis is valid effectively for two-dimensional stressed solids with a single preexisting crack, such as, for example, the case of a large plate with a small thickness. Extension to three-dimensional solids is straightforward.

We assume a thin linear crack of length $2l$ in an infinite elastic continuum subjected to uniform tensile stress σ perpendicular to the length of the crack (see Fig. 1). Stress parallel to the crack does not affect the stability of the crack and has not, therefore, been considered. Because of the crack (which cannot support any stress field, at least on its surfaces), the strain energy density of the stress field ($\sigma^2/2Y$, where Y represents the elastic modulus) is perturbed in a region around the crack, having the dimension of the length of the crack. We assume here that this perturbed or stress-released region has a circular cross section with the crack length as the diameter. The exact geometry of this perturbed region is not important here, and it determines only an (unimportant) numerical factor in the Griffith formula [see, e.g., Lawn (1993)]. Assuming for the purpose of illustration that half of the stress energy of an annular or cylindrical volume having internal radius l, outer radius $l + dl$, and length w (perpendicular to the plane of the stress; here the width w of the plate is very small compared to the other dimensions), to be released as the crack propagates by a length dl, one requires this released strain energy to be sufficient for providing the surface energy of the four new surfaces produced. This suggests

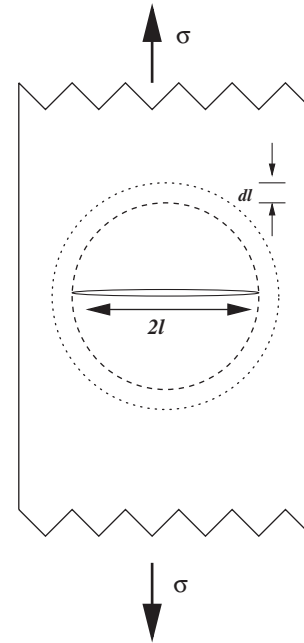$$\tfrac{1}{2}(\sigma^2/2Y)(2\pi wldl) \geq \Gamma(4wdl).$$

FIG. 1. A portion of a plate (of thickness w) under tensile stress σ (model I loading) containing a linear crack of length $2l$. For a further growth of the crack length by $2dl$, the elastic energy released from the annular region must be sufficient to provide the surface energy $4\Gamma wdl$ (extra elastic energy must be released for finite velocity of crack propagation).

Here Γ represents the surface energy density of the solid, measured by the extra energy required to create unit surface area within the bulk of the solid.

We have assumed here that, on average, half of the strain energy of the cylindrical region having a circular cross section with diameter $2l$ is released. If this fraction is different or the cross section is different, it will change only some of the numerical factors, in which we are not very much interested here. Also, we assume here linear elasticity up to the breaking point, as in the case of brittle materials. The equality holds when energy dissipation does not occur, as in the case of plastic deformation or for the propagation dynamics of the crack. One then gets

$$\sigma_f = \frac{\Lambda}{\sqrt{2l}}, \qquad \Lambda = \left(\frac{4}{\sqrt{\pi}}\right)\sqrt{Y\Gamma} \qquad (1)$$

for the critical stress at and above which the crack of length $2l$ starts propagating and a macroscopic fracture occurs. Here Λ is called the critical stress-intensity factor or the fracture toughness.

In a three-dimensional solid containing a single elliptic disk-shaped planar crack parallel to the applied tensile stress direction, a straightforward extension of the above analysis suggests that the maximum stress concentration will occur at the two tips (at the two ends of the major axis) of the ellipse. The Griffith stress for the brittle fracture of the solid is therefore determined by the same formula (1), with the crack length $2l$ replaced by the length of the major axis of the elliptic planar crack. Generally, for any dimension therefore, if a crack of length l already exists in an infinite elastic continuum, subject to uniform tensile stress σ perpendicular

to the length of the crack, then for the onset of brittle fracture, Griffith equates (the differentials of) the elastic energy E_l with the surface energy E_s:

$$E_l \simeq \left(\frac{\sigma^2}{2Y}\right)l^d = E_s \simeq \Gamma l^{d-1}, \qquad (2)$$

where Y represents the elastic modulus appropriate for the strain, Γ the surface energy density, and d the dimension. Equality holds when no energy dissipation (due to plasticity or crack propagation) occurs and one gets

$$\sigma_f \sim \frac{\Lambda}{\sqrt{l}}, \qquad \Lambda \sim \sqrt{Y\Gamma} \qquad (3)$$

for the breakdown stress at (and above) which the existing crack of length l starts propagating and a macroscopic fracture occurs. It may also be noted that the above formula is valid in all dimensions ($d \geq 2$).

This quasistatic picture can be extended (Pradhan and Chakrabarti, 2003a) to fatigue behavior of crack propagation for $\sigma < \sigma_f$. At any stress σ less than σ_f, the cracks (of length l_0) can still nucleate for a further extension at any finite temperature $k_B T$ with a probability $\sim \exp(-E/k_B T)$ and consequently the sample fails within a failure time τ given by

$$\tau^{-1} \sim \exp[-E(l_0)/k_B T], \qquad (4)$$

where

$$E(l_0) = E_s + E_l \sim \Gamma l_0^2 - \frac{\sigma^2}{Y} l_0^3 \qquad (5)$$

is the crack (of length l_0) nucleation energy. One can therefore express τ as

$$\tau \sim \exp\left[A\left(1 - \frac{\sigma^2}{\sigma_f^2}\right)\right], \qquad (6)$$

where (the dimensionless parameter) $A \sim l_0^3 \sigma_f^2 / Y k_B T$ and σ_f is given by Eq. (3). This immediately suggests that the failure time τ grows exponentially for $\sigma < \sigma_f$ and approaches infinity if the stress σ is much smaller than σ_f when the temperature $k_B T$ is small, whereas τ becomes vanishingly small when the stress σ exceeds σ_f; see, e.g., Politi, Ciliberto, and Scorretti (2002) and Sornette (2004)

For disordered solids, we model the solid by a percolating system. For the occupied bond and/or site concentration $p > p_c$, the percolation threshold, the typical preexisting cracks in the solid will have the dimension (l) of correlation length $\xi \sim \Delta p^{-\nu}$ and the elastic strength $Y \sim \Delta p^{T_e}$ (Stauffer and Aharony, 1992). Assuming that the surface energy density Γ scales as ξ^{d_B}, with the backbone (fractal) dimension d_B (Stauffer and Aharony, 1992), by equating E_l and E_s as in Eq. (2), one gets $(\sigma_f^2/2Y)\xi^d \sim \xi^{d_B}$. This gives

$$\sigma_f \sim (\Delta p)^{T_f},$$

with

$$T_f = \tfrac{1}{2}[T_e + (d - d_B)\nu] \qquad (7)$$

for the ''average'' fracture strength of a disordered solid (of fixed value) as one approaches the percolation threshold. Careful extensions of such scaling relations (7) and rigorous

bounds for T_f have been obtained and compared extensively by Chakrabarti and Benguigui (1997), Herrmann and Roux (1990), and Sahimi (2003).

B. Extreme statistics of the fracture stress

The fracture strength σ_f of a disordered solid does not have self-averaging statistics; the most probable and the average σ_f may not match because of the extreme nature of the statistics. This is because the ''weakest point'' of a solid determines the strength of the entire solid, not the average of weak points. As we model here, the statistics of clusters of defects are governed by random percolation processes.

We also discuss how the linear responses, like the elastic moduli of such random networks, can be obtained from the averages over the statistics of such clusters. This possible because of the self-averaging property of such linear responses, which occurs because the elasticity of a random network is determined by all the parellel-connected material portions or paths, contributing their share in the net elasticity of the sample.

The fracture or breakdown property of a disordered solid, however, is determined by only the weakest (often the longest) defect cluster or crack in the entire solid. Except for some indirect effects, most of the weaker or smaller defects or cracks in the solid do not determine the breakdown strength of the sample. The fracture or breakdown statistics of a solid sample is therefore determined essentially by the extreme statistics of the most dangerous or weakest (largest) defect cluster or crack within the sample volume.

We discuss now more formally the origin of this extreme statistics. We consider a solid of linear size L, containing n cracks within its volume. We assume that each of these cracks has a failure probability $f_i(\sigma)$, $i = 1, 2, \ldots, n$, to fail or break (independently) under an applied stress σ on the solid, and that the perturbed or stress-released regions of each of these cracks are separate and do not overlap. If we denote the cumulative failure probability of the entire sample, under stress σ, by $F(\sigma)$, then (Ray and Chakrabarti, 1985; Chakrabarti and Benguigui, 1997)

$$1 - F(\sigma) = \prod_{i=1}^{n}[1 - f_i(\sigma)] \simeq \exp\left[-\sum_i f_i(\sigma)\right]$$
$$= \exp[-L^d \tilde{g}(\sigma)], \qquad (8)$$

where $\tilde{g}(\sigma)$ denotes the density of cracks within the sample volume L^d (coming from the sum $\sum_i$ over the entire volume) that start propagating at and above the stress level σ. Equation (8) comes from the fact that the sample survives if each of the cracks within the volume survives. This is the essential origin of the extreme statistical nature of the failure probability $F(\sigma)$ of the sample.

Noting that the pair correlation $g(l)$ of two occupied sites at distance l on a percolation cluster decays as $\exp[-l/\xi(p)]$, and connecting the stress σ with the length l by using Griffith's law [Eq. (1)] that $\sigma \sim \Lambda/l^a$, one gets $\tilde{g}(\sigma) \sim \exp(-\Lambda^{1/a}/\xi \sigma^{1/a})$ for $p \to p_c$. On substituting this, Eq. (8) gives the Gumbel distribution (Chakrabarti and Benguigui, 1997). If, on the other hand, one assumes a
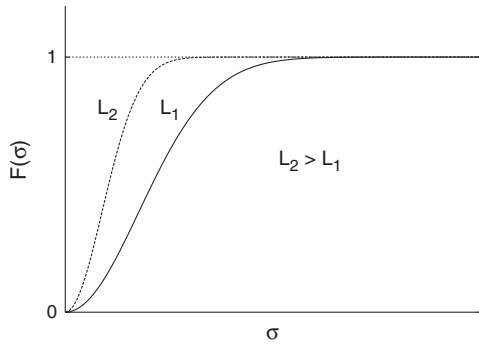
FIG. 2. Schematic variation of failure probability $F(\sigma)$ with stress σ for a disordered solid with volume L_1^d or L_2^d ($L_2 > L_1$).

power-law decay of $g(l)$, $g(l) \sim l^{-b}$, then using the Griffith law (1), one gets $\tilde{g}(\sigma) \sim (\sigma/\Lambda)^m$, giving the Weibull distribution, from Eq. (8), where $m = b/a$ gives the Weibull modulus (Chakrabarti and Benguigui, 1997). The variation of $F(\sigma)$ with σ in both of the cases has the generic form shown in Fig. 2. $F(\sigma)$ is nonzero for any stress $\sigma > 0$ and its value (at any σ) is higher for larger volume (L^d). This is because the possibility of a larger defect (due to fluctuation) is higher in a larger volume and consequently its failure probability is higher. Assuming $F(\sigma_f)$ is finite for failure, the most probable failure stress σ_f becomes a decreasing function of volume if extreme statistics is at work.

The precise ranges of validity of the Weibull and Gumbel distributions for the breakdown strength of disordered solids are not well established yet. However, analysis of the results of detailed experimental and numerical studies of breakdown in disordered solids seems to suggest that the fluctuations of the extreme statistics dominate for small disorder (Herrmann and Roux, 1990; Sahimi, 2003). Very near to the percolation point, the percolation statistics take over and the statistics become self-averaging. One can argue (Bergman and Stroud, 1992) that, arbitrarily close to the percolation threshold, the fluctuations of the extreme statistics will probably be suppressed and the percolation statistics should take over and the most probable breaking stress becomes independent of the sample volume [its variation with disorder being determined,
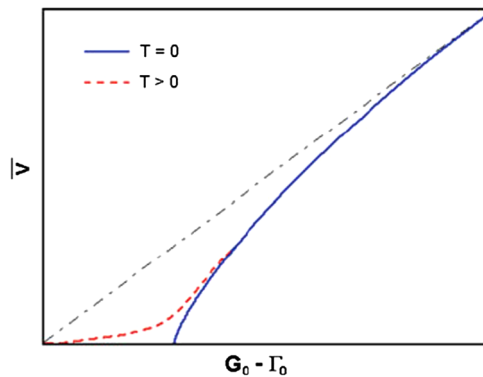
as in Eq. (7), by an appropriate breakdown exponent]. This is because the appropriate competing length scales for the two kinds of statistics are the Lifshitz scale $\ln L$ [coming from the finiteness of the volume integral of the defect probability, $L^d(1 - p)^l$ finite, giving the typical defect size $l \sim \ln L$] and the percolation correlation length ξ. When $\xi < \ln L$, the above scenario of extreme statistics should be observed. For $\xi > \ln L$, the percolation statistics are expected to dominate.

C. Fracture as a dynamical phase transition

When a material is stressed, according to the linear elastic theory discussed above, it develops a proportional amount of strain. Beyond a threshold, cracks appear, and on further application of stress, the material is fractured as it breaks into pieces. In a disordered solid, however, the advancing cracks may be stopped or *pinned* by the defect centers present within the material. So a competition develops between the pinning force due to disorder and the external force. Up to a critical value of the external force, the average velocity of the crack front will disappear in the long-time limit, i.e., the crack will be pinned. However, if the external force crosses this critical value, the crack front moves with a finite velocity. This depinning transition can be viewed as a *dynamical critical phenomenon* in the sense that near criticality universal scaling is observed, independent of the microscopic details of the materials concerned (Bonamy and Bouchaud, 2011). The order parameter for this transition is the average velocity $\bar{v}$ of the crack front. When the external force f^{ext} approaches the critical value f_c^{ext} from a higher value, the order parameter vanishes as

$$\bar{v} \sim (f^{\text{ext}} - f_c^{\text{ext}})^\theta, \tag{9}$$

where θ denotes the velocity exponent. We mention here that the pinning of a crack front by a disorder potential can occur at zero temperature (see Fig. 3). At finite temperature, there can be healing of cracks due to diffusion or there can be subcritical crack propagation (in the so-called creep regime) (Bonamy and Bouchaud, 2011). In the latter case, the velocity is expected to scale as

$$\bar{v} \sim \exp\left[-C\left(\frac{f_c^{\text{ext}}}{f}\right)^\phi\right]. \tag{10}$$

This subcritical scaling agrees well with results of experiments (Koivisto, Rosti, and Alava 2007 and Ponson 2009). In Fig. 4, the experimental result for crack propagation in the Botucatu sandstone (Ponson, 2009) is shown. The average velocity of the crack is plotted against the mechanical energy release rate G ($f = G - \Gamma$, where Γ is the fracture energy). The subcritical creep regime and the supercritical power-law variations are clearly seen (insets), these results give a velocity exponent close to $\theta \approx 0.81$.

Theoretical predictions of this exponent using functional renormalizations group methods have placed its value around $\theta = 0.59$ (Chauve, Le Doussal, and Wiese, 2001), but the experimental findings differ significantly ($\theta \approx 0.80 \pm 0.15$). Here we mention a numerical study of a model of elastic crack-front propagation in a disordered solid. The basic idea is to consider the propagation of the crack front as an elastic string driven through a random medium. The crack front is

FIG. 3 (color online). The average velocity of the crack front is plotted against external force ($f = G - \Gamma$, where G is the mechanical energy release rate and Γ is the fracture energy). For $T = 0$ a depinning transition is seen. For finite temperature the subcritical creep is shown. From Ponson and Bonamy, 2010.
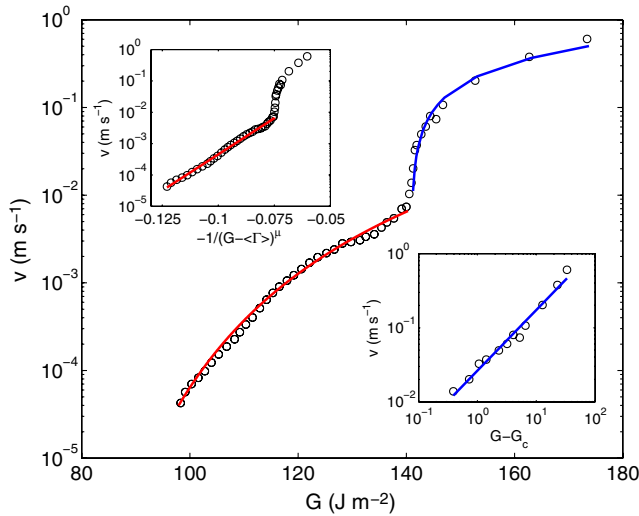
FIG. 4 (color online). Variation of average crack-front velocity against the mechanical energy release rate is shown for Botucatu sandstone. The subcritical creep region and supercritical power- law variations are shown in the top left and bottom right insets, respectively. For the subcritical regime, the data are fitted with a function $v \sim e^{-C/(G-\langle \Gamma \rangle)^\mu}$ for $\mu = 0.60$ and $\langle \Gamma \rangle = 65 \, \mathrm{J \, m^{-2}}$. For the power-law variation [$v \sim (G - G_c)^\theta$] in the supercritical region, $G_c = 140 \, \mathrm{J \, m^{-2}}$ and $\theta = 0.80$. From Ponson, 2009.

characterized by an array of integral height (measured in the direction of the crack propagation) $\{h_1, h_2, \ldots, h_L\}$ with periodic boundary conditions, where the unique values for the height profile suggest that any overhangs in the height profile are neglected. The forces acting on a site can be written as

$$f_i(t) = f_i^{\mathrm{el}} + f^{\mathrm{ext}} + g \eta_i(h_i), \qquad (11)$$

where f^{el} is the elastic force due to stretching, f^{ext} is the applied external force, and η is due to disorder. The dynamics of the driven elastic chain is then given by the simple rule

$$h_i(t+1) - h_i(t) = v_i(t) = \begin{cases} 1 & \text{if } f_i(t) > 0, \\ 0 & \text{otherwise.} \end{cases} \qquad (12)$$

The elastic force may have different forms in various contexts. When this force is short ranged (between nearest neighbors) the well-studied models are the Edwards-Wilkinson (Edwards and Wilkinson, 1982) [see also Amar and Family (1990), Csahok *et al.* (1993)] and Kardar-Parisi-Zhang models [Kardar, Parisi, and Zhang (1986); Moser, Kertész, and Wolf (1991); Sasamoto and Spohn (2010)] [see Barabási and Stanley (1995) for extensive analysis]. The long-range versions include those where the force decays as an inverse square [see, e.g., Duemmer and Krauth (2007)]. The velocity exponent θ, as defined before, turns out to be 0.625 ± 0.005 (Duemmer and Krauth, 2007). Also, mean-field models (infinite range) are studied in this context (Leschhorn, 1992; Vannimenus and Derrida, 2001; Vannimenus, 2002) (with $\theta = 1/2$ exactly). An infinite-range model, where the elastic force depends only upon the total stretching of the string, has also been studied recently (Biswas and Chakrabarti, 2011), where the observed velocity exponent value ($\theta = 0.83 \pm 0.01$) is rather close to that found in some experiments (Ponson, 2009).

D. Rate-dependent and state-dependent friction law

1. General remarks

In a simplified view, an earthquake may be regarded as the rubbing of a fault. From this standpoint, the friction laws of faults play a vital role in understanding and predicting earthquake dynamics. In addition, it should be noted that the Coulomb-Mohr criterion for brittle fracture involves the (internal) friction coefficient and thus the role of a friction law in earthquake physics is considerable. In this section, the phenomenology of friction and its underlying physical processes are briefly reviewed, with a on the recent developments. Some recent remarkable progress in experiments will also be introduced, although, unfortunately, theoretical understanding of such experiments is rather poor. Thus, we try to propose the problems that need to be solved by physicists.

Before explaining the knowledge obtained in the 20th and 21st centuries, it is instructive to look at the ancient (16th-and 17th-century) phenomenology, which has been referred to as the Coulomb-Amonton laws: (i) Frictional force is independent of the apparent area of contact. (ii) Frictional force is proportional to the normal load. (iii) Kinetic friction does not depend on the sliding velocity and is smaller than static friction. The first two laws do not need any modification to this date, whereas the third law needs to be modified and replaced by the rate-dependent and state-dependent friction law, which we introduce in the following sections. The Coulomb-Amonton laws in their original form just represent a phenomenology involving only macroscopic quantities such as the apparent contact area and normal load. It is generally instructive to consider the sublevel (or microscopic) ingredients that underlie this macroscopic phenomenology.

The essential microscopic ingredient in friction is *asperity*, which is a junction of protrusions of the surfaces (Rabinowicz, 1965; Bowden and Tabor, 2001). In other words, the two macroscopic surfaces in contact are indeed detached almost everywhere except for asperities. The total area of asperities defines the *true contact area*, which is generally much smaller than the apparent contact area. Thus, the macroscopic frictional behavior is mainly determined by the rheological properties of asperity. We write the area of asperity i as A_i. Then the total area of true contact reads

$$A_{\mathrm{true}} = \sum_{i \in \mathcal{S}} A_i, \qquad (13)$$

where $\mathcal{S}$ denotes the set of asperities. This set depends on the properties of the surfaces such as topography and is essentially time dependent because the state of the surface is dynamic due to sliding and frictional healing (Brechet and Estrin, 1994).

Because of the stress concentration at asperities, molecules or atoms are directly pushed into contact so that an asperity may be viewed as a grain boundary, possibly with some inclusions and impurities (Rabinowicz, 1965; Bowden and Tabor, 2001). Suppose that each asperity has its own shear strength σ_i, above which the asperity undergoes sliding. It may depend on the degree of grain-boundary misorientation and on the amount of impurities at the asperity. For simplicity,

however, here we assume $\sigma_i = \sigma_Y$; i.e., the yield stress or shear strength of each asperity is the same. Then the frictional force needed to slide the surface reads

$$F = \sum_{i \in \mathcal{S}} A_i \sigma_i \simeq \sigma_Y \sum_{i \in \mathcal{S}} A_i = \sigma_Y A_{\text{true}}. \tag{14}$$

The frictional force is thus proportional to the area of true contact. Dividing Eq. (14) by the normal force N, one obtains the friction coefficient $\mu \equiv F/N$. Using $N = A_a P$, where A_a is the apparent area of contact and P is the normal pressure, one gets

$$\mu = \sum_{i \in \mathcal{S}} \frac{A_i}{A_a} \frac{\sigma_i}{P} \simeq \frac{A_{\text{true}} \sigma_Y}{A_a P}. \tag{15}$$

Alternatively, one can have $A_{\text{true}}/A_a = \mu P/\sigma_Y$. This means that the fraction of true contact area is proportional to the pressure normalized by the yield stress, where the friction coefficient is the proportionality coefficient. Assuming that the yield stress of the asperity is the same as that of the bulk, we may set $\sigma_Y \sim 0.01 G$, where G is the shear modulus. Inserting this and $\mu \simeq 0.6$ into Eq. (15), one has $A_{\text{true}}/A_a \sim 60P/G$. This rough estimate can be confirmed in experiment and numerical simulation (Dieterich and Kilgore, 1994, 1996; Hyun *et al.*, 2004), where the proportionality coefficient is on the order of 10. For example, at a normal pressure on the order of kilopascals, the fraction of true contact is as small as 10^{-5}.

In view of Eq. (14), the first two Coulomb-Amonton laws can be recast in the form that frictional force is proportional to the true contact area, which is independent of the apparent contact area but proportional to the normal load. This constitutes the starting point of a theory on friction, which will be discussed in the following sections. The third Coulomb-Amonton law is just a crude approximation of what we know today. It should be replaced by the modern law, which is now referred to as the rate- and state-dependent friction law. In the next section, we discuss the RSF law based on the first two Coulomb-Amonton laws.

2. Formulation

Extensive experiments on rock friction were conducted in the 1970s and 1980s in the context of earthquake physics. An excellent review of these experimental works is by Marone (1998). Importantly, these experiments reveal that kinetic friction is indeed not independent of sliding velocity. Thus, the third Coulomb-Amonton law must be modified. Dieterich devised an empirical law that describes the behavior of the friction coefficient (for both steady and transient states) based on his experiments on rock friction (Dieterich, 1979). Later, the formulation was to some extent modified by Ruina (1983) who introducing an additional variable(s) other than the sliding velocity. A new set of variables describes the state of the frictional surfaces, so that they are referred to as the *state variables*. Although in general a state variable(s) may be a set of scalars, in most cases a single variable is enough for the purpose. Hereafter, the state variable is denoted by θ'. Using the state variable, the friction law reads

$$\mu = c' + a' \log \frac{V}{V_*} + b' \log \frac{V_* \theta'}{\mathcal{L}}, \tag{16}$$

where a' and b' are positive nondimensional constants, c' is a reference friction coefficient at a reference sliding velocity V_*, and $\mathcal{L}$ is a characteristic length scale interpreted to be comparable to a typical asperity length. In typical experiments, a' and b' are on the order of 0.01, and $\mathcal{L}$ is of the order of micrometers. Note that the state variable θ' has the dimension of time.

The state variable θ' is in general time dependent so that one must have a time evolution law for θ' together with Eq. (16). Many empirical laws have been proposed so far in order to describe time-dependent properties of a friction coefficient. One of the commonly used equations (Ruina, 1983).

$$\dot{\theta}' = 1 - \frac{V}{\mathcal{L}} \theta', \tag{17}$$

which is now referred to as the Dieterich' or aging law. This describes a time-dependent increase of the state variable even at $V = 0$. Meanwhile, other forms of evolution law may also be possible due to the empirical nature of Eq. (16). For example, the following is also known to be consistent with experiments (Ruina, 1983):

$$\dot{\theta}' = -\frac{V \theta'}{\mathcal{L}} \log \frac{V \theta'}{\mathcal{L}}; \tag{18}$$

this is referred to as the Ruina or slip law. In a similar manner, a number of other evolution laws have been proposed so far, such as a composite of the slowness law and the slip law (Kato and Tullis, 2001).

Although there have been many attempts to clarify which evolution law is the most suitable, no decisive conclusions have been reached. As most of them give the identical result if linearized around a steady sliding state, the difference between them becomes apparent only far from a steady sliding state. One may immediately notice that in Eq. (18) the state variable is time independent at $V = 0$ so that it is not very quantitative in describing friction processes for which the healing is relevant. On the other hand, Eq. (18) can describe a relaxation process after an instantaneous velocity switch ($V = V_1$ to V_2) better than Eq. (17), while Eq. (17) predicts different responses for the changes $V = V_1$ to V_2 and $V = V_2$ to V_1. (Experimental data suggest that they are symmetric.) Also, it is known that Eq. (18) can describe a nucleation process better than Eq. (17) (Ampuero and Rubin, 2008). However, we do not go further into the details of the experimental validation of evolution laws and leave it to the review by Marone (1998).

Irrespective of the choice of evolution law, a steady state is characterized by $\theta'_{\text{ss}} = \mathcal{L}/V$ so that the steady-state friction coefficient at sliding velocity V reads

$$\mu_{\text{ss}} = c' + (a' - b') \log \frac{V}{V_*}. \tag{19}$$

Note that, as the nondimensional constants a' and b' are typically on the order of 0.01, the velocity dependence of steady-state friction is very small; a change in sliding velocity by one order of magnitude results in ~ 0.01 (or even less) change in the friction coefficient. It is thus natural that people in the 17th century overlooked this rather minor velocity dependence. However, this velocity dependence is in fact

not minor at all but very important in sliding instability problems, e.g., earthquakes.

We also remark that Eq. (16), together with an evolution law such as Eq. (17) or (18), well describes the behavior of the friction coefficient not only for rock surfaces but also for metal surfaces (Popov *et al.*, 2012), two sheets of paper (Heslot *et al.*, 1994), etc. In this sense, the framework of Eq. (16) is rather universal. This universality is partially because the deformation of asperities involves atomistic processes (i.e., creep). One can assume for creep of asperities $\sigma_Y = k_B T/\Omega \log(V/V_0)$, where Ω is the activation volume and V_0 is a characteristic velocity involving the activation energy. Then Eq. (15) leads to

$$\mu \simeq \frac{k_B T}{\Omega P_{\text{true}}} \log(V/V_0), \qquad (20)$$

where $P_{\text{true}} = PA_a/A_{\text{true}}$ is the actual pressure acting on the asperities. Comparing Eqs. (20) and (16) with $b' = 0$ (no healing), one can infer that $a' = k_B T/\Omega P_{\text{true}}$, as previously derived (Heslot *et al.*, 1994; Nakatani, 2001; Rice, Lapusta, and Ranjith, 2001). However, we are unaware of a microscopic expression for b' to this date. We are also unaware of any microscopic derivations of evolution laws, such as Eqs. (17) and (18), although an interesting effort to understand their physical meaning can be found in Yoshioka (1997).

3. Stability of a steady state within the framework of RSF

As we aim to discuss earthquake dynamics based on the RSF law, it is essential to discuss frictional instability within the framework of RSF. For simplicity, we consider a body on the frictional surface. The body is pulled by a spring at a constant velocity V,

$$M\ddot{X} = -k(X - Vt) - \mu N, \qquad (21)$$

where X is the position, M is the mass, k is the spring constant, and N is the normal load. This may be regarded as the simplest model of frictional instability driven by tectonic loading. Suppose that the friction coefficient μ is given by the RSF law, Eq. (16), together with an evolution law. The choice of the evolution law, i.e., Dieterich's or Ruina's, does not affect the following discussions as they are identical if linearized around a steady state. The motion of the block is uniform in time if the surface is steady state velocity strengthening ($a' > b'$) or if the spring constant is sufficiently large. For a steady-state velocity weakening surface the steadysliding state undergoes Hopf bifurcation below a critical spring constant. A linear stability analysis (Ruina, 1983; Heslot *et al.*, 1994) shows that the steady sliding state is unstable if

$$k < k_{\text{crit}} \equiv \frac{N}{\mathcal{L}}(b' - a'). \qquad (22)$$

This relation plays a central role in various earthquake models, in which a constitutive law is given by the RSF law. This will be discussed in Sec. III. An important consequence of Eq. (22) is that the tectonic motion is essentially stable if $a' - b' > 0$. Namely, steady sliding is realized in the region where $a' - b' > 0$, whereas the motion may be unstable if $a' - b' < 0$. In addition, smaller $\mathcal{L}$ widens the parameter range of unstable motion.

Although the above analyses involve a one-body system, the stability condition, Eq. (22), appears to be essentially the same in many-body and continuum systems. Thus, provided that Eq. (21) applies, it is widely recognized in seismology that the seismogenic zone has negative a, b, and smaller L, whereas the aseismic zone has the opposite tendency.

E. Beyond the RSF law

It should be remarked that the RSF law has a certain limit of its application. Many experiments reveal that it no longer holds at high sliding velocities. This may be due to various mechanochemical reactions that are induced by the frictional heat, which typically lubricate surfaces to a considerable degree; the friction coefficient becomes as low as 0.2 or even less than 0.1 (Tsutsumi and Shimamoto, 1997; Goldsby and Tullis, 2002; Di Toro, Goldsby, and Tullis, 2004; Hirose and Shimamoto, 2005; Mizoguchi *et al.*, 2006). If such lubrication occurs in a fault, the fault motion is considerably accelerated and thus these effects have been much studied during the last decade. Feedback of frictional heat may be indeed very important to faults, because the normal pressure in a seismogenic zone is of the order of 100 MPa. (Note , however, the presence of high-pressure pore fluid may reduce the effective pressure.) As this area of study is relatively new, our current understanding of such mechanochemical effects is rather incomplete. Taking the rapid development of this area into account, here we mention some of the important experiments briefly.

1. Flash heating

Friction under such high pressure may lead to melting of rock. There have been some reports of molten rock observed in fault zones, which implies that the temperature is elevated up to 2000 K during earthquakes.

A series of pioneering works on frictional melting in the context of earthquakes has been conducted by Shimamoto and his co-workers. They devised a facility to study rock friction at high speed under high pressure and found a behavior very different from that of the RSF law. The steady-state friction coefficient typically shows a remarkable negative dependence on sliding velocity and the relaxation to steady state is twofold (Tsutsumi and Shimamoto, 1997; Hirose and Shimamoto, 2005). At higher sliding velocity (e.g., 1 m/s), the friction coefficient decreases to as low as 0.2 (or even less), whereas the typical value in the quasistatic regime is around 0.7. We stress that such a large decrease of the friction coefficient cannot be explained in terms of the RSF law, where the change of the steady-state friction coefficient is of the order of 0.01 even if the sliding velocity changes by a few orders of magnitude [recall Eq. (19), where a' and b' are both on the order of 0.01]. Thus, the mechanism of weakening must be qualitatively different from that of the RSF law. Indeed, in such experiments, molten rock is produced on surfaces due to the frictional heat. It is considered that the melt produced lubricates the surfaces ,resulting in an unusually low friction coefficient.

In view of Eq. (14), frictional melting must take place at asperities, where the frictional heat is produced. Thus, before the entire surface melts, asperities experience very high

temperature, which may change the constitutive law. Such asperity heating is also known in tribology and is referred to as *flash heating*. Rice applied this idea to fault friction in order to estimate the feasibility of flash heating in earthquake dynamics. His argument is as follows (Rice, 2006): The power input to asperity i is $\sigma_Y A_i V$, which is to be stored in the proximity of the asperity. As discussed later, it is essential to assume here that heat conduction is one dimensional; i.e., the temperature gradient is normal to the surface, but uniform along the transverse directions. The produced heat invades the bulk over the distance $\sqrt{D_{\text{th}}t}$, where D_{th} is the thermal diffusivity. Thus, frictional heat is stored in the small volume of $A_i\sqrt{\alpha t}$. Writing the average temperature of this hot volume as $T(t)$, the deposited thermal energy reads $c_P\rho A_i\sqrt{D_{\text{th}}t}[T(t) - T_0]$, where c_P is the isobaric specific heat, ρ is the mass density, and T_0 is the ambient temperature. Then the energy balance leads to

$$T(t) - T_0 \simeq \frac{\sigma_Y V}{\rho c_P}\sqrt{\frac{t}{D_{\text{th}}}}. \tag{23}$$

This indicates that the surface temperature increases with time as $\sqrt{t}$. If T_w symbolizes the critical temperature above which an asperity loses its shear strength, then the duration t_w for the temperature to be elevated up to the critical temperature reads

$$t_w = D_{\text{th}}\left[\frac{\rho c_P(T_w - T_0)}{\sigma_Y V}\right]^2. \tag{24}$$

This heating process is limited to the duration or lifetime of an asperity contact. If we write the longitudinal dimension of each asperity as $\mathcal{L}_i$, the lifetime of an asperity is estimated as $\mathcal{L}_i/V$. Thus, weakening of an asperity occurs if and only if $t_w \leq \mathcal{L}_i/V$. Taking Eq. (24) into account, this condition may be written as

$$V \geq \frac{D_{\text{th}}}{\mathcal{L}_i}\left[\frac{\rho c_P(T_w - T_0)}{\sigma_Y}\right]^2. \tag{25}$$

Neglecting the statistics of $\mathcal{L}_i$, one gets the characteristic sliding velocity V_w above which weakening occurs,

$$V_w = \frac{D_{\text{th}}}{\mathcal{L}}\left[\frac{\rho c_P(T_w - T_0)}{\sigma_Y}\right]^2. \tag{26}$$

Alternatively, from Eq. (25), the maximum size of asperity that does not melt at the sliding velocity V is given by

$$\mathcal{L}_{\text{max}} = \frac{D_{\text{th}}}{V}\left[\frac{\rho c_P(T_w - T_0)}{\sigma_Y}\right]^2. \tag{27}$$

The proportion of nonmelting asperityies may be approximated by $\mathcal{L}_{\text{max}}/\mathcal{L}$. Assuming that the friction coefficients of a molten asperity and a nonmelting one are given by

$$\mu = \begin{cases} f_1 & (T < T_w), \\ f_2 & (T > T_w), \end{cases} \tag{28}$$

the average friction coefficient reads

$$\mu = f_1\frac{\mathcal{L}_{\text{max}}}{\mathcal{L}} + f_2\left(1 - \frac{\mathcal{L}_{\text{max}}}{\mathcal{L}}\right) \tag{29}$$

$$= f_2 + (f_1 - f_2)\frac{V_w}{V}. \tag{30}$$

The friction coefficient decreases as V^{-1} at high slip velocity $V \geq V_w$. Taking $\alpha = 1$ mm^2/s, $\rho c_P = 4$ MJ/m^{3}K, $D = 5$ μm, $T_w - T_0 = 700$ K, and $\sigma_Y = 0.02G$–$0.1G$ (shear modulus) $= 0.6 - 3$ GPa, the characteristic velocity V_w is $0.5 - 14$ m/s. This does not contradict rock experiments on melting-induced weakening. Also, Eq. (30) is not inconsistent with experiments, although f_1 and f_2 are fitting parameters.

Note that the discussion does not depend on the apparent normal pressure, as the pressure on the asperity is approximately the yield stress (of uniaxial compression) irrespective of the apparent normal pressure. Thus, flash melting could occur in principle even when the apparent pressure is very low as long as the sliding velocity is larger than V_w given by Eq. (26). However, in an experiment conducted at relatively low pressures, the threshold velocity is an order of magnitude smaller than the prediction of Eq. (26) (Kuwano and Hatano, 2011). This may be because other relevant mechanisms are responsible for dynamic weakening observed in experiments, but the answer is yet to be given.

It is also important to note that in this discussion the assumption of one-dimensional heat conduction is essential; i.e., the frictional heat is not transferred in the horizontal directions but only in the normal direction. This assumption implies that the thermal diffusion length $\sqrt{\alpha t_w}$ must be smaller than the height of a protrusion that constitutes an asperity. Assuming that the height of a protrusion is proportional to a horizontal dimension L_i, this condition leads to

$$\mathcal{L}_i \geq \frac{D_{\text{th}}\rho c_P(T_w - T_0)}{\sigma_Y V}. \tag{31}$$

Because it is estimated in general that $\rho c_P(T_w - T_0) > \sigma_Y$, Eq. (31) immediately follows from Eq. (25). Thus, the assumption of one-dimensional heat conduction may be sound.

If the asperities are sufficiently small so that the thermal diffusion length exceeds the height of protrusions, the assumption of one-dimensional heat conduction is violated. A good example is friction in nanopowders, in which the typical size of the true contact area is on the order of nanometers (Han *et al.*, 2011). Interestingly, one can still observe dynamic weakening similar to that caused by flash melting, but Han *et al.* did not attribute this behavior to flash melting, because the duration of contact between nanograins was too short to cause a significant temperature increase. The physical mechanism of such weakening is still not clear. (Silica-gel lubrication may be ruled out as the material they used is silica-free.)

2. Frictional melting and thermal pressurization

There is yet another class of weakening phenomena called frictional melting; the melt is squeezed out of asperities to fill the aperture between the two surfaces. Such a situation can occur if the surfaces are rubbed for a sufficiently long time. If this process occurs, the melt layer supports the apparent normal pressure to reduce the effective pressure at asperities, and ultimately hinders solid-solid contact. This leads to the disappearance of the asperities; i.e., there are no solid-solid

contacts between the surfaces but a thin layer of melt under shear. There are some analyses of such systems assuming Arrhenius-type viscosity (Fialko and Khazan, 2005; Nielsen *et al.*, 2008). In such and analysis, one can predict that the shear traction is proportional to $P^{1/4}$, where P is the normal pressure. The quantitative validation of such theories is yet to be done.

It may be noteworthy here that the viscosity of such a liquid film involves a rather different problem: nanofluidics. The melt may be regarded as a nanofluid, the viscosity of which may be very different from that of ordinary fluids. The shear flow of very thin layers of melt (under very high pressure) may be unstable due to partial crystallization (Thompson, Grest, and Robbins, 1992) Until this date, the effect of nanofluidics on frictional melting has not been taken into account and is a problem left open to physicists.

Meanwhile, evidence of frictional melting of a fault is not very often found in core samples or in outcrops. As faults generally contain fluid, frictional heat increases the fluid temperature as well. As a result, the fluid pressure increases and the effective pressure on solid-solid contact decreases. Therefore, the frictional heat production generally decreases in the presence of fluid. In the simplest cases where the fault zone is impermeable, the effective friction (and the produced frictional heat) may vanish as the fluid pressure can be as large as the rock pressure (Sibson, 1973). This is referred to as thermal pressurization, and a large amount of work has been devoted to such dynamic interaction between frictional heat and the fluid pressure. More detailed formulations incorporate the effect of fluid diffusion with nonzero permeability of host rocks (Lachenbruch, 1980; Mase and Smith, 1987). In these analyses, the extent of weakening is enhanced if a fault zone has smaller compressibility and permeability. Although this behavior is rather trivial qualitatively, some nontrivial behaviors are found in a model where the permeability is assumed to be a dynamic quantity coupled with the total displacement (Suzuki and Yamashita, 2010). However, it is generally difficult to judge the validity of a model from observations and thus we do not discuss this problem further.

3. Other mechanochemical effects

In some systems, anomalous weakening of friction ($\mu \sim 0.2$) can be observed at sliding velocities much lower than the critical velocity for flash heating [Eq. (26)]. Typically, one can observe weakening at sliding velocities of the order of mm/s. Thus, there might be mechanisms for great weakening other than frictional melting.

Such experiments are typically conducted with complex materials like a fault gouge taken from a natural fault so that there may be many different mechanisms of weakening depending on the specific compositions of rock species. Among them, a mechanism that might bear some robustness is lubrication by silica-gel production (Goldsby and Tullis, 2002; Di Toro, Goldsby, and Tullis, 2004). In several experiments on silica-rich rock such as granite, scanning election microscope observation of the surfaces reveals a silica gel layer that experienced shear flow. The generation of silica gel may be attributed to chemical reactions between silica and water in the environment. This silica gel intervenes between the surfaces, resulting in lubrication of the fault. Although the

details of the chemical reactions are not very clear, the mechanics of weakening may be essentially the same as that of flash heating and melting, because in both cases the cause of weakening is some soft material (or liquid) that is produced by shear and intervenes at asperities. However, in the case of silica-gel formation, the thixotropic nature of silica gel may result in peculiar behaviors of friction, as observed in the experiment by Di Toro, Goldsby, and Tullis (2004).

In addition, we to add several other mechanisms that lead to anomalous weakening. Han *et al.* (2007) found a friction coefficient as low as 0.06 in marble under relatively high pressure (1.1–13.4 MPa) and high sliding velocity (1.3 m/s). Despite the utilization of several techniques for microstructural observation, they could not observe any evidence of melting such as glass or amorphous texture, but only a layer of nanoparticles produced by thermal decomposition of calcite due to frictional heating. Mizoguchi *et al.* (2006) also found a friction coefficient as low as 0.2 in a fault gouge taken from a natural fault, where they also could not find any evidence for melting. To this date, the mechanism of such frictional weakening at higher sliding velocity is not clear.

It is important to note that these samples inevitably include a large amount of submicrometer grains that are worn down by high-speed friction (Han *et al.*, 2007; Hayashi and Tsutsumi, 2010). They may play an important role in weakening at high sliding velocities. The grain size distribution of the fault gouge is typically well fitted by a power law with exponent -2.6 to -3.0 (Chester and Chester, 1998) so that smaller grains cannot be neglected in terms of volume fraction. The exponent appears to be common to laboratory (Marone and Scholz, 1989) and numerical experiments of wear (Abe and Mair, 2009). The rheology of such fractal grains has not been investigated in a systematic manner, notwithstanding a pioneering computational work (Morgan, 1999). We discuss the influence of grains on friction in detail in the next section.

4. Effect of a third body: Granular friction

Previously, we considered the situation where two surfaces were in contact only at asperities. This is generally not the case if the asperities are worn down to free particles that intervene between the two surfaces. In this case, the system can be regarded as granular matter that is sheared by the two surfaces. The core of a natural fault always consists of powdered rock (Chester and Chester, 1998), which is produced by the fault motion of the past. Thus, friction on a fault is closely related to the rheology of granular rock.

As is briefly mentioned in the previous section, earthquake physics involves a wide range of sliding velocities (or shear rates) ranging from the tectonic (e.g., nm/s) to the coseismic time scale (m/s). It is thus plausible that the rheological properties of granular matter are qualitatively different depending on the range of sliding velocities. Here we define two regimes for granular friction: the quasititatic and dynamic regimes. In the quasistatic regime, the frictional properties of granular matter are described by the RSF law. However, some important properties will be remarked that are not observed for bare surfaces. In the dynamic regime, one may expect dynamic strengthening as observed in numerical simulations

(Midi, 2004; da Cruz *et al.*, 2005). However, at the same time one may also expect weakening due to various mechano-chemical reactions (Mizoguchi *et al.*, 2006; Hayashi and Tsutsumi, 2010). The rheological properties that are experimentally observed are determined by the competition of these two ingredients. Here we review the essential rheological properties of granular matter in these two regimes.

In experiments on quasistatic deformation, friction of granular matter seems to obey the RSF law. However, some important properties that are different from those of bare surfaces should be remarked.

(1) Velocity dependence of steady-state friction appears to be affected by the layer thickness. In particular, the value of $a' - b'$ in Eq. (19) is an increasing function of the layer thickness.

(2) The value of $a' - b'$ appears to have negative dependence on the total displacement applied to a system. This is true for both granular matter and bare surfaces.

(3) Transient behaviors can be described by either Dieterich's or Ruina's law, as in the case of bare surfaces. The characteristic length in an evolution law is proportional to the layer thickness.

These experimental observations are well summarized and discussed in detail by Marone (1998). We thus shall not repeat them here and just note the essential points described above.

As to the first point, there is no plausible explanation to this date. It appears that the second point could be merged into the first point if the effective layer thickness (i.e., the width of the shear band) decreases as the displacement increases. However, we remark that it is also true in the case of bare surfaces, where the effective layer thickness is not a simple decreasing function of the displacement. Thus, the second point cannot be explained in terms of the thickness. The third point indicates that the shear strain is a more appropriate variable than the displacement of the boundary for the description of the time evolution of the friction coefficient. This may be reasonable as the duration of contact between grains is inversely proportional to the shear rate. However, the derivation of evolution laws (either Dieterich's or Ruina's) from the grain dynamics is not known to this date. To construct a theory that can explain these three properties based on the nature of granular matter is still a challenge to statistical physicists.

Next we discuss the dynamic regime. The rheology of granular matter in the dynamic regime is extensively investigated in statistical physics (GDRMidi, 2004; da Cruz *et al.*, 2005). As to the steady-state friction coefficient, the shear-rate dependence is also one of the main interests in statistical physics. There are many ingredients that potentially affect the friction coefficient of granular matter: the grain shape, degree of inelasticity (coefficient of restitution), friction coefficient between grains, stiffness, pore fluid, etc. Shape dependence is very important to granular friction, but theoretical understanding of this effect is still very poor. Thus, for simplicity, we neglect the shape effect and consider only spherical grains. Furthermore, we limit ourselves to the effects of shear rate, stiffness, mass and diameter of grains, coefficient of restitution, and intergrain friction. This means that we neglect time- or slip-dependent deformation of the grain contacts,

such as wear (Marone and Scholz, 1989) or frictional healing (Bocquet *et al.*, 1998). The effects of pore fluid are also neglected; i.e., we discuss only dry granular matter here. With such idealization, one can make a general statement on a constitutive law by dimensional analysis. The friction coefficient of granular matter is formally written as

$$\mu = \mu(P, m, d, \dot{\gamma}, Y, \mu_e, e), \qquad (32)$$

where P is the normal pressure, m is the mass, d is the diameter, $\dot{\gamma}$ is the shear rate, Y is the Young's modulus of grains, μ_e is the intergrain friction coefficient, and e is the coefficient of restitution. [It should be noted that one assumes a single characteristic diameter d in Eq. (32).] From the viewpoint of dimensional analysis, the arguments on the left-hand side of Eq. (32) must be nondimensional numbers,

$$\mu = \mu(I, \kappa, \mu_e, e), \qquad (33)$$

where $I = \dot{\gamma}\sqrt{m/Pd}$ and $\kappa = Y/P$. Thus, the friction coefficient of granular matter depends in principle on these four nondimensional parameters. Many numerical simulations reveal that μ is rather insensitive to κ and ϵ, and the shear-rate dependence is mainly described by I. This nondimensional number I is referred to as the inertial number. Importantly, the dependence on I is positive in numerical simulations (Midi, 2004; da Cruz *et al.*, 2005; Hatano, 2007); namely, the shear-rate dependence is positive. It is important to note that the negative shear-rate dependence that is ubiquitously observed in experiments, cannot be reproduced in numerical simulation. This is reasonable because the origin of the negative velocity dependence is the time-dependent increase in true contact, whereas in simulation the parameters are time independent.

Experiments in the context of earthquake physics are conducted at relatively high pressures at which the frictional heat affects the physical state of granular matter. In some experiments (Mizoguchi *et al.*, 2006; Hayashi and Tsutsumi, 2010), remarkable weakening ($\mu \sim 0.1$) is observed. Because such anomalous behaviors may involve shear banding as well as various chemical reactions such as thermal decomposition or silica-gel formation, the frictional properties should depend on the detailed composition of the rock species contained in the granular matter. These weakening behaviors must be further investigated by extensive experiments.

So far we have discussed the steady-state friction coefficient, but the description of transient states is also important in understanding the frictional instability (and earthquake dynamics). The evolution law for the quasistatic regime is indeed essentially the same as that for bare surfaces; namely, the aging or slip law (Marone, 1998). The evolution law in the dynamic regime is well described by the linear relaxation equation even for relatively large velocity change (Hatano, 2009):

$$\dot{\mu} = -\tau^{-1}[\mu(t) - \mu_{ss}], \qquad (34)$$

where μ_{ss} is the steady-state friction coefficient, which depends on the sliding velocity and τ is the relaxation time. τ is the relaxation time of the velocity profile inside granular matter and it scales with $\sqrt{m/Pd}$. Thus, importantly, the inertial number, which describes steady-state friction may, be written using τ as $I \simeq \tau\dot{\gamma}$; i.e., the shear rate multiplied by

the velocity relaxation time. Note that the inertial number is an example of a Deborah number, which is in general the internal relaxation time normalized by the experimental time scale.

Note the difference from the conventional evolution law in the framework of the RSF law, Eqs. (17) and (18): Eq. (34) does not contain any length scale but only the time scale. This means that the relaxation process of high-speed granular friction takes time rather than the slip distance. However, we stress that the validity of Eq. (34) has been found only in simulations on dry granular matter and it has not been verified in physical experiments.

F. Microscopic theories of friction

Many attempts have been made to explain friction from an atomistic point of view. Of course, such efforts are meaningful only when the surfaces are smooth and the atomistic properties determine friction. This approach has gained importance in recent years, because of advancement of technology in this field. With atomic force microscopy, etc., sliding surfaces can now be probed down to atomic scales. Also, present day computers allow large-scale molecular dynamics simulations that help in understanding the atomic origin of friction. In this approach, the atomic origins of friction forces are investigated [see also Bhushan, Israelachvili, and Landman (1995); Braun and Naumovets (2006); and Hölscher, Schirmeisen, and Schwarz (2008)]. For this purpose, two atomically smooth surfaces are taken and by writing down the equations of motion, friction forces are calculated. The effects of inhomogeneity, impurity, lubrication, and disorder in terms of vacancies of atoms are also considered.

One of the foremost attempts to model friction from an atomic viewpoint was by Tomlinson (1929). In this model, only one atomic layer of each surface in contact is considered. In particular, the lower surface is considered to be rigid and to provide a periodic (sinusoidal) potential for the upper body. The contact layer of the upper body is modeled by mutually disconnected beads (atoms), which are attached elastically to the bulk above. This model is, of course, oversimplified. The main drawback is that no interaction between the atoms of the upper body is considered.

1. Frenkel-Kontorova model

The Frenkel-Kontorova (Frenkel and Kontorova, 1938) model overcomes some of these difficulties. In this model, the surface of the sliding object is modeled by a chain of beads (atoms) connected harmonically by springs. The base is again represented by a sinusoidal potential. The Hamiltonian of the system can, therefore, be written as

$$H = \sum_{i=1}^{N}\left[\frac{1}{2}K(x_{i+1} - x_i - a)^2 + V(x_i)\right], \qquad (35)$$

where x_i is the position of the ith atom, a is the equilibrium spacing of the chain, and $V(x) = -V_0 \cos(2\pi x/b)$. Clearly, there are two competing lengths in this model, viz., the equilibrium spacing of the upper chain (a) and the period of the substrate potential (b). While the first term tries to keep the atoms in their original positions, the second term tries to

bring them into the local minima of the substrate potential. Simultaneous satisfaction of these two forces is possible when the ratio a/b is commensurate. The chain is then always pinned to the substrate in the sense that a finite force is always required to initiate sliding. Below that force, the average velocity vanishes at large times. However, interesting phenomena occur when the ratio a/b is incommensurate. In that case, up to a finite value of the amplitude of the substrate potential, the chain remains "free." In that condition, for arbitrarily small external force, sliding is initiated. The hull function (Peyrard and Aubry, 1983) remains analytic. Beyond the critical value of the amplitude, the hull function is no longer analytic and a finite external force is now required to initiate sliding. This transition is called the breaking-of-analyticity transition or the Aubry transition (Peyrard and Aubry, 1983) [for extensive details see Braun and Kivshar (2004)].

2. Two-chain model

The Frenkel-Kontorova model has been generalized in many ways, viz, extension to higher dimensions, effects of impurity, the Frenkel-Kontorova-Tomlinson model, etc. [see Braun and Naumovets (2006) and references therein]. But one major shortcoming of the Frenkel-Kontorova model is that the substrate or the surface atoms of the lower substance are considered to be rigidly fixed in their equilibrium position. But for the same reason that the upper surface atoms should relax, the lower surface atoms should relax too. In the two-chain model of friction (Matsukawa and Fukuyama, 1994) this question is addressed. In this model, a harmonically connected chain of atoms is pulled over another. The atoms have only one degree of freedom in the direction parallel to the external force. The equations of motion of the two chains are

$$m_a \gamma_a(\dot{x}_i - \langle \dot{x}_i \rangle) = K_a(x_{i+1} + x_{i-1} - 2x_i)$$
$$+ \sum_{j \in b}^{N_b} F_I(x_i - y_j) + F_{\text{ex}}, \qquad (36)$$

$$m_b \gamma_b(\dot{y}_i - \langle \dot{y}_i \rangle) = K_b(y_{i+1} + y_{i-1} - 2y_i)$$
$$+ \sum_{j \in a}^{N_a} F_I(y_i - x_j) - K_s(y_i - ic_b), \qquad (37)$$

where x_i and y_i denote the equilibrium positions of the upper and lower chain, respectively, m's represent the atomic masses, γ's represent the dissipation constants, K's the strengths of the interatomic force, N's the number of atoms in each chain, c's the lattice spacing, and the subscript a denotes upper chain and b the lower chain. F_{ex} is the external force and F_I is the interchain force between the atoms, which is derived from the following potential:

$$U_I = -\frac{K_I}{2}\exp\left[-4\left(\frac{x}{c_b}\right)\right], \qquad (38)$$

where K_I is the interaction strength.

It is argued that the frictional force is of the form

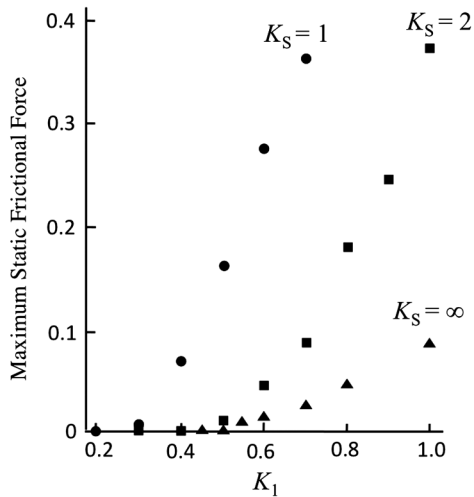$$-\sum_i \sum_j \langle F_I(x_i - y_j)\rangle_t = N_a \langle F_{\text{ex}}\rangle_t. \qquad (39)$$

FIG. 5. The variations of the maximum static friction with the amplitude (K_I) of the interchain potential for different values of the lower-chain stiffness (K_s). The limit $K_s \rightarrow \infty$ corresponds to the Frenkel-Kontorova model. But it is clearly seen that even for finite K_s (i.e., when the lower chain can relax) there is a finite value of interchain potential amplitude up to which the static friction is practically zero and after which it increases , signifying the Aubry transition. From Matsukawa and Fukuyama, 1994.

It is then shown by numerical analysis that the velocity dependence of the kinetic frictional force becomes weaker as the static friction increases (tuned by different K's). The velocity dependence essentially vanishes when the static frictional force is increased, giving one of the Amonton-Coulomb laws.

In this case, the lower-chain atoms, which form the substrate potential, are no longer rigidly placed. Still, the breaking-of-analyticity transition is observed. Figure 5 shows the variation of the maximum static frictional force with interaction potential strength. For different values of the rigidity with which the lower chain is bound (K_s), different curves are obtained. This indicates a pinned state even for finite rigidity of the lower chain.

3. Effect of fractal disorder

The effects of disorder and impurity have been studied in the microscopic models of friction. Also there have been efforts to incorporate the effect of self-affine roughness in friction. Eriksen, Biswas, and Chakrabarti (2010) consider the effect of disorder on static friction. A two-chain version of the Tomlinson model is considered. The self-affine roughness is introduced by removing atoms and keeping the remaining ones arranged in the form of a Cantor set. The Cantor set is a simple prototype of fractals. Instead of considering the regular Cantor set, here a random version of it is used. A line segment [0,1] is taken. In each generation, it is divided into s equal segments and $s - r$ of those are randomly removed. In this way, a self-similar disorder is introduced, which is present only in the statistical sense, rather than in a strict geometric arrangement.

This kind of roughness is introduced in both the chains. Then the interchain interaction is taken to be of very short-range type. Only when there is one atom exactly over another
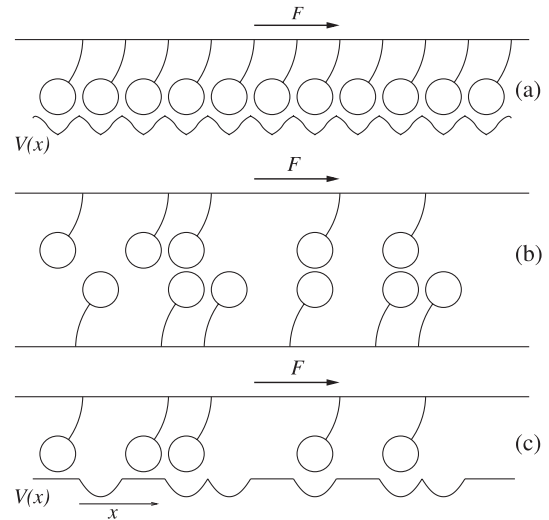

FIG. 6. Schematic representation of the two-chain version of the Tomlinson model with (a) no disorder, (b) Cantor set disorder, and (c) the effective substrate potential. From Eriksen, Biswas, and Chakrabarti, 2010.

(see Fig. 6) is there an attractive interaction. In this way, the maximum static friction force can be calculated by estimating the overlap of these two chains. It turns out that the static friction force has a distribution that is qualitatively different from what is expected if a random disorder or no disorder is present. The scaled (independent of generation) distribution of overlap or static friction is (Eriksen, Biswas, and Chakrabarti, 2010)

$$f^{s,r}(x/R)/R = \sum_{j=1}^{r} \tilde{c}^{s,r}(j)(f^{s,r} \ldots j - 1 \quad \text{terms} \ldots f^{s,r})(x),$$

(40)

where $R = r^2/s$ and $\tilde{c}^{s,r}(x) = rC_x^{s-r}C_{r-x}/sC_r$. For a particular (s, r) combination (9,8), the distribution function is shown in Fig. 7. It clearly shows that the distribution function is
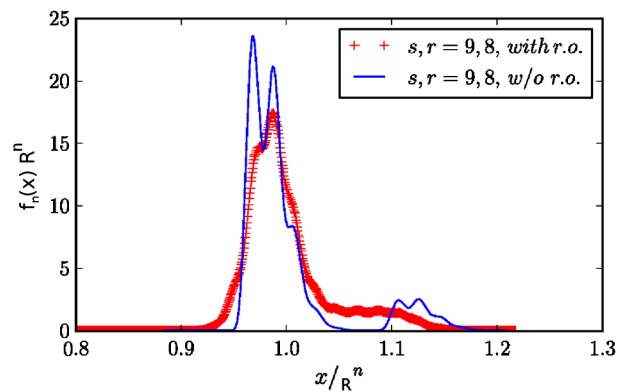

FIG. 7 (color online). The overlap distribution for $s = 9$, $r = 8$ is shown. The dotted curve shows the average distribution with random offset and the continuous curve is that without random offset. The distribution is qualitatively different from the Gaussian distribution expected for random disorder. From Eriksen, Biswas, and Chakrabarti, 2010.

qualitatively different from the Gaussian distribution expected if the disorder were random.

III. EARTHQUAKE MODELS AND STATISTICS I: BURRIDGE-KNOPOFF AND CONTINUUM MODELS

In the previous section, we reviewed the basic physics of friction and fracture, which constitutes a microscopic basis for our study of macroscopic properties of an earthquake as a large-scale frictional instability. Some emphasis was put on the RSF law now regarded as the standard constitutive law in seismology. In this and following sections, we review the present status of our research on various types of statistical physical models of earthquakes introduced to represent their macroscopic properties.

A. Statistical properties of the Burridge-Knopoff model

1. The model

One of the standard models widely employed in the statistical physical study of earthquakes is the Burridge-Knopoff model (Rundle *et al.*, 2003; Ben-Zion, 2008). The model was first introduced by Burridge and Knopoff (1967). Then, Carlson, Langer, and collaborators performed a pioneering study of the statistical properties of the model (Carlson and Langer, 1989a; 1989b; Carlson *et al.*, 1991; Carlson, 1991a; 1991b; Carlson, Langer, and Shaw, 1994), paying particular attention to the magnitude distribution of earthquake events and its dependence on the friction parameter.

In the BK model, an earthquake fault is simulated by an assembly of blocks, each of which is connected via elastic springs to the neighboring blocks and to the moving plate. Of course, the space discretization in the form of blocks is an approximation to the continuum crust, which could in principle give rise to an artificial effect not realized in the continuum. Indeed, such a criticism against the BK model employing a certain type of friction law, e.g., the purely velocity-weakening friction law to be defined below in Sec. III.A.2, was made in the past (Rice, 1993); we shall return to this later.

In the BK model, all blocks are assumed to be subjected to friction force, the source of nonlinearity in the model, which eventually realizes an earthquakelike frictional instability. As mentioned in Sec. II, the standard friction law in modern seismology might be the RSF law. In order to facilitate its computational efficiency, even simpler friction laws have also been used in simulation studies made in the past.

We first introduce the BK model in one dimension (1D). Extension to two dimensions (2D) is straightforward. The 1D BK model consists of a 1D array of N identical blocks, which are mutually connected with the two neighboring blocks via elastic springs of elastic constant k_c, and are also connected to the moving plate via springs of elastic constant k_p, and are driven with a constant rate: See Fig. 8. All blocks are subjected to the friction force Φ, which is the only source of nonlinearity in the model. The equation of motion for the ith block can be written as
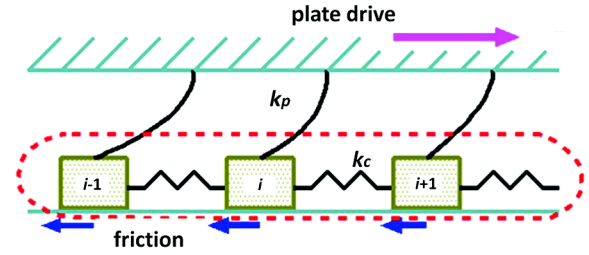

FIG. 8 (color online). The Burridge-Knopoff (BK) model in one dimension.

$$m\ddot{U}_i = k_p(\nu't' - U_i) + k_c(U_{i+1} - 2U_i + U_{i-1}) - \Phi_i,$$
(41)

where t' is the time, U_i is the displacement of the ith block, ν' is the loading rate representing the speed of the moving plate, and Φ_i is the friction force at the ith block.

In order to make the equation dimensionless, the time t' is measured in units of the characteristic frequency $\omega = \sqrt{k_p/m}$ and the displacement U_i in units of the length $L^* = \Phi_0/k_p$, Φ_0 being a reference value of the friction force. Then, the equation of motion can be written in the dimensionless form as

$$\ddot{u}_i = \nu t - u_i + l^2(u_{i+1} - 2u_i + u_{i-1}) - \phi_i,$$
(42)

where $t = t'\omega$ is the dimensionless time, $u_i \equiv U_i/L^*$ is the dimensionless displacement of the ith block, $l \equiv \sqrt{k_c/k_p}$ is the dimensionless stiffness parameter, $\nu = \nu'/L^*\omega$ is the dimensionless loading rate, and $\phi_i \equiv \Phi_i/\Phi_0$ is the dimensionless friction force at the ith block.

The corresponding equation of motion of the 2D BK model is given in the dimensionless form by

$$\ddot{u}_{i,j} = \nu t - u_{i,j} + l^2(u_{i+1,j} + u_{i,j+1} + u_{i-1,j} + u_{i,j-1} - 4u_{i,j}) - \phi_{i,j},$$
(43)

where $u_{i,j} \equiv U_{i,j}/L^*$ is the dimensionless displacement of the block (i, j). It is assumed here that the displacement of each block occurs only along the direction of the plate drive. The motion perpendicular to the plate motion is neglected.

Often (but not always), the motion in the direction opposite to the plate drive is also inhibited by imposing an infinitely large friction for $\dot{u}_i < 0$ (or $\dot{u}_{i,j} < 0$) in either case of 1D or 2D. It is also often assumed in both 1D and 2D that the loading rate ν is infinitesimally small, and $\nu = 0$ during an earthquake event, a very good approximation for real faults (Carlson *et al.*, 1991). Taking this limit ensures that the interval time between successive earthquake events can be measured in units of ν^{-1} irrespective of particular values of ν. Taking the $\nu \to 0$ limit also ensures that, between an ongoing event, no other event takes place at a distant place independently of this ongoing event.

2. The friction law

The friction force Φ: causing a frictional instability is a crucially important element of the model. Here we refer to the following two forms for Φ: (A) a velocity-weakening friction force (Carlson and Langer, 1989a) and (B) a rate-dependent

and state-dependent friction law (Dieterich, 1979; Ruina, 1983; Marone, 1998; Scholz, 1998; Scholz, 2002).

(A) With this velocity-weakening friction force, one simply assumes that the friction force $\phi = \phi(\dot{u}_i)$ is a unique function of the block velocity $\dot{u}_i$. In order for the model to exhibit a frictional instability corresponding to earthquakes, one needs to assume a velocity-weakening force $\phi(\dot{u}_i)$ that needs to be a decreasing function of $\dot{u}_i$. The detailed form of $\phi(\dot{u}_i)$ is irrelevant. The form originally introduced by Carlson and Langer has widely been used in many subsequent works, that is (Carlson *et al.*, 1991),

$$\phi(\dot{u}_i) = \begin{cases} (-\infty, 1] & \text{for } \dot{u}_i \leq 0, \\ \frac{1-\delta}{1+2\alpha\dot{u}_i/(1-\delta)} & \text{for } \dot{u}_i > 0, \end{cases} \quad (44)$$

where the maximum value corresponding to the static friction has been normalized to unity. This normalization condition $\phi(\dot{u}_i = 0) = 1$ has been utilized to set the length unit L^*. The friction force is characterized by the two parameters δ and α. δ, introduced by Carlson *et al.* (1991) as a technical device facilitating the numerics of simulations, represents an instantaneous drop of the friction force at the onset of the slip, while α represents the rate of weaking of the friction force on increasing the sliding velocity. As emphasized by Rice (1993), this purely velocity-weakening friction law applied to the discrete BK model did not yield a sensible continuum limit. To achieve a sensible continuum limit, one then needs to introduce an appropriate short-length cut off by introducing, e.g., the viscosity term as was done by Myers and Langer (1993): See also the discussion in Sec. III.A.6.

We note that, in several simulations on a BK model, a slip-weakening friction force (Ida, 1972; Shaw, 1995; Myers, Shaw, and Langer, 1996), where the friction force is assumed to be a unique function of the slip distance $\phi(u_i)$, was utilized instead of the velocity-weakening friction force. The statistical properties of the corresponding BK model, however, seem not so different from those of the velocity-weakening friction force.

The real constitutive relations is of course more complex, neither purely velocity weakening nor purely slip weakening. As discussed in Sec. II, the RSF friction law was introduced to account for such experimental features, which we now refer to.

(B) From Eq. (16), the friction force in the BK model is given by

$$\phi_i = \left\{ c' + a' \log\left(\frac{v_i'}{v_*'}\right) + b' \log\frac{v_*'\theta_i'}{\mathcal{L}} \right\}\mathcal{N}, \quad (45)$$

where $\mathcal{N}$ is the effective normal load; see Sec. II.D for the other quantities and parameters. Among the several evolution laws, we use the aging (slowness) law [Eq. (17)]

$$\frac{d\theta_i'}{dt'} = 1 - \frac{v_i'\theta_i'}{\mathcal{L}}. \quad (46)$$

Under the evolution law above, the state variable θ_i' grows linearly with time at a complete halt $v_i' = 0$, reaching a very large value just before seismic rupture, while it decays very rapidly during the seismic rupture.

The equation of motion can be made dimensionless by taking the length unit to be the characteristic slip distance $\mathcal{L}$

and the time unit to be the rise time of an earthquake, $\omega^{-1} = (m/k_p)^{1/2}$. Then, one has

$$\frac{d^2u_i}{dt^2} = (\nu t - u_i) + l^2(u_{i+1} - 2u_i + u_{i-1})$$
$$- [c + a\log(v_i/v^*) + b\log(v^*\theta_i)], \quad (47)$$

$$\frac{d\theta_i}{dt} = 1 - v_i\theta_i, \quad (48)$$

where the dimensionless variables are defined by $t = \omega t'$, $u_i = u_i'/\mathcal{L}$, $v_i = v_i'/\mathcal{L}\omega$, $v^* = v_*'/\mathcal{L}\omega$, $\theta_i = \omega\theta_i'$, $\nu = \nu'/\mathcal{L}\omega$, $a = a'\mathcal{N}/k_p\mathcal{L}$, $b = b'\mathcal{N}/k_p\mathcal{L}$, and $c = c'\mathcal{N}/k_p\mathcal{L}$, while $l \equiv (k_c/k_p)^{1/2}$ is the dimensionless stiffness parameter defined above. In some numerical simulations, a slightly different form is used for the a term, where the factor inside the a term, v/v^*, is replaced by $1 + v/v^*$, i.e.,

$$\frac{d^2u_i}{dt^2} = (\nu t - u_i) + l^2(u_{i+1} - 2u_i + u_{i-1})$$
$$- \left[c + a\log\left(1 + \frac{v_i}{v^*}\right) + b\log\theta_i\right], \quad (49)$$

where the constant factor c in Eq. (49) is shifted by $b\log v^*$ from c in Eq. (48).

This replacement enables one to describe the system at a complete halt, whereas, without this replacement, the system cannot stop because of the logarithmic anomaly occurring at $v = 0$. A similar replacement is sometimes made also for the b term, i.e., θ to $1 + \theta$.

The values of various parameters of the model describing natural faults have been estimated (Ohmura and Kawamura, 2007). Typically, ω^{-1} corresponds to the rise time of an earthquake event and is estimated from observations to be a few seconds. Although the characteristic slip distance $\mathcal{L}$ remains largely ambiguous, an estimate of order a few millimeters or centimeters was given by Tse and Rice (1986) and by Scholz (2002). The loading rate associated with the plate motion is typically a few cm/y, and the dimensionless loading rate $\nu = \nu'/\mathcal{L}\omega$ is of order $\nu \simeq 10^{-8}$. The dimensionless quantity $k_p\mathcal{L}/\mathcal{N}$ was roughly estimated to be of order 10^{-4}. The dimensionless parameter c should be of order 10^3–10^4, and the a and b parameters are one or two orders of magnitude smaller than c.

3. The 1D BK model with short-range interaction

The simplest version of the BK model might be the 1D model with only nearest-neighbor interblock interaction. Since this model was reviewed in an earlier RMP review article by Carlson, Langer, and Shaw (1994), we keep the discussion here to a minimum, focusing mainly on recent results obtained after that review.

Earlier studies on the 1D BK model have revealed that, while smaller events persistently obeyed the GR law, i.e., staying critical or near critical, larger events exhibited a significant deviation from the GR law, being off critical or characteristic (Carlson and Langer, 1989a; 1989b; Carlson *et al.*, 1991; Carlson, 1991a; 1991b; Schmittbuhl, Vilotte, and Roux, 1996).
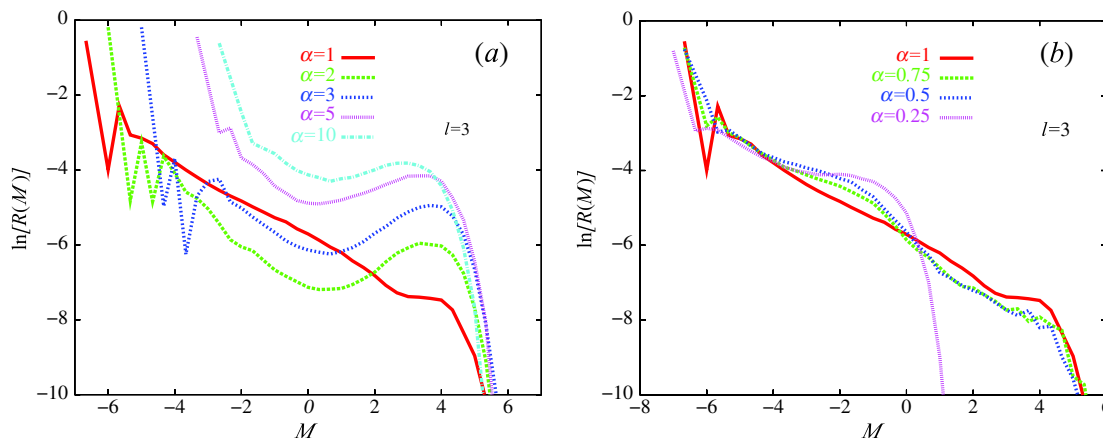
FIG. 9 (color online).   The magnitude distribution of earthquake events of the 1D BK model with nearest-neighbor interaction for various values of the friction parameter α: (a) for larger $\alpha = 1, 2, 3, 5,$ and 10, and (b) for smaller $\alpha = 0.25, 0.5, 0.75,$ and 1. The parameters l and δ are fixed to be $l = 3$ and $\delta = 0.01$. The system size is $N = 800$. From Mori and Kawamura, 2006.

In Fig. 9, we show recent data for the magnitude distribution (Mori and Kawamura, 2005; Mori and Kawamura, 2006). The magnitude of an event, M, is defined by

$$M = \ln\left(\sum_i \Delta u_i\right), \tag{50}$$

where the sum is taken over all blocks involved in the event.

As can be seen from Fig. 9, the form of the calculated magnitude distribution $R(M)$ depends on the value of the velocity-weakening parameter α. The data for $\alpha = 1$ lie on a straight line fairly well, apparently satisfying the GR law, which may be called near-critical behavior. The value of the exponent B describing the power-law behavior is estimated to be $B \simeq 0.50$, corresponding to the b value $b = \frac{3}{2}B \simeq 0.75$. By contrast, the data for larger α deviate from the GR law at larger magnitudes, exhibiting a pronounced peak structure, while the power-law feature still remains for smaller magnitudes; see Fig. 9(a). These features of the magnitude distribution were observed in many simulations (Carlson and Langer, 1989a; 1989b; Carlson *et al.*, 1991). This means that, while smaller events exhibit self-similar critical properties, larger events tend to exhibit off-critical or characteristic properties, which may be called "supercritical." The data for smaller $\alpha < 1$ exhibit considerably different behaviors from those for $\alpha > 1$. Large events are rapidly suppressed, which may be called "subcritical" behavior. For $\alpha = 0.25$, in particular, all events are almost exclusively small; see Fig. 9(b). Here the words critical, supercritical, and subcritical have been defined on the basis of the shape of the magnitude-frequency relationship.

As an example of properties other than the magnitude distribution, we show in Fig. 10 the recurrence-time distribution (Mori and Kawamura, 2005; 2006). The recurrence time T is defined here locally for large earthquakes with $M \geq M_c = 3$ or $M_c = 4$, i.e., a subsequent large event is counted when a large event occurs with its epicenter in the region within 30 blocks from the epicenter of the previous large event. As can be seen from the figure, the tail of the distribution is exponential at longer T irrespective of the value of α. Such an exponential tail of the distribution has also been reported for real seismicity (Corral, 2004). By contrast, the

distribution at shorter T is nonexponential and is greatly different for $\alpha = 1$ and $\alpha > 1$. For $\alpha > 1$, the distribution has an eminent peak corresponding to a characteristic recurrence time, which suggests the near-periodic recurrence of large events, as has been reported for several real faults (Nishenko and Buland, 1987; Scholz, 2002). For $\alpha = 1$, by contrast, the peak located close to the mean $\bar{T}$ is hardly discernible. Instead, the distribution has a pronounced peak at a shorter time, just after the previous large event. In other words, large events for $\alpha = 1$ tend to occur as "twins." A large event for the case of $\alpha = 1$ often occurs as a "unilateral earthquake" where the rupture propagates only in one direction, hardly propagating in the opposite direction.

Possible precursory phenomena exhibited by the model are of much interest, since they might open a way to an earthquake forecast. In fact, certain precursory features were
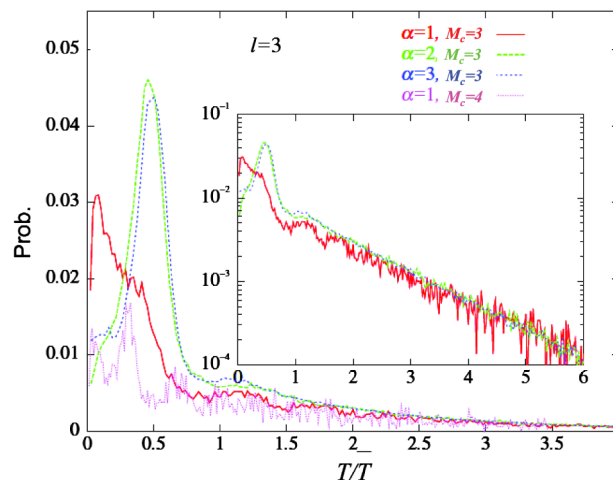

FIG. 10 (color online).   The local recurrence-time distribution of the 1D BK model with nearest-neighbor interaction for various values of the frictional parameter α. Large events with $M > M_c = 3$ or 4 are considered. The parameters l and δ are $l = 3$ and $\delta = 0.01$. The recurrence time T is normalized by its mean $\bar{T}$. The total number of blocks is $N = 800$. The inset represents semilogarithmic plots including the tail part of the distribution. From Mori and Kawamura, 2005.
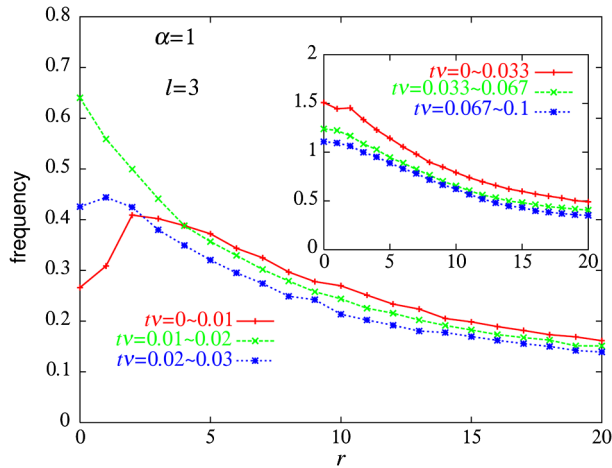
FIG. 11 (color online). The event frequency preceding the large event of $M > M_c = 3$ vs the distance from the epicenter of the upcoming mainshock of the 1D BK model with nearest-neighbor interaction. The parameters α, l, and δ are $\alpha = 1$, $l = 3$, and $\delta = 0.01$. The data are shown for several time periods before the mainshock. The inset represents similar plots with longer time intervals. The system size is $N = 800$. From Mori and Kawamura, 2006.

observed in the 1D BK model. Shaw, Carlson, and Langer examined the spatiotemporal patterns of seismic events preceding large events, observing that the seismic activity accelerates as the large event approaches (Shaw, Carlson, and Langer, 1992). Mori and Kawamura observed that the frequency of smaller events is gradually enhanced preceding the mainshock, whereas, just before the mainshock, it is suppressed in a close vicinity of the epicenter of the upcoming event (Mori and Kawamura, 2005; 2006), a phenomenon closely resembling the "Mogi doughnut" (Mogi, 1969; 1979; Scholz, 2002). Figure 11 represents the space-time correlation function between the large events and the preceding events of arbitrary size (dominated in number by smaller events). It represents the conditional probability that, provided that a large event of $M > M_c = 3$ occurs at a time t_0 and at a spatial point r_0, an event of arbitrary size occurs at a time $t_0 - t$ and at a spatial point $r_0 \pm r$. As can be seen from the inset of Fig. 11, seismic activity is gradually accelerated toward the mainshock either spatially or temporally. As can be seen from the main panel, however, the seismic activity is suppressed just before the mainshock in a close vicinity of the epicenter of the mainshock; see the dip developing around $r = 0$ for $t \lesssim 0.01$.

It turned out that the size of the quiescence region was always of only a few blocks, independent of the size of the upcoming mainshock (Mori and Kawamura, 2006). This may suggest that the quiescence is closely related to the discrete nature of the BK model; see Sec. III.A.6. Thus, the size of the quiescence region cannot be used in predicting the size of the upcoming mainshock. Instead, a correlation was observed between the size of the upcoming mainshock and the size of the seismically active "ring" region surrounding the quiescence region (Pepke, Carlson, and Shaw, 1994; Mori and Kawamura, 2006). Such a correlation was also reported in a real seismic catalog (Kossobokov and Carlson, 1995).

An aftershock sequence obeying the Omori law, although a common observation in real seismicity, is not observed in the BK model, at least in its simplest version (Carlson and Langer, 1989a; 1989b; Mori and Kawamura, 2006). Interestingly, Pelletier reported that the inclusion of the viscosity effect in the form of "dashpots" in the 2D BK model, together with the introduction of inhomogeneity of friction parameters, could realize an aftershock sequence obeying the Omori law (Pelletier, 2000). The frictional force employed by Pelletier was a very simple one, i.e., a constant dynamical vs static friction coefficient. Further analysis is desirable to establish the occurrence of an aftershock sequence obeying the Omori law in the BK model.

We note in passing that the 1D BK model has also been extended in several ways, e.g., by taking account of the effect of the viscosity (Myers and Langer, 1993; Shaw, 1994; De and Ananthakrisna, 2004; Mori and Kawamura, 2008b), modifying the form of the friction force (Myers and Langer, 1993; Shaw, 1995; Cartwright, Garcia, and Piro, 1997; De and Ananthakrisna, 2004), and driving the system only at one end of the system (Vieira, 1992; Vieira, 1996). The effect of the long-range interactions introduced between blocks was also analyzed; we review this effect in Sec. III.A.4.

4. The 2D BK model with short-range interaction

Real earthquake faults are 2D rather than 1D. Hence, it is clearly desirable to study the 2D version of the BK model in order to further clarify the statistical properties of earthquakes. The 2D BK model taken up here is to be understood as representing a fault plane that is itself 2D, where the direction orthogonal to the fault plane is not considered explicitly in the model (Carlson, 1991b). The other possible version is the one where the second direction of the model is taken to be orthogonal to the fault plane (Myers, Shaw, and Langer, 1996).

Extensive numerical studies have revealed that statistical properties of the 2D BK model are more or less similar to those of the 1D BK model reviewed in the previous section, at least qualitatively. The magnitude distribution $R(M)$ of the 2D BK model has been studied by several groups (Carlson and Langer, 1989a; 1989b; Carlson *et al.*, 1991; Kumagai *et al.*, 1999; and Mori and Kawamura, 2008a). In Fig. 12, we show typical behaviors of the magnitude distribution of the 2D BK model with variation of the frictional parameter α (Mori and Kawamura, 2008a). For smaller $\alpha \lesssim 0.5$, $R(M)$ bends down rapidly at larger magnitudes, exhibiting a subcritical behavior. Only small events of $M \lesssim 0.5$ occur in this case. At $\alpha \gtrsim 0.5$, large earthquakes of magnitude $M \simeq 8$ suddenly appear, while earthquakes of intermediate magnitude, say, $2 \lesssim M \lesssim 6$, remain rather scarce. Such a sudden appearance of large earthquakes at $\alpha = \alpha_{c1} \simeq 0.5$ coexisting with smaller ones has a feature of a discontinuous or first-order transition.

In this context, it might be interesting to point out that Vasconcelos observed that a single-block system exhibited a first-order transition at $\alpha = 0.5$ from a stick-slip to a creep mechanism (Vasconcelos, 1996), whereas this discontinuous transition becomes apparently continuous in many-block systems (Vieira, Vasconcelos, and Nagel, 1993; Clancy and
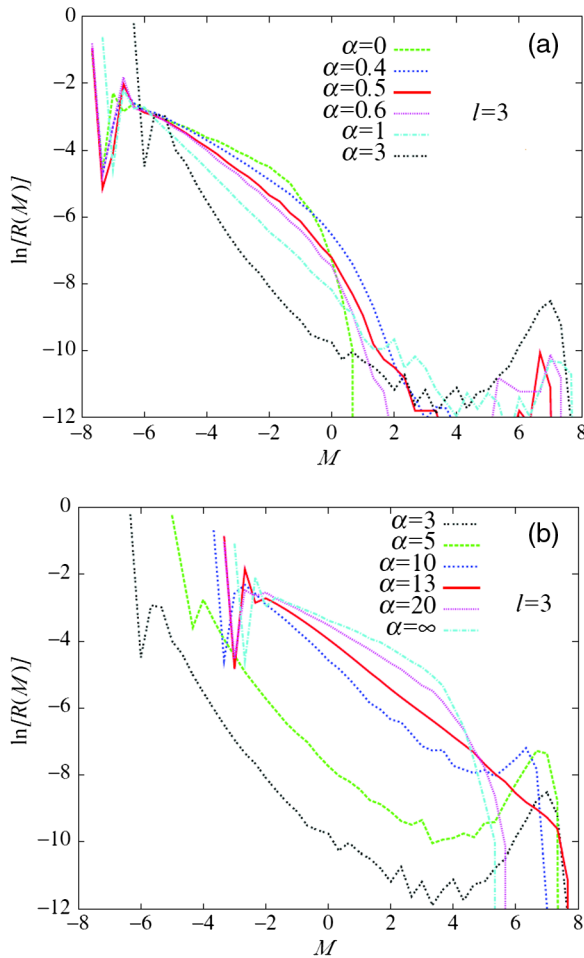
FIG. 12 (color online). The magnitude distribution $R(M)$ of the 2D BK model with nearest-neighbor interaction for various values of the friction parameter α. The other parameters are $l = 3$ and $\delta = 0.01$. (a) $R(M)$ for smaller values of the friction parameter $0 \leq \alpha \leq 3$, (b) $R(M)$ for larger values of the friction parameter $3 \leq \alpha \leq \infty$. The system size is 60×60. From Mori and Kawamura, 2008a.

Corcoran, 2005). The first-order transition observed at $\alpha = \alpha_{c1} \simeq 0.5$ in the 2D model may have some relevance to the first-order transition of a single-block system observed by Vasconcelos, although events observed at $\alpha < \alpha_{c1}$ in the present 2D model are not really creeps, but rather are stick-slip events of small size.

With further increase in α, the frequency of earthquakes of intermediate magnitude gradually increases. Figure 12(b) exhibits $R(M)$ for larger α. In the range of $1 \lesssim \alpha \lesssim 10$, $R(M)$ exhibits a pronounced peak structure at larger magnitude, deviating from the GR law, while it exhibits a near straight-line behavior corresponding to the GR law at smaller magnitudes (supercritical behavior). As α increases further, the peak at a larger magnitude becomes less pronounced. At $\alpha = \alpha_{c2} \simeq 13$, $R(M)$ exhibits a near straight-line behavior for a rather wide magnitude range, although $R(M)$ falls off rapidly at still larger magnitudes $M \gtrsim 7$, indicating that the near-critical behavior observed for $\alpha = \alpha_{c2} \simeq 13$ cannot be regarded as truly asymptotic, since this rapidfalloff of $R(M)$ at very large magnitudes is bulk property, not a finite-size effect.

A "phase diagram" of the model in the elasticity parameter l versus the friction parameter α, as reported by Mori and Kawamura (2008a) is shown in Fig. 13. The regions or the phases called supercritical, near critical, and subcritical are observed. The straight-line behavior of $R(M)$, i.e., the GR law, is realized only in a restricted region in the phase diagram along the phase boundary between the supercritical and subcritical regimes. Even along the phase boundary, the GR relation is characterized by a finite cutoff magnitude above which larger earthquakes cease to occur. Hence, the GR relation, as observed in a ubiquitous manner in real faults, is not realized in this model. Since each phase boundary has a finite slope in the α-l plane, one can also induce the subcritical-supercritical transition by varying the l value for a fixed α (Espanol, 1994; Vieira and Lichtenberg, 1996).

As for other quantities, the recurrence-time distribution of the 2D model exhibits a behavior similar to that of the 1D model. As in the case of 1D, an aftershock sequence obeying the Omori law is not observed even in the 2D model, at least in its simplest version. The 2D model also exhibits precursory phenomena similar to the ones observed in the 1D model (Mori and Kawamura, 2008a). Acceleration of seismic activity prior to the mainshock is observed in the supercritical regime, while it is not realized in the subcritical regime. As in the case of 1D, mainshocks are accompanied by the Mogi-doughnut-like quiescence in both supercritical and subcritical regimes.

As another signature of the precursory phenomena, we show in Fig. 14 the time-resolved local magnitude distribution calculated for time periods before the large event in the supercritical regime of $\alpha = 1$ and $l = 3$ (Mori and Kawamura, 2008a). Only events with their epicenters lying within five blocks of the upcoming mainshock of magnitude $M \geq M_c = 5$. As can be seen from the figure, fine apparent B value describing the samaller-magnitude region gets *smaller* as the mainshock is approached, i.e., it changes from $B \simeq 0.89$ of the long-time value to $B \simeq 0.65$ in the time range $t\nu \leq 0.1$ before the mainshock. In real seismicity, an appreciable decrease of the B value has been reported preceding large earthquakes (Suyehiro, Asada, and Ohtake, 1964; Jaume and Sykes, 1999; Kawamura, 2006). Obviously, a
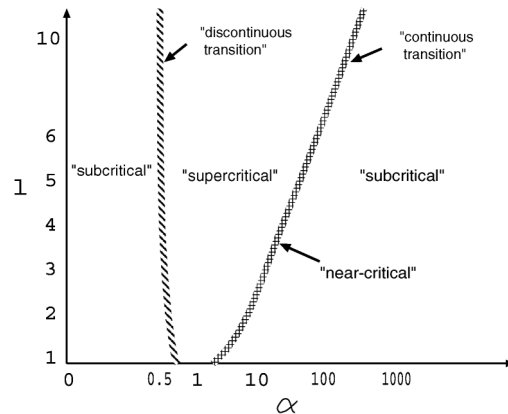

FIG. 13. Phase diagram of the 2D BK model with nearest-neighbor interaction in the plane of the friction parameter α versus the elastic parameter l. The parameter δ is $\delta = 0.01$. From Mori and Kawamura, 2008a.
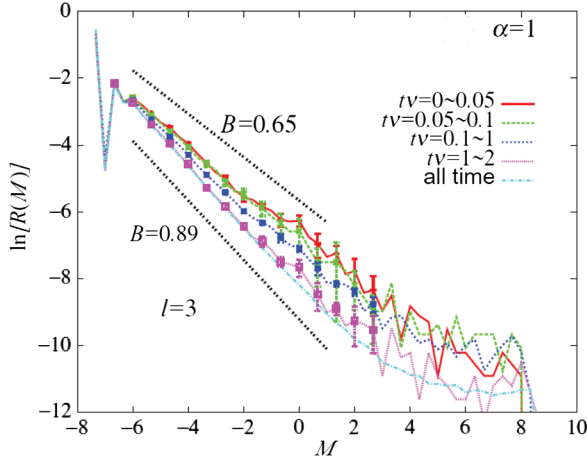
FIG. 14 (color online). The local magnitude distribution preceding a mainshock of $M > M_c = 5$ of the 2D BK model with nearest-neighbor interaction. The parameters are $\alpha = 1$, $l = 3$, and $\delta = 0.01$. The data are shown for several time periods before the mainshock. The system size is 60×60. From Mori and Kawamura, 2008a.

possible change in the magnitude distribution preceding the mainshock possesses potential importance in earthquake forecasting.

5. The BK model with long-range interaction

So far, we have assumed that the interaction between blocks works only between nearest-neighboring blocks. This may correspond to the situation where a thin isolated plate is subject to friction force and is driven by shear force (Clancy and Corcoran, 2006). However, a real fault is not necessarily a thin isolated plate, and the elastic body extends in directions away from the fault plane. Indeed, the BK model extended in the direction orthogonal to the fault plane has also been studied (Myers, Shaw, and Langer, 1996).

Considering the effect of such an extended elastic body adjacent to the fault plane under certain conditions amounts to considering the effective interblock interaction as *long ranged*. Thus, taking account of the effect of long-range interaction might make the model more realistic. Rundle *et al.* studied the properties of the 2D cellular automaton version of the BK model with the long-range interaction decaying as $1/r^3$ (Rundle *et al.*, 1995). Xia *et al.* studied the 1D BK model with a variable-range interaction where a block is connected to its R neighbors with a rescaled spring constant proportional to $1/R$ (Xia *et al.*, 2005; Xia *et al.*, 2008). The long-range model considered by Xia *et al.* may be regarded as of mean-field type, since the model reduces to the mean-field infinite-range model in the $R \rightarrow \infty$ limit.

One can also derive the relevant long-range interaction based on an elastic theory (Mori and Kawamura, 2008b). Suppose that the 3D elastic body in which the 2D BK model lies is isotropic, homogeneous, and infinite, and a fault surface is a plane lying in this elastic body and slipsping along one direction only. Then, a static approximation for an elastic equation of motion for the elastic body would give rise to a spring constant between blocks decaying with their separation r as $1/r^3$. This static assumption is justified

when the velocity of the seismic-wave propagation is high enough compared with the velocity of the seismic-rupture propagation.

Properties of the 2D BK model with the long-range power law interaction derived from an elastic theory, i.e., decaying as $1/r^3$, were investigated by Mori and Kawamura, 2008b. The interaction between the two blocks at sites (i, j) and (i', j') is given in the dimensionless form by

$$\left(l_x^2 \frac{|i' - i|^2}{r^5} + l_z^2 \frac{|j' - j|^2}{r^5} \right)(u_{i',j'} - u_{i,j}), \tag{51}$$

which falls off with distance r as $1/r^3$. Then, the dimensionless equation of motion for the 2D long-range interaction can be written as

$$\ddot{u}_{i,j} = \nu t - u_{i,j} + \sum_{(i',j') \neq (i,j)} \left(l_x^2 \frac{|i' - i|^2}{r^5} + l_z^2 \frac{|j' - j|^2}{r^5} \right)$$
$$\times (u_{i',j'} - u_{i,j}) - \phi_{i,j}. \tag{52}$$

If one restricts the range of interaction to nearest neighbors and takes the spatially anisotropic spring constant to be isotropic, $l_x = l_z = l$, one recovers the isotropic nearest-neighbor model described by Eq. (42). The "isotropy" assumption $l_x = l_z$ is equivalent to a vanishing Lamé constant. In fact, in the short-range model, such spatial anisotropy of the 2D BK model turned out to hardly affect the statistical properties of the model in the sense that the properties of the anisotropic model were quite close to those of the corresponding isotropic model characterized by the *mean* spring constant $l = (l_x + l_z)/2$ (Mori and Kawamura, 2008a).

One might also consider the 1D BK model with long-range interaction (Mori and Kawamura, 2008b). One possible way to construct the 1D model might be to impose the condition on the corresponding 2D model that the systems is completely rigid along the z direction, corresponding to the depth direction, i.e., $u(x, z, t) = u(x, t)$. This yields an effective interblock interaction decaying with distance r as $1/r^2$,

$$l^2 \frac{1}{|i - i'|^2}(u_{i'} - u_i), \tag{53}$$

with the dimensionless equation of motion

$$\ddot{u}_i = \nu t - u_i + l^2 \sum_{i' \neq i} \frac{u_{i'} - u_i}{|i - i'|^2} - \phi_i. \tag{54}$$

In Figs. 15(a) and 15(b), we show the magnitude distribution $R(M)$ of the long-range 2D BK model for smaller and larger values of α, i.e., (a) $0 \leq \alpha \leq 10$ and (b) $10 \leq \alpha \leq \infty$ (Mori and Kawamura, 2008b). As in the short-range case, three distinct regimes are observed depending on the α value. The intermediate-α region corresponds to the supercritical regime where $R(M)$ exhibits a pronounced peak at a larger magnitude, showing a characteristic behavior. A major difference from the short-range case is that the subcritical behavior realized in the short-range model in the smaller-α and larger-α regions is now replaced by near-critical behavior in the long-range model. Namely, for smaller $\alpha < \alpha_{c1} \sim 2$ and for larger $\alpha > \alpha_{c2} \sim 25$, $R(M)$ exhibits a near straight-line behavior over a rather wide magnitude range, and drops off sharply at larger magnitudes. The associated B value is estimated to be $B \simeq 0.59$ ($\alpha < \alpha_{c1}$) and $B \simeq 0.55$ ($\alpha > \alpha_{c2}$),
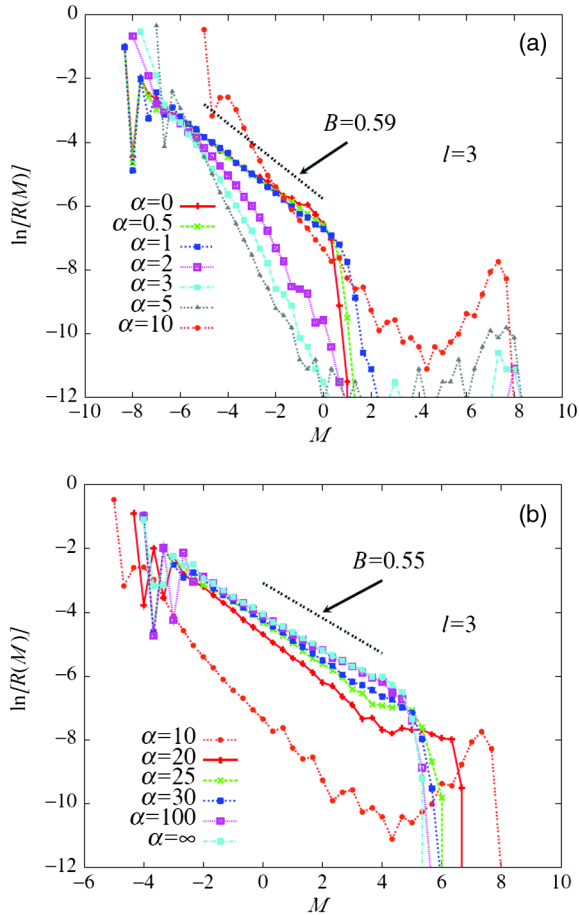
FIG. 15 (color online). The magnitude distribution $R(M)$ of the 2D BK model with long-range interaction for various values of the friction parameter α. The other parameters are $l = 3$ and $\delta = 0.01$. (a) $R(M)$ for smaller values of the frictional parameter $0 \le \alpha \le 10$. (b) $R(M)$ for larger values of the frictional parameter $10 \le \alpha \le \infty$. The system size is 60×60. From Mori and Kawamura, 2008b.
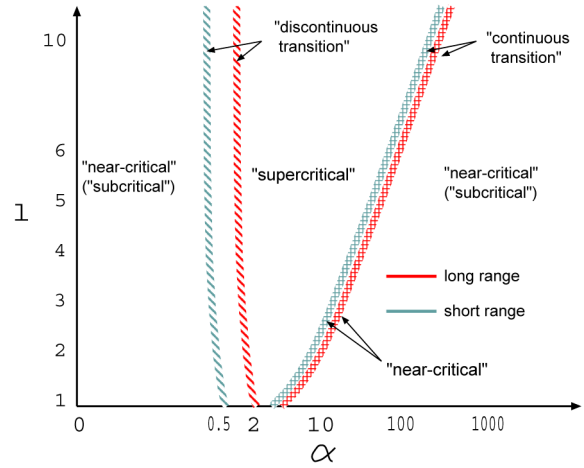

FIG. 16 (color online). The phase diagram of the 2D BK models with long-range interaction in the plane of the friction parameter α vs elastic parameter l, compared with that of the 2D BK model with short-range interaction. The parameter δ is set to $\delta = 0.01$. From Mori and Kawamura, 2008b.

which is rather insensitive to the α value. This straight-line behavior of $R(M)$ cannot be regarded as truly critical, since $R(M)$ drops off sharply at very large magnitudes. As in the short-range case, the change from the supercritical to the near-critical behavior at $\alpha = \alpha_{c2} \simeq 25$ is continuous, while it is discontinuous at $\alpha = \alpha_{c1} \simeq 2$.

Such near-critical behavior realized over a wide parameter range is in sharp contrast to the behavior of the corresponding short-range model, where $R(M)$ at smaller and larger α exhibits only a down-bending subcritical behavior, while a straight-line near-critical behavior is realized only by fine-tuning the α value to a special value $\alpha \simeq \alpha_{c2}$. The robustness of the near-critical behavior of $R(M)$ observed in the 2D long-range model might have an important relevance to real seismicity, since the GR law is ubiquitously observed for different types of faults. Note also that the associated B value observed here turns out to be close to the one observed in real seismicity (Mori and Kawamura, 2008b).

In Fig. 16, the behavior of $R(M)$ is summarized in the form of a phase diagram in the plane of the friction parameter α versus the elastic parameter l (Mori and Kawamura, 2008b). As can be seen from the figure, the phase diagram of the long-range model consists of three distinct regimes, two of which

are near-critical while one is supercritical. The phase boundary between the smaller-α near-critical regime and the supercritical regime represents a discontinuous transition, while the one between the larger-α near-critical regime and the supercritical regime represents a continuous transition. For comparison, the corresponding phase boundary of the short-range model is also shown. The near-critical phases in the long-range model are replaced by subcritical phases in the short-range model.

Note that the system in different phases of Fig. 16 really shows different properties. For example, we show in Fig. 17 the magnitude dependence of the mean displacement $\Delta \bar{u}$ at a seismic event (Mori and Kawamura, 2008b). As can be seen from the figure, the data in the two near-critical regimes (the data in the upper horizontal branch and in the lower horizontal branch) are grouped into two distinct branches,
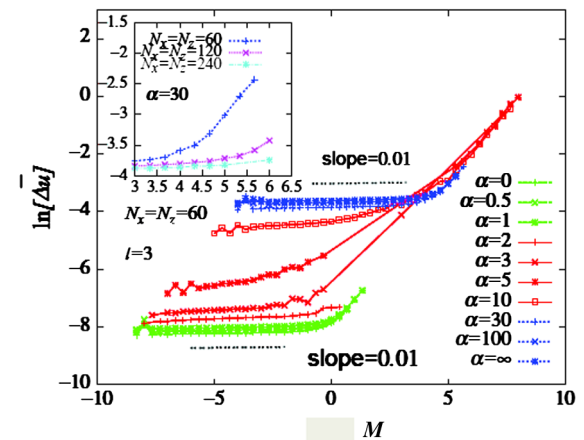

FIG. 17 (color online). The magnitude dependence of the mean displacement $\Delta \bar{u}$ at each seismic event of the 2D BK model with long-range interaction. In the main panel, the friction parameter α is varied with a fixed system size 60×60, while in the inset the system size N is varied for the case of $\alpha = 30$. The parameters l and δ are fixed to $l = 3$ and $\delta = 0.01$. From Mori and Kawamura, 2008b.

while the data in the supercritical regime (the data in between) exhibit a significantly different behavior. Interestingly, the mean displacement in the near-critical regimes hardly depends on the event magnitude.

It was observed that the mean stress drop at a seismic event also hardly depends on the event magnitude in the near-critical regimes of the 2D long-range BK model (Mori and Kawamura, 2008b). A similar independence was also reported in the mean-field-type 1D long-range BK model (Xia *et al.*, 2005; Xia *et al.*, 2008) and in the 1D long-range BK model (Mori and Kawamura, 2008b).

6. Continuum limit of the BK model

Although the BK model has been widely used as a useful tool to investigate statistical properties of earthquakes, the block discretization inherent to the model construction is a crude approximation of the original continuum earthquake fault. It introduces a short-length cutoff scale into the problem. Therefore, in order to check the validity of the model, it is crucially important to examine the continuum limit of the BK model carefully. Indeed, Rice criticized the discrete BK model with the velocity-weakening friction law as "intrinsically discrete," lacking in a well-defined continuum limit (Rice, 1993). Rice argued that the spatiotemporal complexity observed in the discrete BK model was due to the inherent discreteness of the model and should disappear in the continuum. Indeed, he applied the RSF law, which possesses an intrinsic length scale corresponding to the characteristic slip distance, and showed that the system tended to exhibit a quasiperiodic behavior if the grid spacing d' was taken smaller than the characteristic length scale, while if the grid spacing d' was taken longer than that, the system exhibited an apparently complex or critical behavior. This problem of the continuum limit of the BK model was also addressed by Myers and Langer (1993) within the velocity-weakening friction law; they introduced a Kelvin viscosity term to produce a small length scale, which allowed a well-defined continuum limit. Myers and Langer, and subsequently Shaw (1994), observed that the added viscosity term smoothed the rupture dynamics, apparently giving rise to the continuum limit accompanied by spatiotemporal complexity. More recently, the continuum limit of the 1D BK model with and without viscosity was examined by Mori and Kawamura within the velocity-weakening friction law (Mori and Kawamura, 2008c).

Thus, two different ways of taking the continuum limit of the BK model have been tried so far, each introducing a short length scale via (A) the viscosity term or (B) the RSF law. In this section, we examine the former (A), while the latter (B) is discussed in the next section.

As mentioned, the naive continuum limit of the discrete BK model with a velocity-weakening friction force without viscosity has a problem in that the pulse of the slip tends to become increasingly narrow in the limit, i.e., the dynamics becomes sensitive to the grid spacing $d' \to 0$. One way to circumvent this problem is to introduce the viscosity term $\eta' \partial^3 U_i / \partial x'^2 \partial t'$ into Eq. (41) to produce a small length scale, where η' is the viscosity coefficient. Myers and Langer showed that, owing to the added viscosity term, the system becomes independent of the grid spacing d' as long as the new small length scale ϵ', defined by

$$\epsilon' = \pi \sqrt{\frac{\eta'}{\alpha \omega}}, \tag{55}$$

is sufficiently larger than the grid spacing d' (Myers and Langer, 1993). With ξ' being the wave velocity in the continuum limit, this small length scale ϵ' can also be given in dimensionless form as

$$\epsilon \equiv \epsilon' / (\xi' / \omega) = \pi \sqrt{\frac{\eta}{\alpha}}, \tag{56}$$

where $\eta \equiv \eta' / (\xi'^2 / \omega)$ is the dimensionless viscosity coefficient. The dimensionless distance r between the blocks i and i' is measured by

$$r = d|i - i'|, \tag{57}$$

where $d \equiv d' / (\xi' / \omega)$ is the dimensionless grid spacing. The continuum limit corresponds to taking the limit $d \to 0$ with fixed $L = Nd$ and r, which means $N \to \infty$ and $l \to \infty$. Thus, taking the continuum limit in the BK model corresponds to making the model infinitely rigid, $l \to \infty$. Numerically, various observables were calculated with successively smaller d to examine its asymptotic $d \to 0$ limit.

Shaw showed, by adding the viscosity term to the 1D BK model, that the magnitude distribution becomes independent of the grid spacing d' for sufficiently small d' (Shaw, 1994). Mori and Kawamura studied the 1D BK model with successively smaller grid spacings d' to examine how various statistical properties of the model changed and approached the continuum limit for both cases of nonzero ($\eta > 0$) and zero ($\eta = 0$) viscosity (Mori and Kawamura, 2008c). It was then observed that, in the viscous case, the results converged to the continuum limit when the condition $d < \epsilon$ was met, whereas, in the nonviscous case, such a convergence was obscure.

As an example, we show in Fig. 18 the convergence of the magnitude distribution function $R(M)$ for $\alpha = 1$ (a) and $\alpha = 3$ (b), in the viscous case ($\eta = 0.02$). For both cases of $\alpha = 1$ and 3, the continuum limit seems to be well reached, i.e., $R(M)$ seems to converge to an asymptotic form for smaller d, except that the minimum magnitude continuously gets lower as the grid spacing d gets smaller. A similar result was reported by Shaw (1994). From Fig. 18(a), one also sees that a nonzero viscosity tends to weaken the GR character of the magnitude distribution somewhat. Such a deviation from the GR law at smaller magnitudes probably originates from the fact that the viscosity tends to make the relative displacement of neighboring blocks smoother, enhancing the correlated motion of neighboring blocks, which considerably reduces the frequency of smaller events of one or a few blocks (Mori and Kawamura, 2008c).

The small length-cutoff scale ϵ as given by Eq. (56) is estimated here to be $\epsilon \simeq 0.44$ and 0.26 for $\alpha = 1$ and 3, respectively. As can be seen from Figs. 18(a) and 18(b), $R(M)$ converges to an asymptotic form for d values smaller than $d \simeq 1/4$ and 1/8 for $\alpha = 1$ and 3, respectively, which is consistent with the expected condition of the continuum limit $d < \epsilon$.

As mentioned in Sec. III.A.3, the BK model generally gives rise to a seismic quiescence phenomenon prior to mainshock, i.e., the Mogi doughnut. Then, a natural question
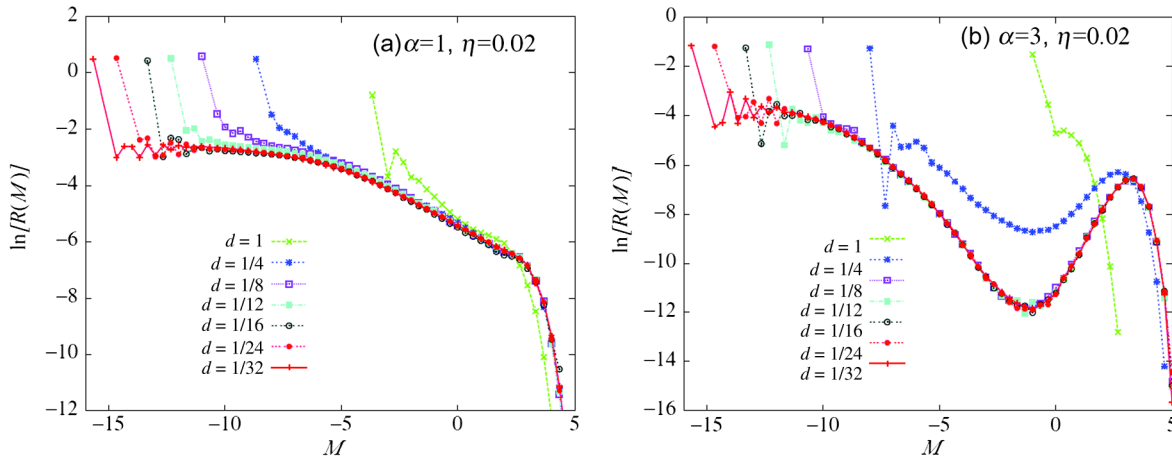
FIG. 18 (color online). The magnitude distribution $R(M)$ of earthquake events of the 1D viscous BK model ($\eta = 0.02$) with $\delta = 0.01$. The dimensionless grid spacing d is varied in the range $1 \geq d \geq 1/32$. (a) and (b) represent the cases of $\alpha = 1$ and 3, respectively. The system size is $L = dN = 200$. From Mori and Kawamura, 2008c.

is whether the doughnutlike quiescence observed in the discrete BK model survives the continuum limit, or it is a phenomenon intrinsically originating from the short cutoff-length scale of the model. This question was addressed by Mori and Kawamura (2008c). Figure 19 exhibits the time-dependent spatial correlation functions before the mainshock in the case of the viscous model with $\alpha = 1$. As the grid spacing d gets smaller, the spatial range of the quiescence gets narrower, tending to vanish for small enough d; see the inset of Fig. 19. This observation strongly suggests that the doughnutlike quiescence might vanish altogether in the continuum limit $d \rightarrow 0$. Thus, the doughnutlike quiescence observed in the discrete BK model is likely to be a phenomenon

closely related to the short length-cutoff scale of the model. This seems fully consistent with the observation that the one-block events are responsible for the observed doughnutlike quiescence (Mori and Kawamura, 2006; 2008a).

The observation might have some implications to real seismicity. While the real crust is obviously a continuum, it is often not very uniform, and possibly has a short-length cutoff. In any case, in real earthquakes the Mogi doughnut is occasionally reported to occur (Mogi, 1969; 1979; Scholz, 2002), although establishing its statistical significance is sometimes not easy. Thus, our present result may suggest that, if the real crust possesses a cutoff length scale due to the inhomogeneity of the crust, the ''Mogi doughnut'' quiescence might occur at such a length scale. In other words, spatial inhomogeneity might be an essential ingredient for the Mogi doughnut to occur in real seismicity (Mori and Kawamura, 2008c).
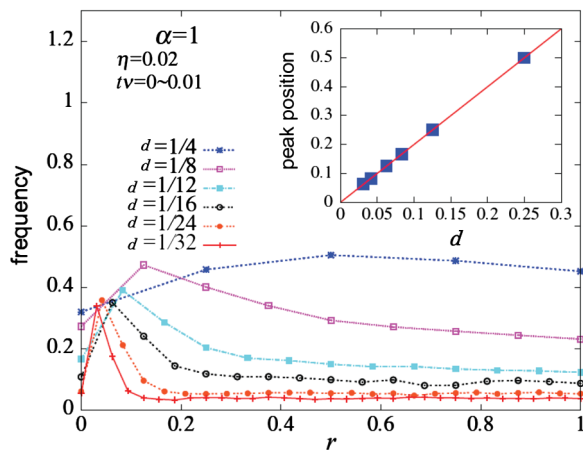
7. The BK model with RSF law

So far, we mostly assumed a simple velocity-weakening friction law where the friction force is a single-valued function of the velocity. As detailed in Sec. II and in III.A.2, the RSF law is now regarded in seismology as the standard constitutive law.

Tse and Rice employed this RSF constitutive relation in their numerical simulations of earthquakes (Tse and Rice, 1986). They studied the stick-slip motion of a two-dimensional strike-slip fault within an elastic continuum theory, assuming that the fault motion is rigid along the strike. It was then observed that large events repeated periodically. Since then, similar RSF constitutive laws have been widely used in numerical simulations (Stuart, 1988; Horowitz and Ruina, 1989; Rice, 1993; Ben-Zion and Rice, 1997; Kato and Hirasawa, 1999a; Kato, 2004; Bizzarri and Cocco, 2006a, 2006b). A somewhat different type of slip-dependent and state-dependent constitutive law has also been used (Cochard and Madariaga, 1996).

Cao and Aki performed a numerical simulation of earthquakes by combining the 1D BK model with a RSF law in

FIG. 19 (color online). The event frequency in the time period $t\nu = 0$–0.01 immediately before the mainshock of $M > M_c = 2$ of the 1D viscous BK model ($\eta = 0.02$) with $\alpha = 1$ plotted vs r, the distance from the epicenter of the upcoming mainshock. The dimensionless grid spacing d is varied in the range $1/4 \geq d \geq 1/32$. The parameter δ is fixed to $\delta = 0.01$. The system size is $L = dN = 200$. The inset represents the peak position of the event frequency, corresponding to the range of the doughnutlike quiescence, as a function of the dimensionless grid spacing d. The doughnutlike quiescence vanishes in the continuum limit $d \rightarrow 0$. From Mori and Kawamura, 2008c.

which various constitutive parameters were set nonuniformly over blocks (Cao and Aki, 1986). Ohmura and Kawamura extended an earlier calculation by Cao and Aki to study the statistical properties of the 1D BK model combined with RSF constitutive law with uniform constitutive parameters (Ohmura and Kawamura, 2007). Clancy and Corcoran also performed a numerical simulation of the 1D BK model based on a modified version of the RSF law (Clancy and Corcoran, 2009).

Rice and collaborators argued that the slip complexity of the BK model might be caused by its intrinsic discreteness (Rice, 1993; Ben-Zion and Rice, 1997). In this context, it is important to clarify the statistical properties of the model where the discrete BK structure is combined with the RSF law, to compare its statistical properties with those of the standard BK model with the velocity-weakening or slip-weakening friction law reviewed in the previous sections.

A recent study by Morimoto and Kawamura revealed that the model exhibits very different behaviors depending on whether the frictional instability is "strong" or "weak" (Morimoto and Kawamura, 2011). The condition of strong or weak frictional instability is given by $b > 2l^2 + 1$ or $b < 2l^2 + 1$, respectively, for the 1D BK model. In the case of a weaker frictional instability, the model exhibits a *precursory process* where a slow nucleation process occurs prior to the mainshock. In the next section, we discuss such a precursory process realized in the BK model in more detail. Interestingly, the presence or absence of such a nucleation process also affects statistical properties of the model. From a simulation point of view, the case of a weaker friction instability is much harder to deal with, since a slow and long-standing nucleation process prior to the mainshock generally requires a lot of CPU time.

The statistical properties of the 1D BK model with the RSF law Eq. (47) [or Eq. (49)] and Eq. (48) were investigated by Ohmura and Kawamura for the case of a strong frictional instability (Ohmura and Kawamura, 2007), and by Yamamoto and Kawamura for the case of a weak frictional instability (Yamamoto and Kawamura, 2011). Typical behaviors of the magnitude distribution are, respectively, shown in Figs. 20(a) and 20(b). As can be seen from the figure, when the frictional instability is strong, an almost flat distribution spanning from small to large magnitudes is realized, while, as the critical value is approached, the peak at larger magnitude becomes more pronounced, giving rise to an enhanced characteristic behavior. In the weak frictional instability regime, the distribution has no weight at smaller magnitudes, with a pronounced peak only at a large magnitude. This means that only large earthquakes of more or less similar magnitude occur in the regime of a weak frictional instability.

The statistical properties of the corresponding 2D model were investigated by Kakui and Kawamura for both cases of weak and strong frictional instabilities (Kakui and Kawamura, 2011). In the 2D BK model, the condition of strong or weak frictional instability is given by $b > 4l^2 + 1$ or $b < 4l^2 + 1$, respectively. Typical behaviors of the magnitude distribution are shown in Figs. 21(a) and 21(b) for the cases of strong and weak instabilities, respectively. As can be seen from the figure, when the frictional instability is strong, a behavior more or less close to the GR law, characterized by an
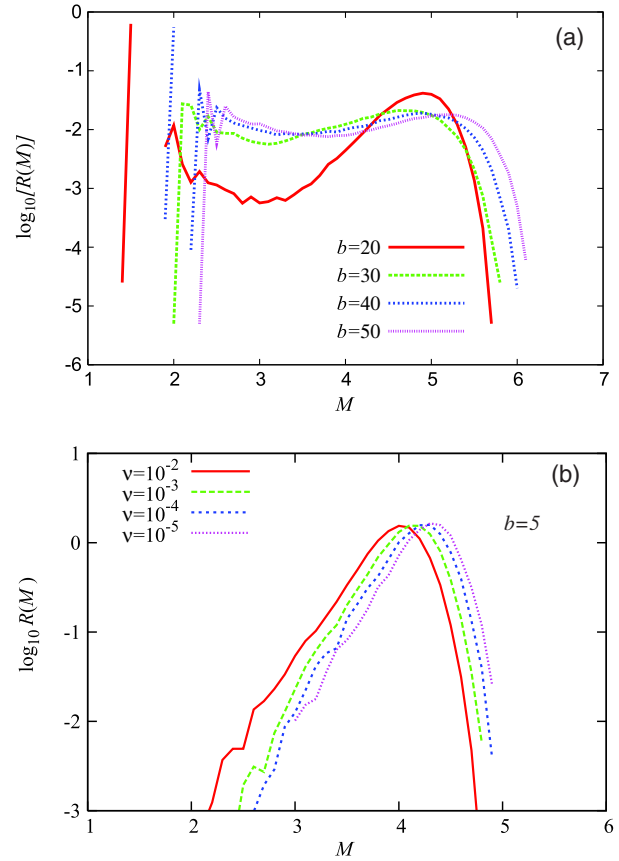

FIG. 20 (color online). The magnitude distribution of the 1D BK model with the RSF law, for the cases of (a) a strong frictional instability $b > b_c$ and (b) a weak frictional instability $b < b_c$, with $b_c = 2l^2 + 1$. The parameter values are $a = 0$, $c = 1000$, $\nu = 10^{-8}$, $v^* = 1$, and $l = 3$ in (a) and $a = 1$, $b = 5$, $c = 1000$, $v^* = 1$, and $l = 5$ in (b). The borderline b value is $b_c = 19$ in (a) and $b_c = 51$ in (b). The system size is $N = 800$ in (a) and $N = 1200$ in (b). (a) From Ohmura and Kawamura, 2007. (b) From Morimoto and Kawamura, 2011.

exponent close to $B \sim 2/3$, is realized, although there is a weak shoulderlike structure superimposed at larger magnitudes. The observation of a near-critical behavior close to the GR law would be of much interest in conjunction with real seismicity. As the critical value is approached, on the other hand, the peak at larger magnitude is further developed, giving rise to an enhanced characteristic behavior. In the weak frictional instability regime, the distribution has double peaks, exhibiting more characteristic behavior; see Fig. 21(b).

8. Nucleation process of the BK model

In this section, we touch upon the nucleation process as a precursory phenomenon prior to the mainshock as realized in the BK model obeying the RSF law. It was observed that the nucleation process is realized even in the BK model with the RSF law for both cases of 1D and 2D, if the model lies in the regime of a weak frictional instability (Morimoto and Kawamura, 2011; Kakui and Kawamura, 2011). Namely, prior to seismic rupture, the system exhibits a slow rupture process localized to a compact seed area with its rupture velocity orders of magnitude smaller than the seismic-wave
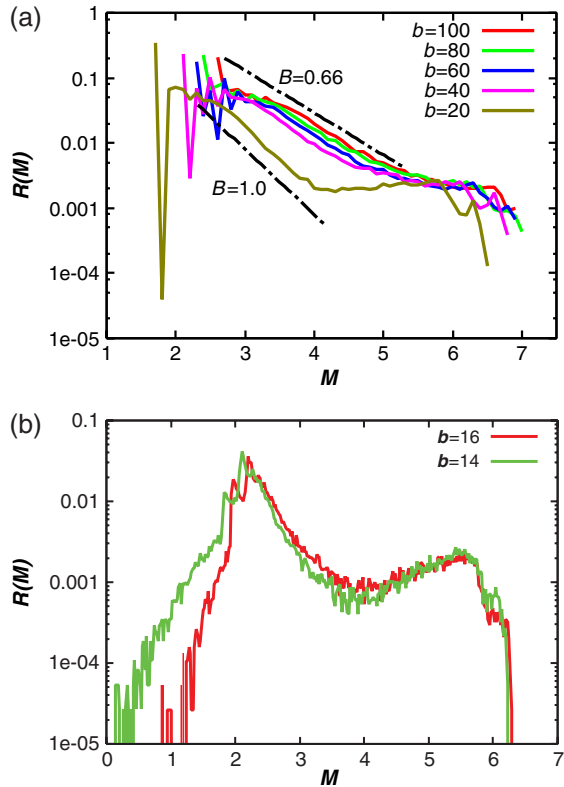
FIG. 21 (color online). The magnitude distribution of the 2D BK model with the RSF law, for the case of (a) a strong frictional instability $b > b_c$, and of (b) a weak frictional instability $b < b_c$, with $b_c = 4l^2 + 1$. The parameter values are $a = 1$, $c = 1000$, $\nu = 10^{-8}$, $\nu^* = 1$, and $l = 2$ in (a), and $a = 1$, $c = 1000$, $\nu = 10^{-8}$, $\nu^* = 1$, and $l = 2$ in (b). The borderline value is $b_c = 17$ in both (a) and (b). The system size is $N = 60 \times 60$ in (a), and $N = 30 \times 30$ in (b). From Kakui and Kawamura, 2011.

velocity. The system spends a very long time in this nucleation process, and then, at some stage, exhibits a rapid acceleration process accompanied by a rapid growth of the rupture velocity and a rapid expansion of the rupture zone, finally getting into the final seismic rupture or a mainshock (Dieterich, 2009). Such a nucleation process has also been observed and extensively studied in the continuum model; see, e.g., Ampuero and Rubin (2008). We illustrate in Fig. 22 a typical example of seismic events realized in the 1D BK model with the RSF law for each case of a weak frictional instability (b) and of a strong frictional instability (a). As can be seen from the figure, a slow nucleation process with a long duration time is observed only in (b), while such a nucleation process is absent in (a).

As mentioned, the condition for the appearance of such a nucleation process is given by $b < b_c = 2l^2 + 1$ in 1D and by $b < b_c = 4l^2 + 1$ in 2D (for a square array of blocks). Indeed, Morimoto and Kawamura found that the critical nucleation size at which the slow nucleation process ends and the acceleration stage begins is given by $X_c = \pi\{\arccos[1 - (b - 1)/2l^2]\} - 1$ in units of block size (Morimoto and Kawamura, 2011). Indeed, this length X_c corresponds in its physical meaning to the length h^* of Rice (1993), although its detailed functional form, e.g., the dependence on b, is somewhat different from the standard
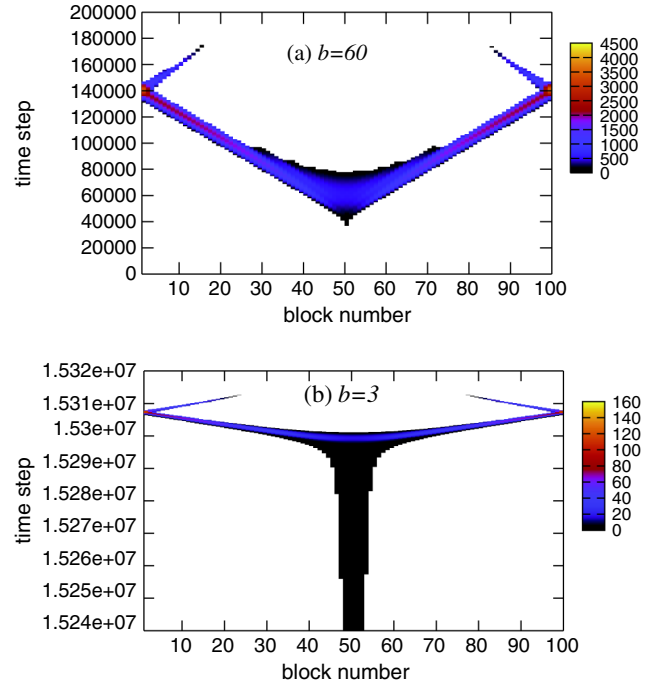

FIG. 22 (color online). The typical rupture process realized in the 1D BK model with the RSF law for (a) a strong and (b) a weak frictional instability, corresponding to (a) $b > b_c$ and (b) $b < b_c$ with $b_c = 2l^2 + 1$. The color represents the rupture velocity. The parameter values are $a = 1$, $c = 1000$, $\nu = 10^{-2}$, $\nu^* = 1$, and $l = 5$ for both (a) and (b), corresponding to $b_c = 51$, whereas $b = 60$ in (a) and $b = 3$ in (b). From Morimoto and Kawamura, 2011.

one. The condition of this critical nucleation size being greater than the block size, $X_c > 1$, yields the condition of weak frictional instability $b < b_c$. In other words, when $b > b_c$, the nucleation process cannot be realized in the BK model due to its intrinsic discreteness. Indeed, this is exactly the situation discussed by Rice (1993).

This observation means that, if one takes the continuum limit of the BK model with the RSF law, the system should necessarily lie in the limit of a weak frictional instability, since the continuum limit means $l \to \infty$. Hence, at least as long as one considers a uniform fault obeying the RSF law without any discretization short length scale, earthquakes should exhibit characteristic properties rather than critical properties. This fully corroborates an earlier criticism by Rice against the SOC view of earthquakes based on the BK model (Rice, 1993). Indeed, in seismology the concept of earthquake cycles has been used in long-term probabilistic earthquake forecasts (Scholz, 2002; Nishenko and Buland, 1987; Working Group on California Earthquake Probabilities, 1995). Of course, a big issue to understand is what is then the true origin of the GR law, which is widely observed in real seismicity.

B. Continuum models

As discussed in Sec. III.A.6, Rice (1993) criticized inherently discrete models, where simulated earthquake sequences depend on the computation grid size. He confirmed in numerical simulations that complex earthquake sequences

disappear when the grid size is sufficiently smaller than the critical size of the slip nucleation zone for almost spatially uniform frictional properties. Moreover, he argued that geometrical and/or material disorder is the origin of complexity of earthquakes. The models with sufficiently small grid sizes may be called continuum models, which generate simulation results independent of the grid size, in contrast to inherently discrete models. Note that if a model does not have a finite critical size for nucleating unstable slip, such as a model with constant static and dynamic friction, it is always inherently discrete. In this section, we discuss continuum models of earthquakes, especially models using the rate- and state-dependent friction law. In the RSF law, the critical size of slip nucleation can be defined as a function of frictional constitutive parameters, and the computation grid sizes are sufficiently smaller than the critical size in the studies mentioned below. We use elastic continuum models below, in contrast to spring-block models in the previous section. The "continuum model" is thus used in two senses.

The RSF law has commonly been used in models for understanding earthquake phenomena (Scholz, 2002; Dieterich, 2009). These models were sometimes constructed for reproducing and understanding particular earthquakes, earthquake cycles, or sliding processes observed by seismometers, strainmeters, global positioning systems (GPS), etc. We will see deterministic aspects of earthquake phenomena, in addition to statistical characteristics of earthquakes. Note that comprehensive reviews were presented by Ben-Zion (2008), Rundle *et al.* (2003), and Turcotte, Shcherbakov, and Rundle (2009) for models of statistical properties of earthquakes using friction laws other than the RSF law.

1. Earthquake cycles, asperities, and aseismic sliding

Before introducing earthquake models, we briefly review observational facts about earthquakes and fault slip behavior. Earthquakes repeatedly occur at the same fault segment. At the Parkfield segment along the San Andreas fault, California, interplate earthquakes of magnitude about 6 have occurred at recurrence intervals of 23 ± 9 yr since 1857 (Sykes and Menke, 2006). Great earthquakes of magnitude 8 have repeatedly occurred along the Nankai trough, where the Philippine Sea plate subducts beneath southwestern Japan, every 100 years (Sykes and Menke, 2006). Quasiperiodic earthquake recurrence has been used for long-term forecasts of earthquakes (Working Group on California Earthquake Probabilities, 1995; Matthews, Ellsworth, and Reasenberg, 2002). One of the most remarkable examples of regularity of earthquakes was found off Kamaishi, where the Pacific plate subducts beneath northern Honshu, Japan. Earthquakes of magnitude of 4.8 ± 0.1 have repeatedly occurred at recurrence intervals of 5.5 ± 0.7 yr in the same region since 1957. Okada, Matsuzawa, and Hasegawa (2003) estimated coseismic slip distributions of recent Kamaishi earthquakes from seismic waveform data and found that they overlap with each other (Fig. 23). Although many smaller earthquakes occur around the source area of the Kamaishi earthquakes, no comparable or larger earthquakes occur there. This observation suggests that aseismic sliding surrounds the source area of the Kamaishi earthquakes, where stick-slip motion occurs, and steady loading by the surrounding aseismic sliding to the
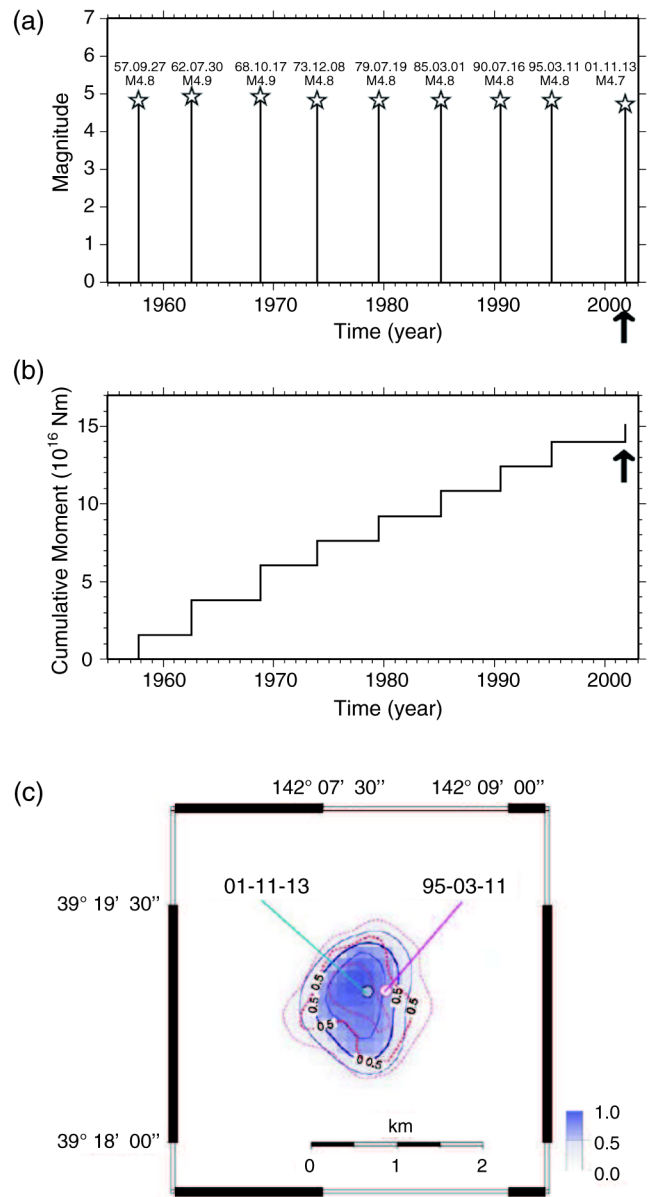

FIG. 23 (color online). (a) Recurrence of Kamaishi earthquakes of nearly the same magnitudes and recurrence intervals. (b) Cumulative seismic moment of Kamaishi earthquakes. (c) Coseismic slip distribution of the 1995 and 2001 Kamaishi earthquakes estimated from seismic waveforms. Broken contours and blue contours denote the seismic slip of the 1995 and 2001 earthquakes, respectively. From Okada, Matsuzawa, and Hasegawa, 2003.

source area leads to the quasiperiodic recurrence of earthquakes of almost the same magnitude. It has been suggested that the variance in the recurrence interval came from temporal variation of the aseismic sliding rate surrounding the earthquake source (Uchida *et al.*, 2005). The significant afterslip of the 2011 great Tohoku-oki earthquake ($M = 9.0$) rapidly loaded the source area of the Kamaishi earthquake, generating earthquakes at much shorter recurrence intervals. Recurrences of small earthquakes in the same source areas in mainly creeping (aseismic sliding) regions have been found in many places and these earthquakes are

called small repeating earthquakes (Nadeau and Johnson, 1998; Igarashi, Matsuzawa, and Hasegawa, 2003). Although small earthquakes occur, most strain is released by aseismic sliding on these fault planes. The seismic coupling coefficient is defined by the long-term average of the ratio of seismic slip to total (seismic and aseismic) slip expected from relative plate motion. The seismic coupling coefficient is variable, dependent on the locality. It is close to unity at some segments in Chile and the Aleutians, indicating little aseismic sliding and nearly complete locking during interseismic periods, and is nearly equal to zero in the Marianas, indicating no or few large interplate earthquakes (Pacheco, Sykes, and Scholz 1993). These facts show that aseismic sliding is a common phenomenon and plays an important part in strain release at plate boundaries and that frictional properties differ from place to place.

A patch where stick-slip motion occurs, that is, a fault region where earthquakes repeatedly occur, is often called an asperity, from the rock mechanics term for a contact spot between sliding surfaces as used in Sec. II.D. Note that an asperity of an earthquake occupies a considerable part of the earthquake fault area and its size is orders of magnitude larger than the amount of seismic slip. In contrast, an asperity of a sliding surface is much smaller and its size may be comparable to the slip amount. The asperity model has been developed for explaining spatial heterogeneity in seismic slip on faults and complex source processes of earthquakes (Kanamori and McNally, 1982; Lay, Kanamori, and Ruff, 1982; Thatcher, 1990). When the asperity model was developed around 1980, sliding behavior surrounding asperities had not been clarified from observations because aseismic sliding cannot be detected by seismometers. To detect aseismic sliding, geodetic observations as by GPSs are required. Since dense GPS networks were established in the 1990s (Segall and Davis, 1997), many aseismic sliding phenomena have been reported, such as afterslip (postseismic sliding) and slow (silent) earthquakes. The source areas of afterslip are usually located near coseismic slip areas (asperities), and the afterslip area and the asperity do not overlap, as shown in Fig. 24 (Yagi, Kikuchi, and Nishimura, 2003; Miyazaki *et al.*, 2004; Johnson, Bürgmann, and Larson, 2006), which also supports spatial heterogeneity of frictional properties. It was confirmed that locations of asperities of large earthquakes are locked during interseismic periods from geodetic observations (Chlieh *et al.*, 2008; Hashimoto *et al.*, 2009; Perfettini *et al.*, 2010). For instance, Fig. 25 clearly shows that the seismic slip areas of large interplate earthquakes off the island of Sumatra coincide with the locked areas during interseismic periods. For the 2011 great Tohoku-oki earthquake (*M* = 9.0), a significant peak of seismic slip larger than 30 m was estimated from inversions of seismic waveform and tsunami data (Koketsu *et al.*, 2011). This also suggests nonuniform friction on the plate interface.

The spatial distribution of asperities on plate boundaries has been estimated from source areas of past large interplate earthquakes, and earthquakes repeatedly occurred on the same asperities (Yamanaka and Kikuchi, 2004). This suggest that the locations of asperities are unchanged for at least a few earthquake cycles. Apparently complex earthquake cycles, where earthquake rupture areas are variable, may be
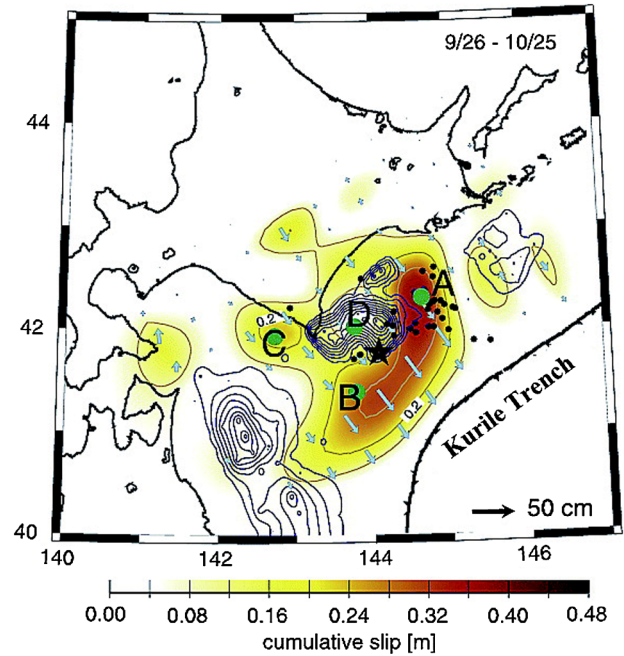

FIG. 24 (color online). Spatial distribution of cumulative slip for 30 days of afterslip of the 2003 Tokachi-oki earthquake (*M* = 8.0), off Hokkaido, northern Japan, estimated from GPS data (color contours) by Miyazaki *et al.* (2004). Black contours with an 0.5 m interval show seismic slip in the 1973 Nemuro-oki (right), 1968 Tokachi-oki (left), and 2003 Tokachi-oki (center) earthquakes (Yamanaka and Kikuchi, 2004). The black star and small circles denote the epicenter and aftershocks of the 2003 earthquake.

understood by a change in the combination of simultaneously ruptured asperities. For example, two adjacent asperities are simultaneously ruptured, resulting in a large earthquake in some cases, and one of them is ruptured to generate a smaller event in other cases. Note that some researchers do not accept persistent asperities, on the basis of seismic waveform analyses (Park and Mori, 2007).

2. Models for nonuniform fault slip using the RSF law

The asperity model indicates that spatial heterogeneity of material properties is important, and it is compatible with the RSF law discussed in Sec. II.D. Regions of velocity-weakening friction ($a - b < 0$) correspond to asperities, where stick-slip occurs, and aseismic sliding occurs at regions of velocity-strengthening friction ($a - b > 0$). Afterslip occurs in velocity-strengthening areas, and it slowly relaxes the stress increases generated by nearby earthquakes. Using a single-degree-of-freedom spring-block model, Marone, Scholtz, and Bilham (1991) obtained a theoretical slip time function $u(t)$ for afterslip, occurring on a fault with velocity-strengthening friction ($a - b > 0$), as follows:

$$u(t) = \frac{(a - b)\sigma_n}{k} \ln\left[\frac{kV_{cs}}{(a - b)\sigma_n} t + 1\right] + V_0 t, \qquad (58)$$

where σ_n is the normal stress on the fault plane, k is the spring stiffness, V_{cs} is the coseismic slip velocity, V_0 is the preseismic slip rate, and the time t is measured from the earthquake occurrence time. A quantitative comparison
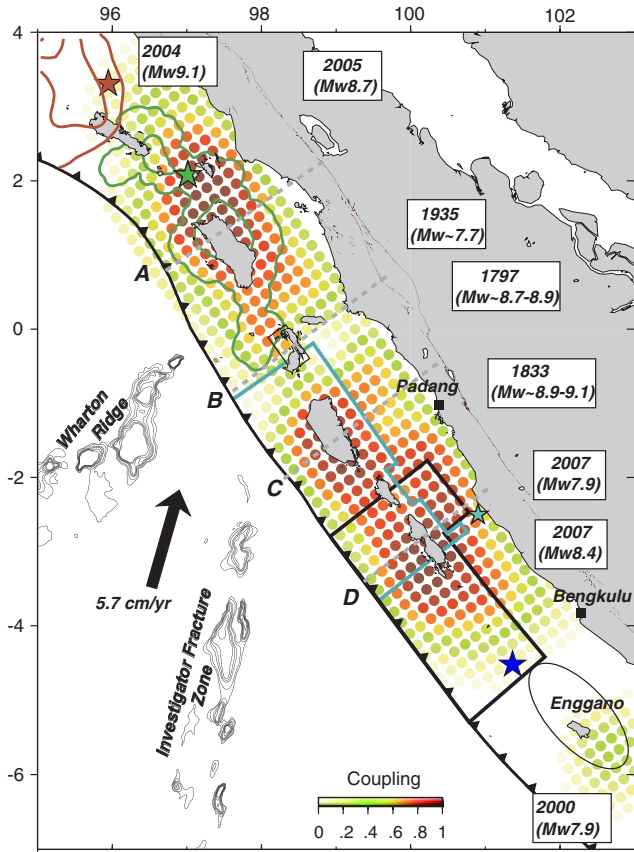
FIG. 25 (color online).   Spatial distribution of interplate coupling estimated from geodetic data (colored circles) along the Sunda trench, where the Australian plate subducts beneath the island of Sumatra. Dark circles indicate that the plate interface is nearly locked and strain is accumulated during an interseismic period, and light circles indicate that continuous aseismic sliding occurs and strain is not accumulated. Contours with a 5 m interval show seismic slip in the 2004 Sumatra-Andaman ($M = 9.1$) and the 2005 Nias-Simeulue ($M = 8.7$) earthquakes. Lines show the approximate source are as of the 1797 and 1833 great earthquakes. From Chlieh *et al.*, 2008.

between afterslip observations and models indicates that the RSF law well explains afterslip (Perfettini and Avouac, 2004; Freed, 2007).

When the stiffness is larger than the critical stiffness defined by Eq. (22) for a velocity-weakening fault, it is called conditionally stable (Scholz, 1998). Although aseismic sliding usually occurs under quasistatic loading for a conditionally stable case, rapid stress increase may generate seismic slip (Gu *et al.*, 1984). This fact indicates that sliding behavior at a fault is not determined only by the fault properties but by a loading condition, suggestive of variable sliding behavior of a fault. Note that the effective stiffness of a fault may be related to fault size as will be shown in the next section.

Since the RSF law takes into consideration a time-dependent healing process, it can be used in simulations of earthquake cycles. Tse and Rice (1986) first published an earthquake cycle model for a strike-slip fault in an elastic continuum using the RSF law to successfully explain stick-slip behavior at a shallower part of a fault, continuous stable sliding at a deeper part, and afterslip at intermediate depths. In the simulation, the quasidynamic equilibrium between frictional stress and elastic stress generated by fault slip and relative plate motion is numerically solved. The assumption of Tse and Rice of a depth dependence of $a - b$ is consistent with laboratory data, which indicate that $a - b$ changes from negative to positive at about 300° C (Blanpied, Lockner, and Byerlee, 1995). Similar models have been presented for earthquake cycles in particular regions to compare the simulations with observed earthquake recurrence and/or crustal deformation. Figure 26 shows an example simulation result of spatiotemporal evolution of the slip velocity on a model plate interface, where great interplate earthquakes repeatedly occur at a shallower part and stable sliding at a deeper part (Hori *et al.*, 2004).

If a single asperity exists on a fault plane without any interactions with other asperities, regular stick-slip at a constant recurrence interval is expected to occur. Note that when the asperity size is close to the critical nucleation zone size, an irregular stick-slip cycle is observed even for a single-asperity model (Liu and Rice, 2007). When some asperities exist close together, they interact with each other, resulting

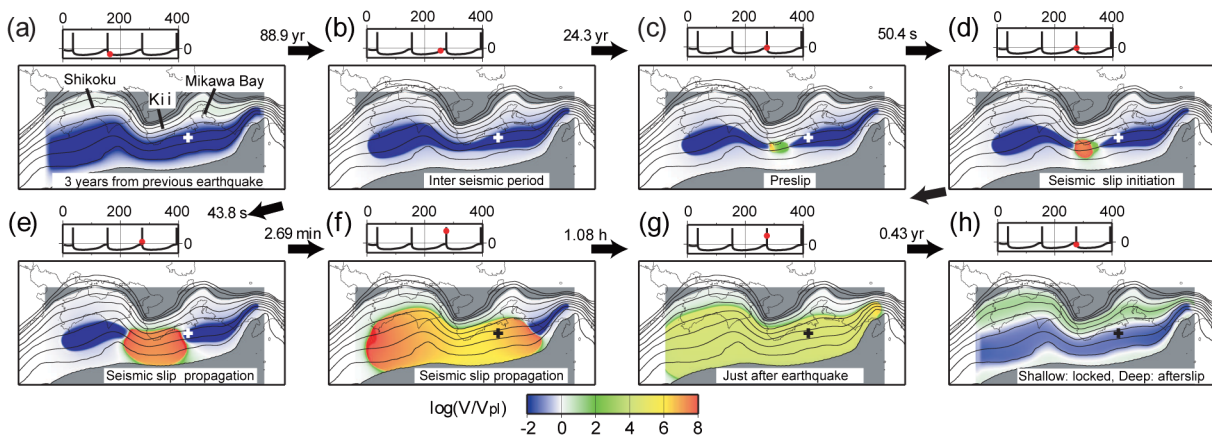FIG. 26 (color online).   Snapshots of simulated slip rate V on the model plate interface normalized by the relative plate velocity V_{pl} in a model for recurrence of great earthquakes along the Nankai trough, central Japan. Different colors show seismic slip rates, stable sliding with sliding velocity nearly equal to the plate velocity, and nearly locked, respectively. Adapted from Hori *et al.*, 2004.

in complex earthquake sequences including single- and multiple-asperity ruptures. Numerical simulations of complex earthquake sequences due to interactions between some asperities have been carried out by Kato and Hirasawa (1999b), Kato (2004), Lapusta and Liu (2009), and Kaneko, Avouac, and Lapusta (2010). In these studies, friction obeying the RSF law was assumed and different values of friction parameters (a', b', $\mathcal{L}$) are assigned for model asperities with velocity-weakening friction, to reproduce compound earthquakes, where some asperities are ruptured simultaneously or with some time delays, which resembles some observations. Kato (2008), for instance, reproduced a complex earthquake cycle similar to that observed in the Sanriku-oki region, northeastern Japan, where simulated earthquakes included the 1968 Tokachi-oki earthquake ($M = 8.2$) and the 1994 Sanriku-oki earthquake ($M = 7.7$) and its largest aftershock ($M = 6.9$) and afterslip. These studies suggest that spatial distribution of asperities or friction parameters controls the regularity and complexity of earthquake recurrence. This further suggests that numerical forecasts of earthquakes may be possible if we can obtain a detailed map of friction parameters on a fault. Friction parameters have actually been estimated through comparison of observed data and simulations in California (Johnson, Brgmann, and Larson, 2006) and Japan (Miyazaki *et al.*, 2004; Fukuda *et al.*, 2009) from afterslip data.

Preseismic sliding, which is aseismic sliding during a slip nucleation process, is expected from the RSF law before earthquake occurrence. It is almost ubiquitously observed in laboratory experiments, where the amount of preseismic sliding is of the order of micrometers (Ohnaka and Shen, 1999). Using a spring-block system implemented with the RSF law, one can show that the preseismic sliding amount is approximately given by $\mathcal{L}$ (Popov *et al.*, 2012). Some model studies with the RSF law discussed the crustal deformation expected from preseismic sliding for particular earthquakes (Stuart and Tullis, 1995; Kuroki, Ito, and Yoshida, 2002). However, it is difficult to predict precise amplitudes of crustal deformation, because friction parameters that influence preseismic sliding are not well constrained by the presently available data. There are some reports of observations of preseismic sliding, although insignificant or questionable observations are included (Wyss, 1997). For example, close and dense geodetic observations of the Parkfield segment of the San Andreas fault could not detect any precursory slip prior to the 2004 earthquake, although it should be remarked that observation of the tremor may suggest accelerated creep on the fault $\sim$16 km beneath the eventual earthquake hypocenter (Shelly, 2009). Kanamori and Cipar (1974) detected precursory signals in long-period strain seismograms before the occurrence of the 1960 great Chilean earthquake ($M = 9.5$). Since no earthquake that could explain the observed strain signals was detected, they inferred that the signals were caused by preseismic sliding on a deeper extension of the mainshock fault plane. Linde and Sacks (2002) examined crustal deformation data before the occurrence of the 1944 Tonankai ($M = 8.0$) and 1946 Nankai ($M = 8.1$) earthquakes, southwestern Japan, to construct a model for preseismic sliding of these earthquakes. Their model indicates that preseismic sliding took place at a deeper extension

of the mainshock fault plane. However, in models with the common RSF law, accelerating preseismic sliding just before the earthquake occurrence takes place within the source area of seismic slip because spontaneous accelerating slip can be nucleated only in the velocity-weakening region, being inconsistent with these models of preseismic sliding. Kato (2003a) proposed a model for earthquake cycles at a subduction zone to explain large preseismic sliding at deeper extensions of the seismogenic plate interface. He assumed velocity-weakening friction ($d\mu_{ss}/d\ln V < 0$) at low velocities and velocity-strengthening friction ($d\mu_{ss}/d\ln V > 0$) at high velocities, where μ_{ss} is the steady-state friction coefficient given by Eq. (19). Preseismic sliding relaxes regional stresses, which may decrease seismic activity, while it increases stresses around the edges of the slipped region, which tends to increase seismic activity (Kato, Ohatake, and Hirasawa, 1997). This may explain precursory seismic quiescence observed for some large earthquakes (Kanamori, 1981; Wyss, Klein, and Johnston, 1981). Preseismic sliding perturbs the regional stress field, resulting in an increase or decrease of seismicity. Taking this effect into consideration, Ogata (2005) systematically researched seismicity changes in Japan to find possible crustal stress changes due to preseismic sliding.

3. Slow earthquakes

Slow earthquakes are episodic fault slip events that generate few or no seismic waves because their source durations are longer than the periods of observable seismic waves. Slip events without seismic wave radiation are often called silent earthquakes or slow slip events. Slow earthquakes have been studied by using records of very-long-period seismographs (Kanamori and Stewart, 1979), creepmeters that directly detect fault creep at the ground surface (King, Nason, and Tocher, 1973), and strainmeters (Linde *et al.*, 1996). Afterslip and the preseismic sliding mentioned earlier may be included in slow earthquakes.

Recent development of dense geodetic observation networks including GPS networks and borehole tiltmeters has accelerated studies of slow earthquakes (Schwartz and Rokosky, 2007). Hirose *et al.* (1999) found from GPS data that episodic aseismic slip with duration of about 300 days took place in 1997 on the plate boundary in the Hyuganada region, southwestern Japan. The estimated slip and source area indicated that it released a seismic moment corresponding to a magnitude of 6.6. Later, almost the same-size aseismic slip events occurred at the same area in 2003 and 2010. In the Tokai region, central Japan, another large slow earthquake from 2000 to 2005 released a seismic moment nearly equal to that of an $M = 7.0$ earthquake (Ozawa *et al.*, 2002; Miyazaki *et al.*, 2006). The source area of this slow earthquake was estimated to be at the deeper extension of the locked plate boundary, where a magnitude-8 interplate earthquake is expected to occur. In almost the same area, smaller slow earthquakes, corresponding to moment magnitudes of about 6.0, with shorter durations of a few days, were found to occur repeatedly (Hirose and Obara, 2006). These slow earthquakes are often called short-term slow-slip events (SSEs), to be discriminated from long-term SSEs of durations of several months or longer. Furthermore, Hirose and Obara (2006) found low-frequency tremors, which radiate seismic

waves with long durations, from high-sensitivity borehole seismometer array data. These events are clearly distinguished from long durations of wave trains and lack of high-frequency components of seismic waves. Short-term SSEs and low-frequency tremors occur simultaneously in almost the same locations. Synchronized occurrence of short-term SSEs and low-frequency tremors were observed in other regions such as the Cascadia subduction zone, North America (Rogers and Dragert, 2003), and Shikoku, southwestern Japan (Obara *et al.*, 2004).

These findings of slow earthquakes and low-frequency tremors force us to reconsider the simple view of earthquakes as brittle fracture. Many mechanical models for slow earthquakes has been proposed. Since both seismic and aseismic slips can be easily modeled with the RSF law, it is natural to consider that slow earthquakes can be modeled with the RSF law. In fact, sustaining aseismic oscillation, similar to the recurrence of slow earthquakes, occurs in a single-degree-of-freedom spring-block model if the spring stiffness k is equal to the critical stiffness k_{crit} given by Eq. (22) (Ruina, 1983). Using a more realistic elastic continuum model, Kato (2004) showed that slow earthquakes occur when the size of the velocity-weakening region is close to the critical size of the slip nucleation zone. The effective stiffness k_{eff} of a fault may be defined by

$$k_{eff} = \Delta\tau/\Delta u, \qquad (59)$$

where $\Delta\tau$ is the shear-stress change on the fault due to slip Δu (Dieterich, 1986). For a circular fault of radius r with a constant stress drop in an infinite uniform elastic medium with Poission ratio $= 0.25$, k_{eff} is given by

$$k_{eff} = \frac{7\pi}{24}\frac{G}{r}, \qquad (60)$$

where G is the rigidity. Recalling that unstable slip occurs for $k < k_{crt}$ for a spring-block model, unstable slip is expected to occur for $k_{eff} < k_{crt}$ on a fault in an elastic medium. This leads to the condition for occurrence of unstable slip: that the fault radius r is larger than the critical fault size r_c given by

$$r_c = \frac{7\pi}{24}\frac{G}{(b'-a')\sigma_n}\mathcal{L}, \qquad (61)$$

where σ_n is the normal stress. Note that the critical nucleation zone size r_c obtained by considering the stability around steady-state sliding may not be realistic in natural conditions during earthquake cycles. Other forms of critical nucleation zone sizes were obtained by considering more realistic conditions (Dieterich, 1992; Rubin and Ampuero, 2005). It is confirmed in numerical simulations that the usual earthquakes with short slip duration occur for a circular fault with $r > r_c$, continuous stable sliding for $r \ll r_c$, and slow earthquakes for $r \sim r_c$, where slip duration increases with a decrease in r/r_c as shown in Fig. 27 (Kato, 2003b; 2004). The same idea was adopted by Liu and Rice (2007) in their model for slow earthquakes at a subduction zone, where they showed that high pore fluid pressure in the fault zone is required to explain the observed recurrence intervals and slip amounts of slow earthquakes. Although these models are simple and plausible, slow earthquakes may occur under
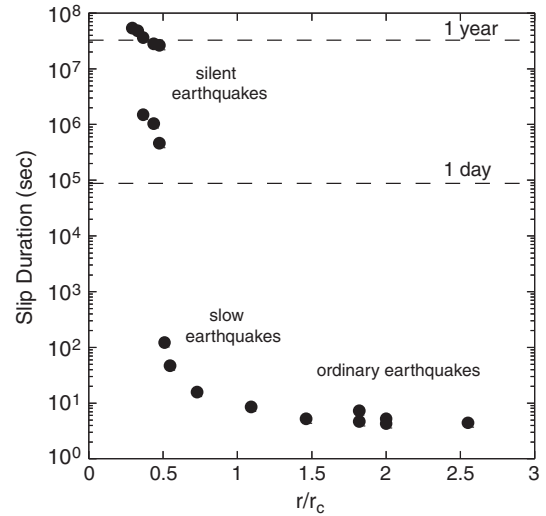

FIG. 27. The duration of slip events vs r/r_c in numerical simulations using the RSF law, where a circular asperity of radius r with velocity-weakening friction is embedded in a fault of velocity-strengthening friction. r_c denotes the critical fault radius for unstable slip defined in the text. From Kato, 2003b.

limited conditions of $r \sim r_c$. This seems to be inconsistent with the observations that slow earthquakes are common phenomena in some regions. Using a two-degree-of-freedom spring-block model, Yoshida and Kato (2003) showed that slow earthquakes may occur under wider conditions by considering the interaction between an unstable block where the usual earthquakes repeatedly occur and a conditionally stable block where slow earthquakes occur. Shibazaki and Iio (2003) and Shibazaki and Shimamoto (2007) introduced a cutoff velocity to the state evolution effect in Eq. (16) to obtain the frictional properties of velocity weakening ($d\mu_{ss}/d\ln V < 0$) at low velocities and of velocity strengthening ($d\mu_{ss}/d\ln V > 0$) at high velocities, which is similar to the model of Kato (2003a) for deep preseismic sliding. Similar complex frictional behavior with $d\mu_{ss}/d\ln V$ depending on velocity was actually observed in the laboratory for halite (Shimamoto, 1986) and for serpentine (Moore *et al.*, 1997). In this case, slip is accelerated at low velocities with $d\mu_{ss}/d\ln V < 0$ and is decelerated at high velocities with $d\mu_{ss}/d\ln V > 0$, leading to slow earthquakes. Repeated slow earthquakes at transition depths from a shallow locked zone to a deeper stable sliding zone were simulated in Shibazaki and Iio (2003) and Shibazaki and Shimamoto (2007). This kind of model was further extended to simulate short and long-term SSEs and their interaction with shallower large interplate earthquakes (Matsuzawa *et al.*, 2010). A weakness of these models is that experimental data for the velocity dependence of $d\mu_{ss}/d\ln V$ are insufficient, and frictional properties at depths where slow earthquakes occur are unknown. Rubin (2008) reviewed models for slow earthquakes based on the RSF law and pointed out that the existing models seem to be unable to explain the common occurrence of slow earthquakes at subduction zones. He suggested that variation of pore-fluid pressure due to inelastic dilation of the fault zone and fluid diffusion is required for generating slow earthquakes.

4. Origin of complexities of earthquakes and aftershock decay law

Rice (1993) claimed that complex earthquake sequences simulated in inherently discrete models may be artifacts and geometrical and/or material heterogeneity is required to explain the observed complexity of earthquakes. Continuum models with relatively homogeneous frictional properties produce simple patterns of earthquakes such as the periodic recurrence of large earthquakes that break the entire seismogenic zone. Using a continuum model with the RSF law, Ben-Zion and Rice (1995) introduced heterogeneity in the effective normal stress on the fault and successfully produced moderately complex earthquake sequences. They pointed out that abrupt change in the effective normal stress is necessary to produce complex earthquakes. Hillers *et al.* (2007) introduced spatial heterogeneity in the characteristic slip distance $\mathcal{L}$ in the model of a vertical strike-slip fault to produce complex earthquake sequences that include a wide range of earthquake magnitudes. The obtained relation between earthquake magnitude and frequency mimics the Gutenberg-Richter law, and the statistical properties of simulated earthquakes depend on the degree of heterogeneity in $\mathcal{L}$. These authors also found temporal clustering of simulated earthquakes and a tendency for nucleation sites of smaller $\mathcal{L}$. Hillers and Miller (2007) introduced spatial variation of pore pressure to generate complex earthquake sequences.

An important fact about the relation between the magnitude and frequency of earthquakes obtained in observations is that the GR law may not always be valid for each individual fault. For some faults and plate boundaries, the number of small earthquakes is fewer than expected from the GR law and the frequency of large earthquakes that rupture the entire fault, indicating violation of the GR law (Stirling, Wesnousky, and Shimazaki, 1996; Ishibe and Shimazaki, 2009). This behavior of fewer small earthquakes than expected from the frequency of large earthquakes is referred to as the characteristic earthquake model. The highly coupled plate interface in the Tokai region, central Japan, is nearly quiescent, while many small earthquakes occur in the overriding plate and subducting oceanic plate (Matsumura, 1997). This suggests that except for great earthquakes, few small earthquakes occur at the plate interface in the Tokai region. Considering large earthquakes along the San Andreas fault, California, and smaller earthquakes at secondary faults around the San Andreas, Turcotte (1997) argued that the observed GR law comes from a fractal distribution of faults and characteristic earthquakes at each fault.

Another important empirical law that demonstrates the complexities of earthquakes is the modified Omori (Omori-Utsu) law for decay in the aftershock occurrence rate (Utsu, Ogata, and Matsuura, 1995). The aftershock rate n at time t from the occurrence of the mainshock is well approximated by

$$n(t) = \frac{K}{(t + T_{\text{MOL}})^p}, \tag{62}$$

where K, T_{MOL}, and p are constants. The constant p is ~1 for many cases. For $T_{\text{MOL}} = 0$, this relation is simply referred to as the Omori law. Aftershocks have been thought to be a manifestation of relaxation of stress generated by the mainshock. To explain the delay times of aftershocks, subcritical cracking due to stress corrosion (Yamashita and Knopoff, 1987) and the variation of effective normal stress due to diffusion of pore fluid, whose pressure is perturbed by the mainshock (Bosl and Nur, 2002), have been invoked. Dieterich (1994) considered the responses of many fault patches, where friction is assumed to obey the RSF law, to instantaneous stress change due to the mainshock. He further assumed that a constant seismicity rate is achieved under a constant loading rate without any stress perturbation. This model successfully explains the power-law decay of the seismicity rate for $p = 1$, which is consistent with observations, and has been applied to analyses of aftershocks of some large earthquakes (Toda *et al.*, 1998). Another important model for aftershocks using the RSF law is related to afterslip. Afterslip perturbs stresses around its source area, causing aftershocks. Differentiating the slip function Eq. (58) of afterslip with respect to time, we have a slip rate approximately proportional to $(t + c)^{-1}$, which may be related to the stress rate and therefore seismicity rate (Perfettini and Avouac, 2004). This expected seismicity rate coincides with the Omori-Utsu formula with $p = 1$. Moreover, afterslip propagates outward from a mainshock slip area, leading to expansion of the aftershock area (Kato, 2007). The aftershock expansion pattern obtained from a numerical model with the RSF law is consistent with observed expansions of aftershock areas (Tajima and Kanamori, 1985; Peng and Zhao, 2009).

5. Earthquake dynamics: Critical slip distance

Here we consider the dynamics of unstable motion. The unstable slip of a spring-block system given by Eq. (21) is accompanied by a drop in the frictional force. If one plots the frictional force as a function of the slip distance (Fig. 28), one can define the distance D_c over which the frictional force drops. This behavior of decreasing frictional force with increasing slip is referred to as the slip-weakening model (Ida, 1972; Andrews, 1976), and the slip distance D_c is called the critical slip distance in seismology. D_c is on the same order of (or at most several tens of) the characteristic length $\mathcal{L}$ in an evolution law (Bizzarri and Cocco, 2003). This is so irrespective of the number of degrees of freedom: discrete or continuum.
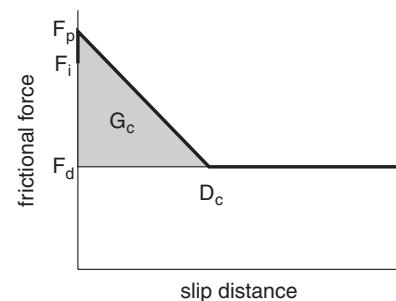

FIG. 28. Schematic diagram of the relation between frictional force and slip distance during the slip-weakening process, where F_i, F_p, F_d, and D_c denote the initial force, the peak frictional force, the dynamic frictional force, and the critical slip distance, respectively. The shaded area indicates the fracture energy G_c.

Importantly, one can estimate D_c of earthquakes by analyzing the seismic wave. Such analyses show that D_c is on the order of several tens of centimeters or a meter (Ide and Takeo, 1997). Note that the fracture energy G_c, which is equal to twice the surface energy density Γ, can rather stably be estimated from seismic waveform data, although accurate estimate of D_c is difficult because of poor resolution of rupture process modeling from seismic waves (Guatteri and Spudish, 2000). The characteristic slip distance $\mathcal{L}$ estimated for afterslip of a large interplate earthquake by GPS data is on the order of millimeters (Fukuda *et al.*, 2009). This makes quite a contrast to laboratory experiments, where $\mathcal{L}$ is typically estimated as several micrometers. Because $\mathcal{L}$ is a typical longitudinal dimension of the true contact patch, application of the RSF law to a natural fault implies that the natural fault also consists of true contact patches, the linear dimension of which is several tens of centimeters. Although the aperture of a fault is not empty but filled with fluid and gouge, a fault generally has nonplaner structure (e.g., jogs) that can interlock to resist displacement. Such jogs may effectively act as the true contact area. However, it is not obvious at all if the RSF law still holds for such true contact area on a macroscopic scale.

At least, we believe that the RSF law should not be used except for very-low speed friction. Namely, the RSF law no longer holds at seismic slip rates due to physical processes caused by frictional heat: flash heating, melting, mechanochemical effects, etc. In such cases, the critical slip distance D_c is proportional to ϵ_c/P, where ϵ_c is the critical energy per unit area for a weakening process (e.g., melting) to occur and P is the normal stress. (As the frictional force is proportional to P, the produced heat is proportional to P and to the slip distance D. Thus, the weakening process may occur if PD is on the order of ϵ_c.) Namely, the critical slip distance is inversely proportional to the normal pressure. This implies that the critical slip distance must be smaller for deeper faults. However, unfortunately, such depth dependence has not been observed so that the mechanism that determines the critical slip distance must be different.

Another important process that affects the critical slip distance is off-fault fracture accompanied by crack propagation on the fault. Andrews (2005) analyzes a model for slip propagation on a fault supplemented with the Coulomb yield condition for off-fault material. He finds that the effective critical slip distance depends on the distance from the crack initiation point. This is because the plastic zone is wider for larger cracks. Thus, the critical slip distance is essentially scale dependent, which is consistent with the observational facts.

IV. EARTHQUAKE MODELS AND STATISTICS II: SOC AND OTHER MODELS

A. Statistical properties of the OFC model

1. The model

In the previous section, we reviewed the properties of statistical physical models of earthquakes such as the spring-block BK model and the continuum model. In the present section, we deal with further simplified statistical

physical models of earthquakes (Turcotte, 1997; Hergarten, 2002; Turcotte, Shcherbakov, and Rundle, 2009). Many of them are coupled-map lattice models originally introduced as SOC models (Bak, Tang, and Wiesenfeld, 1987; Bak and Tang, 1989; Ito and Matsuzaki, 1990, Nakanishi, 1990; Brown, Scholz, and Rundle, 1991; Olami, Feder, and Christensen, 1992; Hainzl, Zöllar, and Kurths, 1999; Hainzl *et al.*, 2000; Hergarten and Neugebauer, 2000; Helmstetter, Hergarten, and Sornette, 2004).

The one introduced by Olami, Feder, and Christensen as a further simplification of the BK model, now called the OFC model, is particularly popular (Olami, Feder, and Christensen, 1992). It is a two-dimensional coupled-map lattice model where the rupture propagates from a lattice site to its nearest-neighboring sites in a nonconservative manner, often causing multisite "avalanches." Extensive numerical studies have also been devoted to this model, mainly in the field of statistical physics, which we review in the present section (Christensen and Olami, 1992; Grassberger (1994); Middleton and Tang (1995); Bottani and Delamotte (1997); de Carvalho and Prado (2000); Pinho and Prado, 2000; Lise and Paczuski (2001); Miller and Boulter (2002); Hergarten and Neugebauer (2002); Boulter and Miller (2003); Helmstetter, Hergarten, and Sornette (2004); Peixoto and Prado (2004, 2006); Wissel and Drossel (2006); Ramos, Altshuler, and Maloy (2006); Kotani, Yoshino, and Kawamura (2008); Jagla (2010) and Kawamura *et al.* (2010)).

In the OFC model, a "stress" variable f_i ($f_i \geq 0$) is assigned to each site on a square lattice with $L \times L$ sites. Initially, a random value in the interval [0, 1] is assigned to each f_i, while f_i is increased with a constant rate uniformly over the lattice until, at a certain site i, the f_i value reaches a threshold, $f_c = 1$. Then, the site i "topples," and a fraction of stress αf_i ($0 < \alpha < 0.25$) is transmitted to its four nearest neighbors, while f_i itself is reset to zero. If the stress of some of the neighboring sites j exceeds the threshold, i.e., $f_j \geq f_c = 1$, the site j also topples, distributing a fraction of stress αf_j to its four nearest neighbors. Such a sequence of topplings continues until the stress of all sites on the lattice becomes smaller than the threshold f_c. A sequence of toppling events, which is assumed to occur instantaneously, corresponds to one seismic event or an avalanche. After an avalanche, the system goes into an interseismic period where uniform loading of f is resumed, until some of the sites reach the threshold and the next avalanche starts.

The transmission parameter α measures the extent of nonconservation of the model. (This α should not be confused with α describing the velocity-weakening friction force employed in the study of the BK model of Sec. III.A. We are using α as a conservation parameter of the OFC model throughout Sec. IV.A.) The system is conservative for $\alpha = 0.25$, and nonconservative for $\alpha < 0.25$. The unit of time is taken to be the time required to load f from zero to unity.

In the OFC model, boundary conditions play a crucial role. For example, the SOC state is realized under open or free boundary conditions but not under periodic boundary conditions. Thus, most of the studies made in the past employed open (or free) boundary conditions.

2. Properties of the homogeneous model

Earlier studies concentrated mostly on the event size distribution of the model (Olami, Feder, and Christensen (1992); Cristensen and Olami (1992); Grassberger (1994); de Carvalho and Prado (2000); Lise and Paczuski (2001); Miller and Boulter (2002); Boulter and Miller (2003); Wissel and Drossel, 2006). The avalanche size s is defined by the total number of topples in a given avalanche, which could be larger than the number of toppled sites because multitoppling is possible in a given avalanche. (In fact, it is observed that multitoppling rarely occurs in the model except in the conservation limit or in the regime very close to it.) It turns out that the size distribution of the model exhibits a power-law-like behavior close to the GR law. Yet there still remains controversy concerning whether the model is strictly critical (Lise and Paczuski, 2001) or only approximately so (de Carvalho and Prado (2000); Miller and Boulter (2002); Boulter and Miller (2003); Wissel and Drossel, 2006).

In Fig. 29, we show the size distribution of the model under open boundary conditions for several values of the transmission parameter α (Kawamura *et al.*, 2010). As can be seen from the figure, a near-straight-line behavior corresponding to a power law is observed. The slope representing the B value is not universal, varying from $\simeq 0.90$ to $\simeq 0.22$ as α is varied from 0.17 to 0.245. The power-law feature is weakened as one approaches the conservation limit.

Hergarten and Neugebauer (2002) observed that the OFC model also exhibits another well-known power-law feature of seismicity, i.e., the Omori law (inverse Omori law) describing the time evolution of the frequency of aftershocks (foreshocks) (Hergarten and Neugebauer, 2002; Helmstetter, Hergarten, and Sornette, 2004). We show in Fig. 30(a) on a log-log plot the frequency of aftershocks as a function of the time elapsed after the mainshock, t (Kawamura *et al.*, 2010). The slope representing the Omori exponent p is again not universal, depending on the parameter α, as $p = 0.84$, 0.69, and 0.03 for $\alpha = 0.17$, 0.20 and 0.23, respectively. Since the p value is known to be around unity in real seismicity, the p value of the OFC model is not necessarily close to reality. Similar results are obtained also for foreshocks; see Fig. 30(b) . Aftershocks and foreshocks are defined here as events of
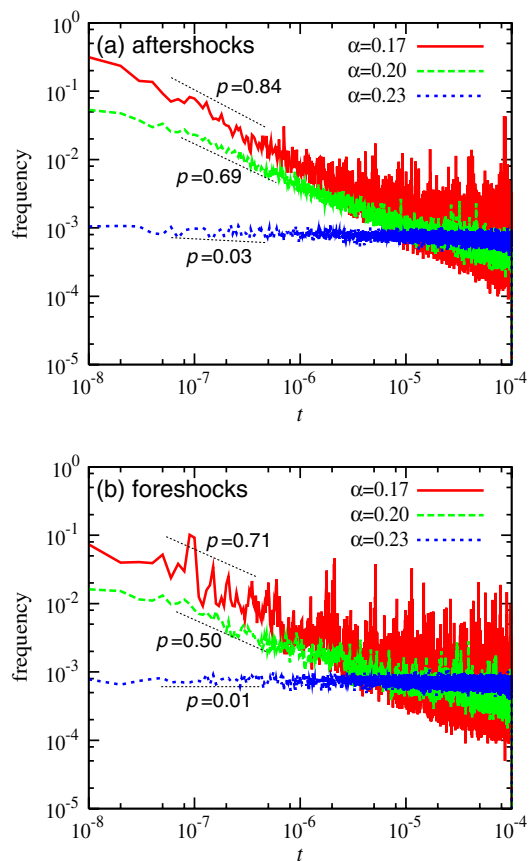
FIG. 30 (color online). The time dependence of the frequency of aftershocks (a) and of foreshocks (b) of the OFC model under open boundary conditions on a log-log plot for several values of the transmission parameter α. Mainshocks are events of size greater than $s \geq s_c = 100$. The time t is measured with the occurrence of a mainshock as the origin. The range parameter is $r_c = 10$. From Kawamura *et al.*, 2010.

arbitrary sizes which occur in the vicinity of the mainshock with epicenters lying at distance $r \leq r_c$ (the range parameter r_c is taken to be $r_c = 10$ in Fig. 30). As one approaches the conservation limit $\alpha = 0.25$, both aftershocks and foreshocks tend to go away.

As mentioned, the properties of the model depend on the applied boundary conditions. Middleton and Tang observed that the model under open boundary conditions goes into a special transient state where events of size 1 (single-site events) repeat periodically with period $1 - 4\alpha$ (Middleton and Tang, 1995). These single-site events occur in turn in a spatially random manner, but after time $1 - 4\alpha$, the same site topples repeatedly. Although such a periodic state consisting of single-site events is a steady state under periodic boundary conditions, it is not a steady state under open boundary conditions because of the boundary. Indeed, clusters are formed near the boundary, within which the stress values are more or less uniform, and gradually invades the interior, destroying the periodic state. Eventually, such clusters span the entire lattice, giving rise to a SOC-like steady state. Middleton and Tang pointed out that such clusters might be formed via synchronization between the interior site and the boundary site, the latter having a slower effective loading rate
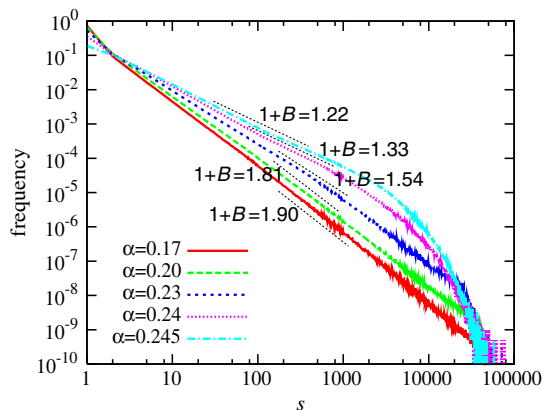

FIG. 29 (color online). The size distribution of the OFC model under open boundary conditions for various values of the transmission parameter α. The slope of the data gives the value of $1 + B$, which is shown in the figure. From Kawamura *et al.*, 2010.

due to the boundary. Large-scale synchronization occurring in the steady state of the OFC model was further investigated by Bottani and Delamotte (1997).

In contrast to the aforementioned critical properties of the model, recent studies also unraveled the *characteristic* features of the OFC model (Ramos, Altshuler, and Maloy, 2006; Kotani, Yoshino, and Kawamura, 2008; Kawamura *et al.*, 2010). By investigating the time series of events, Ramos found the nearly periodic recurrence of large events (Ramos, Altshuler, and Maloy, 2006). Kotani *et al.* studied the spatiotemporal correlations of the model and identified in the OFC model a phenomenon resembling an asperity (Kotani, Yoshino, and Kawamura, 2008; Kawamura *et al.*, 2010). They computed the local recurrence-time distribution, $P(T)$ of the model. The computed $P(T)$, shown in Fig. 31, exhibits a sharp δ-function-like peak at $T = T^* = 1 - 4\alpha$, indicating that many (though not all) events of the OFC model are repeated with a fixed time interval $T = T^*$. While the peak at $T = T^*$ is sharp, it is not infinitely sharp with a finite intrinsic width; see the inset. The peak position turned out to be independent of the range parameter r_c, the size threshold s_c, and the lattice size (as long as it was not too small). As α is increased toward $\alpha = 0.25$, the δ-function peak is gradually suppressed, keeping its position strictly at $T = 1 - 4\alpha$. The δ-function peak of $P(T)$ goes away toward the conservation limit $\alpha = 0.25$; see Fig. 31.

In the longer time regime $T > T^*$, $P(T)$ exhibits behaviors close to power laws (Kotani, Yoshino, and Kawamura, 2008; Kawamura *et al.*, 2010). Furthermore, the periodic events contributing to a sharp peak of $P(T)$ ("peak events") possess a power-law-like size distribution very similar to those observed for other aperiodic events (Kotani, Yoshino, and Kawamura, 2008; Kawamura *et al.*, 2010). Hence, in earthquake recurrence in the model, the characteristic or periodic feature, i.e., a sharp peak in $P(T)$ at $T = T^*$, and the critical feature, i.e., power-law-likebehaviors of $P(T)$ at $T > T^*$ and power-law-like size distribution, coexist.
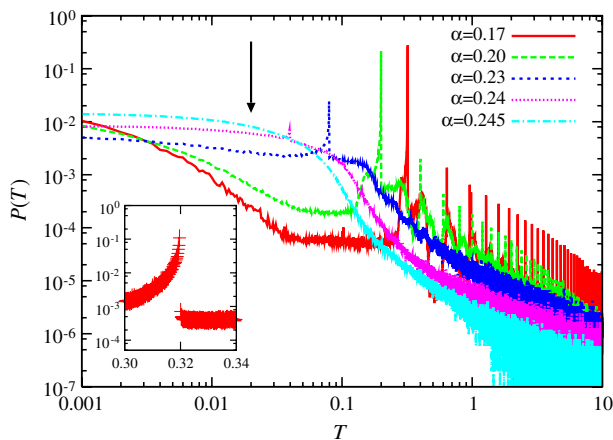

FIG. 31 (color online). Log-log plots of the local recurrence-time distributions of large avalanches of their size $s \geq s_c = 100$ for a fixed range parameter $r_c = 10$, with variation of the transmission parameter α. The arrow in the figure represents the expected peak position for $\alpha = 0.245$ corresponding to the period $T^* = 1 - 4\alpha = 0.02$. The inset is a magnified view of the main peak for the case of $\alpha = 0.17$. From Kawamura *et al.*, 2010.

3. Asperity-like phenomena

In fact, it turns out that the δ-function peak of $P(T)$ is created by "asperitylike" events, i.e., events which rupture repeatedly with almost the same period $1 - 4\alpha$ and with a common rupture zone and a common epicenter. In seismology, the concept of asperity is now quite popular. A typical example might be the one observed along the subduction zone in northeastern Japan, particularly in repeating earthquakes off Kamaishi (Matsuzawa, Igarashi, and Hasegawa, 2002; Okada, Matsuzawa, and Hasegawa, 2003).

In Fig. 32, we show typical examples of such asperity-like events as observed in the OFC model (Kawamura *et al.*, 2010). In the upper panel, we show for the case of $\alpha = 0.2$ typical snapshots of the stress-variable distribution immediately before and after a large event which occurs at time $t = t_0$. A discontinuous drop of the stress associated with a rupture of a synchronized cluster is discernible. Then, at time $t = t_0 + T^*$, the same cluster (except for a minor difference) ruptures again. In the lower panel, we show snapshots of the stress-variable distribution immediately before and after this subsequent avalanche occurring at $t = t_0 + T^*$. In this particular example, a rhythmic rupture of essentially the same cluster is repeated more than ten times.

The asperitylike events go away in the conservation limit $\alpha \rightarrow 1/4$ (Kawamura *et al.*, 2010). It is also observed that an epicenter site tends to lie at the tip or at the corner of the rupture zone rather than in its interior (Kawamura *et al.*, 2010). The asperitylike events observed in the OFC model closely resemble those familiar in seismology (Scholz, 2002),
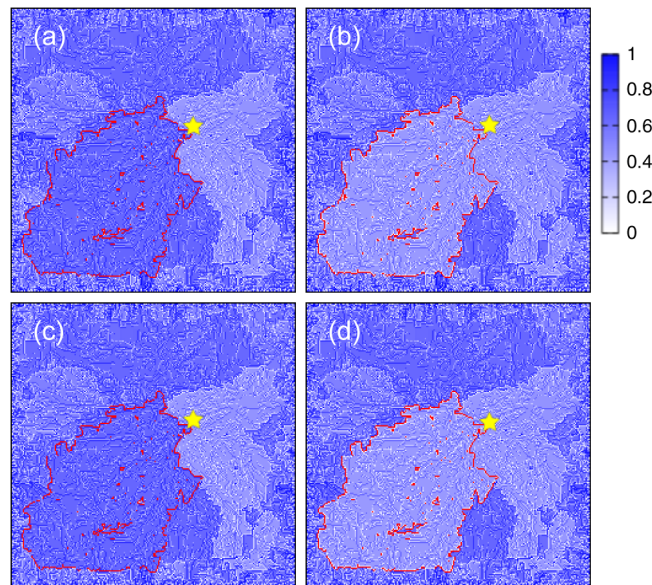

FIG. 32 (color online). Snapshots of the stress-variable distribution of the OFC model under open boundary conditions for the case of $\alpha = 0.2$: (a) immediately before a large event at time $t = t_0$, (b) immediately after this event, (c) immediately before the following event which occurs at time $t = t_0 + T^*$ ($T^* = 0.2$), and (d) immediately after this second event. The two events are of sizes $s = 15\,891$ and $15\,910$ on an $L = 256$ lattice. The region surrounded by bold lines represents the rupture zone, while the star symbol represents an epicenter site which is located at the tip of the rupture zone. From Kawamura *et al.*, 2010.
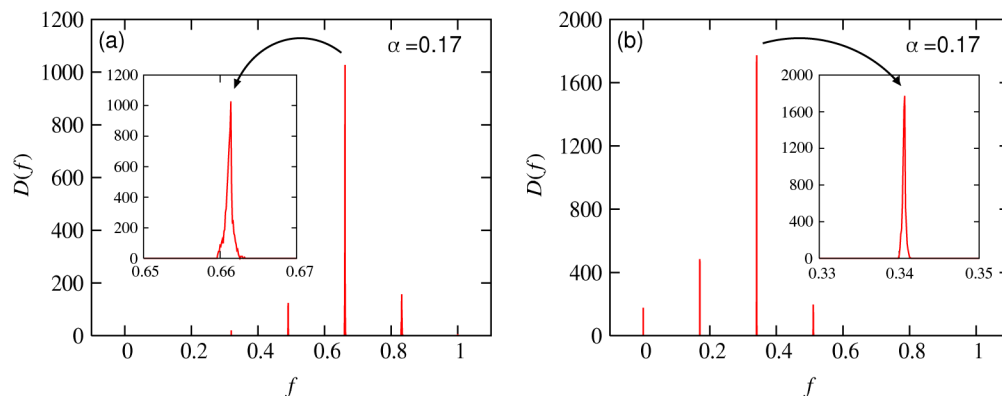
FIG. 33 (color online). The stress-variable distribution $D(f)$ of each site contained in the rupture zone of an asperity event of the OFC model under open boundary conditions, just before (a) and after (b) the asperity event. An asperity event is defined here as an event of size greater than $s \geq s_c = 100$ belonging to the main peak of the local recurrence-time distribution function. The transmission parameter is $\alpha = 0.17$. The inset is a magnified view of the main peak. From Kawamura *et al.*, 2010.

in the sense that almost the same spatial region ruptures repeatedly with a common epicenter site and with a common period.

In fact, not all large events of the OFC model occur in the form of asperities. Many clusters forming large events are left out of the rhythmic recurrence and rupture more critically with widely distributed recurrence times, thereby bearing the observed power-law-like part of $P(T)$.

A key ingredient in the asperity formation is a self-organization of the highly concentrated stress state (Kawamura *et al.*, 2010). The stress-variable distribution in the asperity region tends to be "discretized" to certain values. In Fig. 33, we show for the case of $\alpha = 0.17$ the stress-variable distribution $D(f)$ of the asperity sites immediately before (a) and after (b) an avalanche, averaged over asperity events. As can be seen from the figure, $D(f)$ now consists of several "spikes" located at appropriate multiples of the transmission parameter α, i.e., at $1 - n\alpha$ before the rupture and at
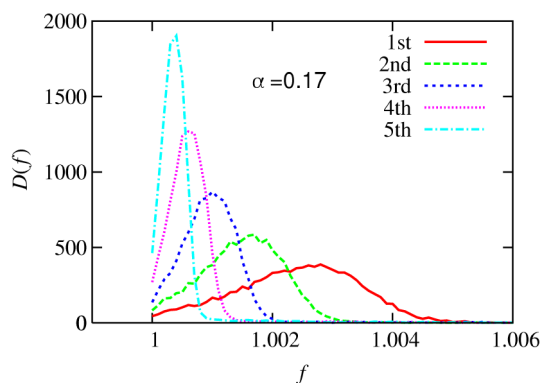

FIG. 34 (color online). The time sequence of the stress-variable distribution $D(f)$ at the time of toppling of each site contained in the rupture zone of the asperity events. An asperity event is defined here as an event of size greater than $s \geq s_c = 100$ belonging to the main peak of the local recurrence-time distribution function. The transmission parameter is $\alpha = 0.17$. As the events repeat, the stress-variable distribution at the time of toppling becomes more and more concentrated on the borderline value $f_c = 1$. From Kawamura *et al.*, 2010.

$f = n\alpha$ after the rupture, with n being an integer. Furthermore, as the asperity events repeat, the tendency to stress-variable concentration is more and more enhanced. In Fig. 34, we show the time sequence of the stress-variable distribution at the time of toppling for the asperity events. As the asperity events repeat, the stress-variable distribution tends to be narrower, being more concentrated on the threshold value $f_c = 1$ (Kawamura *et al.*, 2010; Hergarten and Krenn, 2011).

In fact, one can prove that the stress-variable distribution at the time of toppling tends to be more concentrated on the threshold value $f_c = 1$ as the asperity events repeat (Kawamura *et al.*, 2010). Namely, once each site starts to topple at more or less similar stress values close to the threshold value $f_c = 1$, this tendency evolves more and more as the asperity events repeat. The stress-variable concentration tends to be self-organized. Such a stress-variable concentration immediately explains why the interval time of the asperity events is equal to $1 - 4\alpha$, and why the same site becomes an epicenter in the asperity sequence (Kawamura *et al.*, 2010). For example, the reason why the interval time is $1 - 4\alpha$ when all sites topple at a stress value close to the threshold $f_c = 1$ in the asperity events can easily be seen just by remembering the conservation law of the stress, i.e., the stress variable dissipated at the time of toppling, which is $1 - 4\alpha$ per site if the toppling occurs exactly at $f = 1$, should match the stress loaded during the interval time T; see Kawamura *et al.* (2010), for further details. More recently, Hergarten and Krenn further analyzed this stress-concentration phenomenon, demonstrating that the mean stress excess representing the extent of the stress concentration approaches zero exponentially with a certain decay time which is dependent on the number of "internal" sites (the sites contained in the rupture zone) connected to an epicenter site (Hergarten and Krenn, 2011). Thus, the epicenter site with the smallest number of internal nearest-neighbor sites, i.e., the one lying at the tip of the rupture zone, has the longest decay time and turns out to be the most stable. This observation gives an explanation of the finding of Kawamura *et al.* (2010) that the majority of epicenter sites of the asperitylike events are located at the tip of the rupture zone.

Although the origin of the asperity is usually ascribed in seismology to possible inhomogeneity of the material properties of the crust or of the external conditions of that particular region, we stress that, in the present OFC model, there is no built-in inhomogeneity in the model parameters nor in the external conditions. The asperity in the OFC model is self-generated from the spatially uniform evolution rule and model parameters.

As mentioned, the asperity in the OFC model is not a permanent one: In the long term, its position and shape change. After all, the model is uniform. Nevertheless, recovery of spatial uniformity often takes a long time, and the asperity exists stably over many earthquake recurrences. Although one has to be careful in immediately applying the present result for the OFC model to real earthquakes, it might be instructive to recognize that the observation of asperitylike earthquake recurrence does not immediately mean that the asperity region possesses different material properties or different external conditions from other regions.

Thus, critical and characteristic features coexist in the OFC model in an intriguing manner. Although the critical features were emphasized in earlier works, the model certainly includes the eminent characteristic features as well. Thus, the OFC model, though an extremely simplified model, may capture some of the essential ingredients necessary to understand the apparent coexistence of critical and characteristic properties in real earthquakes.

4. Effects of inhomogeneity

Note that the original OFC model is a spatially homogeneous model, where homogeneity of an earthquake fault is implicitly assumed. Needless to say, a real earthquake fault is more or less spatially inhomogeneous, which might play an important role in real seismicity. A natural next step is to extend an original homogeneous OFC model to an inhomogeneous one where the evolution rule and/or the model parameters are taken to be random from site to site.

Spatial inhomogeneity can be either static or dynamic. As a cause of possible temporal variation of spatial inhomogeneity, one may consider two distinct processes, i.e., the fast dynamical process during earthquake rupture changing the fault state via, e.g., wear, frictional heating, melting, etc., and many slower processes taking place during the long interseismic period until the next earthquake, e.g., water migration, plastic deformation, chemical reactions, etc. (Scholz, 2002). Thus, to introduce spatial inhomogeneity into the OFC model, there are two possible extreme methods: First, one might assume that the randomness is quenched in time, namely, spatial inhomogeneity is fixed over many earthquake recurrences. In the other extreme, spatial inhomogeneity is assumed to vary with time in an uncorrelated way over earthquake recurrences.

Several studies have been made on the inhomogeneous OFC model for both types of inhomogeneity. For the first type of inhomogeneity, i.e., quenched or static randomness, Janosi and Kertesz introduced spatial inhomogeneity into the stress threshold and found that the inhomogeneity destroyed the SOC of the model (Jánosi and Kertész, 1993). Torvund and Froyland studied the effect of spatial inhomogeneity in the stress threshold and observed that the inhomogeneity induced

a periodic repetition of system-size avalanches (Torvund and Froyland, 1995). Ceva introduced defects associated with the transmission parameter α and observed that the SOC was robust against a small number of defects (Ceva, 1995). Mousseau and Bach *et al.* introduced inhomogeneity into the transmission parameter at each site. They observed that the bulk sites were fully synchronized in the form of a system-wide avalanche over a wide parameter range of the model (Mousseau, 1996; Bach, Wissel, and Drossel, 2008).

For the second type of inhomogeneity, i.e., the dynamical randomness, Ramos *et al.* considered the randomness associated with the stress threshold, and observed that the nearly periodic recurrence of large events persisted (Ramos, Altshuler, and Maloy, 2006). More recently, Jagla studied the same stress-threshold inhomogeneity, to find that the GR law was weakened by randomness (Jagla, 2010). An interesting observation by Jagla is that, once the slow structural relaxation process is added to the inhomogeneous OFC model, both the GR law and the Omori law are realized with exponents that are stable against the choice of the model parameter values and are close to the observed values. Yamamoto *et al.* studied the dynamically inhomogeneous model with a variety of implementations of the form of the inhomogeneities and found the general tendency that critical features in the original homogeneous OFC model, e.g., the Gutenberg-Richter law and the Omori law, were weakened or suppressed in the presence of inhomogeneity, whereas the characteristic features of the original homogeneous OFC model, e.g., the near-periodic recurrence of large events and the asperitylike phenomena, tended to persist (Yamamoto, Yoshino, and Kawamura, 2010).

Thus, the properties of the dynamically inhomogeneous models are quite different from those of the static or quenched inhomogeneous models. In the latter case, introduced inhomogeneity often gives rise to a full synchronization and a periodic repetition of system-size events. Such a system-wide synchronization is never realized in the dynamically homogeneous models. Presumably, temporal variation of the spatial inhomogeneity may eventually average out the inhomogeneity over many earthquake recurrences, giving rise to behavior similar to that of the homogeneous model.

B. Fiber bundle models

The fiber bundle model, initiated by Peirce (1926) in the context of testing the strength of cotton yarns, represents various aspects of fracture processes of disordered systems, through its self-organized dynamics [for a detailed review, see Pradhan, Hansen, and Chakrabarti (2010)]. The fiber bundle (see Fig. 35) consists of N fibers or Hookean springs, each having an identical spring constant κ. The bundle supports a load $W = N\sigma$ and the breaking threshold $(\sigma_{th})_i$ of the fibers is assumed to be different for different fibers (i). For the equal-load-sharing model we consider here, the lower platform is absolutely rigid, and therefore no local deformation and hence no stress concentration occurs anywhere around the failed fibers. This ensures equal load sharing, i.e., the intact fibers share the applied load W equally and the load per fiber increases as more and more fibers fail. The strength of each of the fibers $(\sigma_{th})_i$ in the bundle is given by the stress
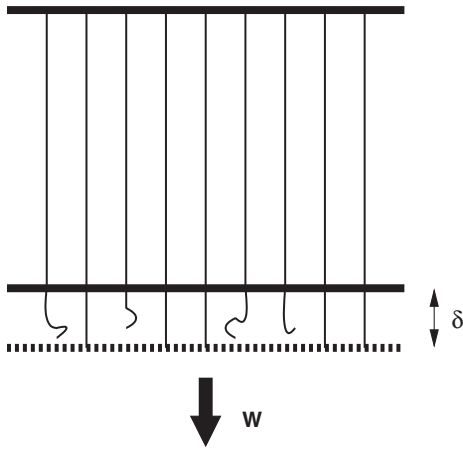
FIG. 35. The fiber bundle consists initially of N fibers attached in parallel to a fixed and rigid plate at the top and a downwardly movable platform from which a load W is suspended at the bottom. In the equal-load-sharing model considered here, the platform is absolutely rigid and the load W is consequently shared equally by all the intact fibers.

value it can bear and beyond which it fails. The strengths of the fibers are taken from a randomly distributed normalized density $\rho(\sigma_{\text{th}})$ within the interval 0 and 1 such that

$$\int_0^1 \rho(\sigma_{\text{th}}) d\sigma_{\text{th}} = 1.$$

The equal-load-sharing assumption neglects "local" fluctuations in stress (and its redistribution) and renders the model as a mean-field one.

The breaking dynamics starts when an initial stress σ (load per fiber) is applied on the bundle. The fibers having strength less than σ fail instantly. Because of this rupture, the total number of intact fibers decreases and the rest of the (intact) fibers have to bear the applied load on the bundle. Hence the effective stress on the fibers increases and this compels some more fibers to break. These two sequential operations, namely, stress redistribution and further breaking of fibers, continue until an equilibrium is reached, where the surviving fibers are either strong enough to bear the applied load on the bundle or all fibers fail.

This breaking dynamics can be represented by recursion relations in discrete time steps. For this, we consider a very simple model of fiber bundles where the fibers (having the same spring constant κ) have a white or uniform strength distribution $\rho(\sigma_{\text{th}})$ up to a cutoff strength normalized to unity, as shown in Fig. 36: $\rho(\sigma_{\text{th}}) = 1$ for $0 \le \sigma_{\text{th}} \le 1$ and $\rho(\sigma_{\text{th}}) = 0$ for $\sigma_{\text{th}} > 1$. We also define $U_t(\sigma)$ to be the fraction of fibers in the bundle that survive after (discrete) time step t, counted from the time $t = 0$ when the load is applied (the time step indicates the number of stress redistributions). Thus, $U_t(\sigma = 0) = 1$ for all t and $U_t(\sigma) = 1$ for $t = 0$ for any σ; $U_t(\sigma) = U^*(\sigma) \ne 0$ for $t \to \infty$ and $\sigma < \sigma_f$, the critical or failure strength of the bundle, and $U_t(\sigma) = 0$ for $t \to \infty$ if $\sigma > \sigma_f$.

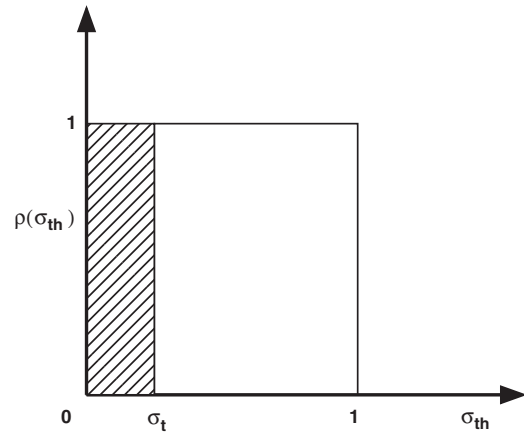Therefore, $U_t(\sigma)$ follows the simple recursion relation (see Fig. 36)

FIG. 36. The simple model considered here assumes uniform density $\rho(\sigma_{\text{th}})$ of the fiber strength distribution up to a cutoff strength (normalized to unity). At any load per fiber level σ_t at time t, the fraction σ_t fails and $1 - \sigma_t$ survives.

$$U_{t+1} = 1 - \sigma_t, \qquad \sigma_t = \frac{W}{U_t N}, \qquad \text{or}$$
$$U_{t+1} = 1 - \frac{\sigma}{U_t}. \tag{63}$$

In the equilibrium state ($U_{t+1} = U_t = U^*$), the above relation takes a quadratic form of U^*:

$$U^{*2} - U^* + \sigma = 0.$$

The solution is

$$U^*(\sigma) = \tfrac{1}{2} \pm (\sigma_f - \sigma)^{1/2}; \qquad \sigma_f = \tfrac{1}{4}.$$

Here σ_f is the critical value of initial applied stress beyond which the bundle fails completely. The solution with the $+$ sign is the stable one, whereas the one with the $-$ sign gives an unstable solution (Pradhan and Chakrabarti, 2001; Pradhan, Bhattacharyya, and Chakrabarti, 2002; Bhattacharyya, Pradhan, and Chakrabarti, 2003). The quantity $U^*(\sigma)$ must be real valued as it has a physical meaning: it is the fraction of the original bundle that remains intact under a fixed applied stress σ when the applied stress lies in the range $0 \le \sigma \le \sigma_f$. Clearly, $U^*(0) = 1$. Therefore, the stable solution can be written as

$$U^*(\sigma) = U^*(\sigma_f) + (\sigma_f - \sigma)^{1/2},$$
$$U^*(\sigma_f) = \tfrac{1}{2} \quad \text{and} \quad \sigma_f = \tfrac{1}{4}. \tag{64}$$

For $\sigma > \sigma_f$, we cannot get a real-valued fixed point as the dynamics never stops until $U_t = 0$, when the bundle breaks completely.

a. At $\sigma < \sigma_f$—Note that the quantity $U^*(\sigma) - U^*(\sigma_f)$ behaves as an order parameter that determines a transition from a state of partial failure ($\sigma \le \sigma_f$) to a state of total failure ($\sigma > \sigma_f$):

$$O \equiv U^*(\sigma) - U^*(\sigma_f) = (\sigma_f - \sigma)^\beta \qquad \beta = \tfrac{1}{2}. \tag{65}$$

To study the dynamics away from criticality ($\sigma \to \sigma_f$ from below), we replace the recursion relation (63) by a differential equation

$$-\frac{dU}{dt} = \frac{U^2 - U + \sigma}{U}.$$

Close to the fixed point we write $U_t(\sigma) = U^*(\sigma) + \epsilon$ (where $\epsilon \to 0$). This, following Eq. (65), gives

$$\epsilon = U_t(\sigma) - U^*(\sigma) \approx \exp(-t/\tau), \qquad (66)$$

where $\tau = \frac{1}{2}[\frac{1}{2}(\sigma_f - \sigma)^{-1/2} + 1]$. Near the critical point we can write

$$\tau \propto (\sigma_f - \sigma)^{-\alpha}, \qquad \alpha = \frac{1}{2}. \qquad (67)$$

Therefore the relaxation time diverges following a power law as $\sigma \to \sigma_f$ from below.

One can also consider the breakdown susceptibility χ, defined as the change of $U^*(\sigma)$ due to an infinitesimal increment of the applied stress σ:

$$\chi = \left| \frac{dU^*(\sigma)}{d\sigma} \right| = \frac{1}{2}(\sigma_f - \sigma)^{-\gamma}, \qquad \gamma = \frac{1}{2} \qquad (68)$$

from Eq. (65). Hence the susceptibility diverges as the applied stress σ approaches the critical value $\sigma_f = \frac{1}{4}$. Such a divergence in χ was already observed in numerical studies.

b. *At $\sigma = \sigma_f$*—At the critical point ($\sigma = \sigma_f$), we observe a different dynamic critical behavior in the relaxation of the failure process. From the recursion relation (63), it can be shown that the decay of the fraction $U_t(\sigma_f)$ of unbroken fibers that remain intact at time t follows a simple power law,

$$U_t = \frac{1}{2}\left(1 + \frac{1}{t+1}\right), \qquad (69)$$

starting from $U_0 = 1$. For large t ($t \to \infty$), this reduces to $U_t - 1/2 \propto t^{-\delta}$, $\delta = 1$; a strict power law which is a robust characterization of the critical state [see, however, Zapperi *et al.* (1997)].

1. Universality class of the model

The universality class of the model has been checked with two other types of fiber strength distributions: (I) linearly increasing and (II) linearly decreasing density distribution within the ($\sigma_{\rm th}$) limits 0 and 1. One can show that while σ_f changes with different strength distributions; $\sigma_f = \sqrt{4/27}$ for case I and $\sigma_f = 4/27$ for case II, the critical behavior remains unchanged: $\alpha = 1/2 = \beta = \gamma$, $\delta = 1$ for all these equal-load-sharing models (Pradhan, Hansen, and Chakrabarti, 2010).

2. Precursors of global failure in the model

In any such failure case, it is important to know when the failure will take place. In this model, there exist several precursors. The growth of susceptibility χ with σ, following Eq. (68), indeed suggests one such possibility: $\chi^{-1/2}$ decreases linearly with increasing σ to 0 at $\sigma = \sigma_f$. Pradhan and Hemmer (2009) studied the rate $R(t)$ ($\equiv -dU_t/dt$) of failure of fibers following dynamics as in Eq. (63) for $\sigma > \sigma_f$ and found that the rate becomes minimum at a time t_0, which is half of the failure time t_f of the bundle (see Fig. 37). This relation is shown to be independent of the breaking strength distribution of the fibers. A similar relation was also found

(Pradhan and Hemmer, 2011) for the rate of energy released in a bundle. This is, of course, easier to measure using acoustic emissions.

3. Strength of local-load-sharing fiber bundles

So far, we have studied models with fibers sharing the external load equally. This type of model shows (both analytically and numerically) the existence of a critical strength (nonzero σ_f) of the macroscopic bundle beyond which it collapses. The other extreme model, i.e., the local-load-sharing model has proved to be difficult to tackle analytically.

It is clear, however, that the extreme statistics come into play for such local-load-sharing models, for which the strength $\sigma_f \to 0$ as the bundle size (N) approaches infinity. Essentially, for any finite load (σ), depending on the fiber strength distribution, the size of the defect cluster can be estimated using the Lifshitz argument (see, Sec. II.A) as $\ln N$, giving the failure strength $\sigma_f \sim 1/(\ln N)^a$, where the exponent a assumes a value appropriate for the model [see, e.g., Pradhan and Chakrabarti (2003b)]. If a fraction f of the load of the failed fiber goes for global redistribution and the rest (the fraction $1 - f$) goes to the fibers neighboring the failed one, then we see that there is a crossover from extreme to self-averaging statistics at a finite value of f [see, e.g., Pradhan, Hansen, and Chakrabarti (2010)].

4. Burst distribution: Crossover behavior

In fiber bundle models, when the load is slowly increased until a new failure occurs, a burst can be defined as the number (Δ) of fiber failures following that failure. The distribution of such bursts [$D(\Delta)$] shows power-law behavior. It was shown for a generic case (independent of threshold distribution) that the form of this distribution (for continuous loading) is

$$D(\Delta)/N = C\Delta^{-\xi} \qquad (70)$$
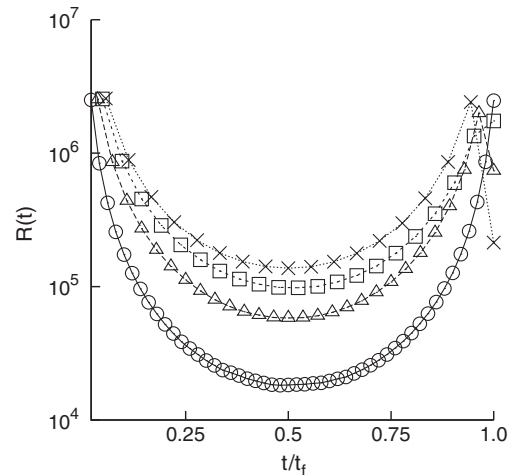
in the limit $N \to \infty$.

FIG. 37.   The breaking rate $R(t)$ vs the rescaled step variable t_f/t for the uniform threshold distribution for a bundle of $N = 10^7$ fibers. Different symbols are for different excess stress levels $\sigma - \sigma_f$: 0.001 (circles), 0.003 (triangles), 0.005 (squares), and 0.007 (crosses). From Pradhan and Hemmer, 2009.

The burst exponent ζ has a value $\frac{5}{2}$ on average over all σ ($= 0$ to σ_f) and it is universal (Hemmer and Hansen, 1992). However, the burst exponent value depends, e.g., on the details of the loading process and also from which point of the loading the burst statistics are recorded. If the burst distribution is recorded only near the critical point ($\sigma \lesssim \sigma_f$), the burst exponent (ζ) value becomes $3/2$ (Pradhan, Hansen, and Hemmer, 2005). For the equal-load-sharing model with uniform strength distribution, the burst distribution is shown (Fig. 38) for recording that starts from different points of effective loading denoted by x_0, where $x_t = \sigma/U_t$ is the elongation or the effective loading (for linear elastic behavior) at any point t. The crossover behavior is clearly seen. In these studies, the load increase rate is extremely slow and the increase is assumed to stop once a fiber fails. The consequent avalanches are studied at that load. Once the avalanche stops, the load is increased again. This process is realistic in the case of earthquakes where stress accumulation takes place over years. However, if the increase in load is fixed ($d\sigma$), then the above exponent value of ζ becomes 3: $\Delta \sim d(1 - U^*)/d\sigma$, giving $\Delta^{-2} = \sigma - \sigma_f$ [from Eq. (64)] and since $D(\Delta)d\Delta \sim d\sigma$, $D(\Delta) \sim d\sigma/d\Delta \sim \Delta^{-\zeta}$, $\zeta = 3$ (Pradhan, Bhattacharyya, and Chakrabarti, 2002).

In fact, the earthquake frequency statistics may indeed show the crossover behavior mentioned above: If the event frequency is denoted by $D(M)$, then it is known that $D(M) \sim M^{-\zeta}$, where M denotes the magnitude (which may be assumed to be related to avalanche size Δ in the models) and the ζ value is found (Kawamura, 2006) to be larger ($\zeta \approx 0.9$) for statistics over a smaller time period (before the mainshock), compared to the long-time average value ($\zeta \approx 0.6$); see Fig. 39.

C. Two-fractal-overlap models

The common geometrical property observed in seismic faults is its fractal nature. It is now well known that, like other fractured surfaces, fault surfaces also posses self-affine
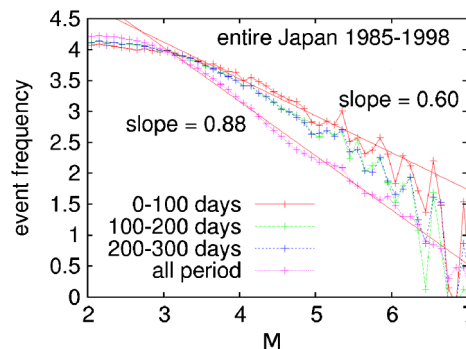
FIG. 39 (color online).   Crossover signature in the local magnitude distribution of earthquakes in Japan. During the 100 days before the mainshock the exponent is 0.60, much smaller than the average value 0.88. From Kawamura, 2006.

roughness [see, e.g., Santucci *et al.* (2007) and references therein]. Therefore, it is worth investigating if earthquake phenomena can be modeled as the outcome of relative movement of two self-affine surfaces over each other. Chakrabarti and Stinchcombe (1999), in a simplistic model, studied the overlap statistics of two Cantor sets in order to understand the underlying physics of such phenomena.

The Cantor set is a prototype example of a fractal. In order to construct a triadic Cantor set, in the first step the middle third of a base interval [0,1] is removed. In successive steps, the middle thirds of the remaining intervals ([0, 1/3] and [2/3, 1] and so on) are removed. After n such steps, the remaining set is called a Cantor set of generation n. When this process is continued *ad infinitum*, i.e., in the limit $n \rightarrow \infty$, it becomes a true fractal.

In this model, the solid-solid contact surfaces of both the Earth's crust and the tectonic plate are considered as average self-affine surfaces (see Fig. 40). The strain energy growing between the two surfaces due to a stick period is taken to be proportional to the overlap between them. During a slip event, this energy is released. Considering that such slips occur at intervals proportional to the length corresponding to that area, a power law for the frequency distribution of the energy release is obtained. This compares well with the GR law [see, e.g., Bhattacharyya and Chakrabarti (2006)].

1. Renormalization group study: Continuum limit

Let the sequence of generators G_n define the Cantor set in the nth generation within the interval [0,1]: $G_0 = [0, 1]$, $G_1 \equiv RG_0 = [0, a] \cup [b, 1], \ldots, G_{n+1} = RG_n, \ldots$. The mass density of the set G_n is represented by $D_n(r)$, i.e., $D_n(r) = 1$
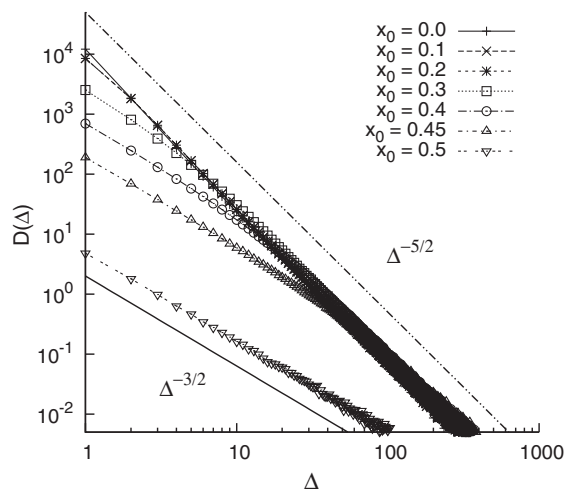
FIG. 38.   The burst size distribution for different values of x_0 in the equal-load-sharing model with uniform threshold distribution. The number of fibers is $N = 50000$. From Pradhan, Hansen, and Hemmer, 2006.
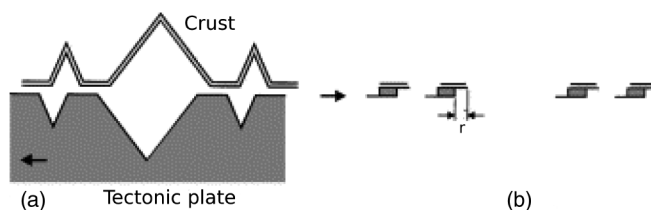
FIG. 40.   (a) Schematic representation of the rough Earth surface and a tectonic plate. (b) The one-dimensional projection of the surfaces, forming overlapping Cantor sets.
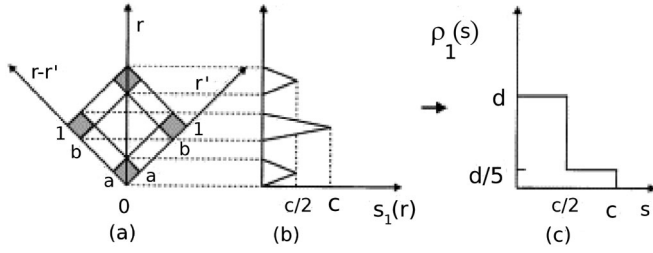
FIG. 41.   (a) Two Cantor sets along the axes r and $r - r'$. (b) The overlap $s_1(r)$ along the diagonal. (c) The corresponding density $\rho_1(s)$.

if r is in any of the occupied intervals of G_n and 0 elsewhere. The overlap magnitude between the sets at any generation n is then given by the convolved form $s_n(r) = \int dr' D_n(r') D_n(r - r')$ (for symmetric fractals). One can express the overlap integral s_1 in the first generation by the projection of the shaded region along the vertical diagonals in Fig. 41(a). That gives the form shown in Fig. 41(b). For $a = b \le 1/3$, the nonvanishing $s_1(r)$ regions do not overlap and are symmetric on both sides, with the slope of the middle curve being exactly double those on the sides. One can then easily check that the distribution $\rho_1(s)$ of overlap s in this generation is given by Fig. 41, with both c and d greater than unity, maintaining the normalization condition with $cd = 5/3$. The successive generations of the density $\rho_n(s)$ may therefore be represented by Fig. 42, where

$$\rho_{n+1}(s) = \tilde{R}\rho_n(s) \equiv \frac{d}{5}\rho_n\left(\frac{s}{c}\right) + \frac{4d}{5}\rho_n\left(\frac{2s}{c}\right). \tag{71}$$

In the infinite-generation limit of the renormalization group equation, if $\rho^*(s)$ denotes the fixed point distribution such that $\rho^*(s) = \tilde{R}\rho^*(s)$, then assuming $\rho^*(s) \sim s^{-\gamma}\tilde{\rho}(s)$, one gets $(d/5)c^\gamma + (4d/5)(c/2)^\gamma = 1$. Here $\tilde{\rho}(s)$ represents an arbitrary modular function, which also includes a logarithmic correction for large s. This agrees with the normalization condition $cd = 5/3$ for the choice $\gamma = 1$, giving

$$\rho^*(s) \equiv \rho(s) \sim s^{-\gamma}; \qquad \gamma = 1. \tag{72}$$

This analysis is for the continuous relative motion of the overlapping fractals. For discrete steps, the contact area distribution can be found exactly for two Cantor sets having the same dimension ($\log 2/\log 3$) (Bhattacharyya, 2005). The step size is taken as the minimum element in the generation at which the distribution is found.
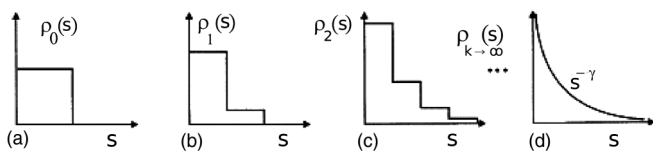

FIG. 42.   The overlap densities (probabilities) $\rho(s)$ at various generations; (a) zeroth, (b) first, (c) second, and (d) infinite generation.

2. Discrete limit

Let $s_n(t)$ represent the amount of overlap between two Cantor sets of generation n at time t. Initially ($t = 0$) the two identical Cantor sets are placed on top of each other, generating the maximum overlap (2^n for the nth-generation sets). Then in every time step (discrete) the length of the shift is chosen to be $1/3^n$ for the nth generation, such that a line segment in one set either completely overlaps with one such segment on the other set or does not overlap at all, i.e., partial overlap of two segments of the two sets is not allowed. Periodic boundary conditions are assigned in both of the sets. The magnitude of overlap $[s_n(t)]$, therefore, in this discrete version, is given by the number of overlapping pairs in the line segment of the two sets. Because of the structure of the Cantor sets, the overlap magnitudes can only have certain discrete values which are in geometric progression: $s_n = 2^{n-k}$, $k = 0, \ldots, n$.

Let $Nr(s_n)$ denote the number of times an overlap s_n has occurred in one period of the time series for the nth generation (i.e., 3^n time steps). It can be shown that (Bhattacharyya and Chakrabarti, 2006)

$$Nr(2^{n-k}) \stackrel{n}{=} C_k 2^k, \qquad k = 0, \ldots, n. \tag{73}$$

Now, if $\text{Prob}(s_n)$ denotes the probability that after time t there are s_n overlapping segments, then for the general case of $s_n = 2^{n-k}$, $k = 0, \ldots, n$, it is given by

$$\text{Prob}(2^{n-k}) = \frac{Nr(2^{n-k})}{\sum_{k=0}^{n} Nr(2^{n-k})} = \frac{2^k}{3^n}{}^n C_k$$

$$= {}^n C_{n-k}\left(\frac{1}{3}\right)^{n-k}\left(\frac{2}{3}\right)^k. \tag{74}$$

3. Gutenberg-Richter law

Since the allowed values of the overlap are $s_n = 2^{n-k}$, $k = 0, \ldots, n$, one can write $\log_2 s_n = n - k$. Then Eq. (74) becomes

$$\text{Prob}(s_n) = {}^n C_{\log_2 s_n}\left(\frac{1}{3}\right)^{\log_2 s_n}\left(\frac{2}{3}\right)^{n-\log_2 s_n} \equiv F(\log_2 s_n). \tag{75}$$

Near the maxima it may be written as

$$F(M) = \frac{3}{2\sqrt{n\pi}} \exp\left[-\frac{9}{4}\frac{(M - n/3)^2}{n}\right], \tag{76}$$

where $M = \log_2 s_n$. To obtain the GR law analog from this distribution we have to integrate $F(M)$ from M to ∞:

$$F_{\text{cum}}(M) = \int_M^\infty F(M')dM'$$

$$= \int_M^\infty \frac{3}{2\sqrt{n\pi}} \exp\left(-\frac{9}{4}\frac{(M' - n/3)^2}{n}\right)dM'. \tag{77}$$

Substituting $p = (3/2\sqrt{n})(M' - n/3)$, we get

$$F_{\text{cum}}(M) = \frac{1}{\sqrt{\pi}} \int_{\frac{3}{2\sqrt{n}}(M-n/3)}^\infty \exp(-p^2)dp. \tag{78}$$

On simplification, this gives

$$F_{\text{cum}}(M) = \frac{1}{3}\sqrt{\frac{n}{\pi}} \exp\left[-\frac{9}{4}\frac{(M-n/3)^2}{n}\right](M-n/3)^{-1}. \tag{79}$$

$F_{\text{cum}}(M)$ in the above equation suggests that the "average" quakes are of magnitude $n/3$, while

$$F_{\text{cum}}(M) \sim \exp[-(9/4)(M-n/3)^2/n] \tag{80}$$

can be simplified for large M. Using $e^{-a^2} = (1/\sqrt{2\pi}) \times \int_{-\infty}^{+\infty} e^{-x^2/2+\sqrt{2}ax} dx$ and $\int_{-\infty}^{+\infty} e^{-f(x)} dx \sim e^{-f(x_0)}$, where x_0 refers to the extremal point with $\partial f/\partial x|_{x=x_0} = 0$, one finds $F_{\text{cum}}(M) \sim e^{-(9/4)[M(m_0/n)-2M/3]} \sim e^{-3M/4}$, where $x_0 = (3/\sqrt{2n})m_0$; $m_0 = n$. It gives (Bhattacharya *et al.*, 2009)

$$\log F_{\text{cum}}(M) = A - \tfrac{3}{4}M, \tag{81}$$

where A is a constant depending on n. This is the Gutenberg-Richter law in the model and clearly holds for the high-magnitude end of the distribution. Also, one can equate easily the magnitude M with the released energy E by noting that $M = \log_2 s$ here. The overlap s is related to the energy E and hence the relation $M \sim \log E$, giving $F_{\text{cum}} \sim E^{-3/4}$.

Similar to the outcome of the simple fractal models considered here, a power-law behavior for the overlap distribution also occurs for two overlapping random Cantor sets, Sierpinsky gaskets and Sierpinsky carpets overlapping on their respective replicas (Pradhan *et al.*, 2003), and one fractional Brownian profile overlapping on another (De Rubeis *et al.*, 1996,). In view of the generality of the power-law distribution and the fractal geometry of the fault surfaces, it is suggested that the GR law owes its origin to a significant extent to the fractal geometry of the fault surfaces. It may be noted that, by identifying the aftershocks as these adjusted overlaps, with average size given by Eq. (79), one can define an average magnitude ($n/3$) dependent on the fractal geometry generator fraction ($= 1/3$ here) and the generation number (n). This agrees with the observed data quite satisfactorily [see Bhattacharya, Chakrabarti, and Kamal (2011)].

4. Omori law

Let $N^{(M_0)}(t)$ denote the cumulative number of aftershocks (of magnitude $M \geq M_0$, where M_0 is some threshold) after the mainshock. Then the Omori law states that

$$\frac{dN^{(M_0)}(t)}{dt} = \frac{1}{t^p}. \tag{82}$$

The value of the exponent p is close to unity for a tectonically active region, although a range of p values is also observed [for review see Bhattacharya *et al.* (2009)]. In practice, a particular value of p is observed when the threshold M_0 is given. For this model, when the threshold is fixed at the minimum (i.e., $M_0 = 1$), then $p = 0$ due to the fact that aftershock occurs at every step in this model. However, interesting facts are seen when the threshold is set at the second highest possible value $n-1$ (recall that the second highest overlap was 2^{n-1}). Then for $t = 2.3^{r_1}$ (where $r_1 = 0, \dots, n-1$) there is an aftershock of magnitude $n-1$. Therefore, neglecting the prefactor 2, an aftershock of magnitude $n-1$ occurs in a geometric progression with

the common ratio 3. Therefore, we get the general rule $N(3t) = N(t) + 1$, leading to

$$N(t) = \log_3(t). \tag{83}$$

On integration, the Omori law gives $N(t) = t^{1-p}$, and therefore from this model we get $p = 1$, which is the value suggested by the Omori law for p. The model therefore gives a range of p values between 0 and 1 which systematically increases within the range of threshold values.

V. DISCUSSION AND CONCLUSIONS

Earthquakes, due to their devastating consequences, have been the subject of extensive studies in various disciplines, ranging from seismology to physics. Although the efforts were not always commensurate [see also Kagan (2006) for a critical view of the inherent difficulties of the present approach in theoretical physics], in the last decade considerable progress has been made in studying different aspects of this vast topic. In this review, the progress in such studies is discussed from the point of view of statistical physics.

Because an earthquake is mainly a large-scale dynamic failure process, it is necessary to formulate the background of friction and fracture in order to understand the physics of earthquakes. In Sec. II such issues are discussed: After describing the Griffith theory for crack nucleation and the fracture stress statistics of disordered solids, we discuss the RSF law and microscopic models for solid-solid friction. The effects that could lead to violations of RSF laws are also discussed.

Several statistical approaches to model earthquake dynamics are discussed. The BK model is discussed in one and two spatial dimensions, as well as its long-range version. In Sec. III.A.6, the continuum limit is also discussed, which gives "characteristic" earthquakes. The BK model has also been discussed in terms of the RSF law. In addition to relatively complex modeling like that of BK models and continuum models, we also discuss simplistic models such as OFC models, fiber bundle models, and purely geometrical models like the two-fractual-overlap model. While many details are lost in any such model, they still capture the complex nature of the dynamics and the different statistical aspects, helping us to gain new insights.

As one can easily see, in spite of considerable progress in the study of such an important and complex dynamical phenomenon as an earthquake, our knowledge is far short of any satisfactory level. We believe major collaborative efforts, involving physicists and seismologists, in particular, are urgently necessary to unfold the dynamics and allow us to employ our knowledge of the precursor events to save us from catastrophic disasters in the future.

GLOSSARY

aftershocks: Small earthquakes that follow a large earthquake (main shock).
afterslip: Aseismic sliding that follows an earthquake.
asperity: (a) A region where stick-slip motion occurs on a fault or a plate boundary. Strain energy is accumulated at an asperity during a stick stage between earthquakes and it is

released by seismic slip at the occurrence of an earthquake. (b) Junction of protrusions of the two contacting surfaces.

Cantor set: Start with the set of real numbers in the interval [0:1], divide the set into a few subsets, and remove one of the subsets in the first step. As the removal scheme is repeated *ad infinitum*, one is left with a dust of real numbers called the Cantor set. It is a fractal object.

characteristic earthquakes: Earthquakes that repeatedly rupture approximately the same segment of a fault. The magnitudes and slip distributions of characteristic earthquakes are similar to one another.

dynamical critical phenomena: Critical behaviors that are associated with the dynamical properties of the system, rather than the equilibrium properties (e.g., the thermal transition in the Ising model), are called dynamical critical phenomena (e.g., the depinning transition of a fracture front, the time-dependent field-induced transitions in the Ising model, etc.).

fiber bundle model: Originating from textile engineering, the fiber bundle model is often used as a prototype model for fracture dynamics. In its simplest form, it consists of a large number of fibers or Hooke springs. The bundle hangs from a rigid ceiling and supports a load via a platform at the bottom. Each fiber has identical spring constants but the breaking stress for each differs. Depending on the breaking stress of the fibers, the fibers fail and successive failures occur due to load redistribution, showing complex failure dynamics.

fractals: A fractal is a geometrical object having self-similarity in its internal structure.

fractional Brownian profile: Fractional Brownian motion (FBM) is a continuous-time random walk with zero mean. However, the directions of the subsequent steps of a FBM are correlated (positively or negatively). A fractional Brownian profile is the trajectory of such a walk. It is self-similar.

Gutenberg-Richter (GR) law: The power law describing the magnitude-frequency relation of earthquakes. The frequency of earthquakes of energy (seismic moment) E decays with E proportionally to $E^{-(1+B)} = E^{-(1+\frac{2}{3}b)}$ where B and $b = \frac{3}{2}B$ are appropriate exponents.

Hamiltonian: It is essentially the total energy of a system. For a closed system, is the sum of kinetic and potential energies.

Omori law: The power law describing the decay of the number (frequency) of aftershocks with the time elapsed after the mainshock.

power law distribution: (Also called a "scale free distribution") A distribution of the generic form $P(x) \sim x^{\alpha}$. Note that there is no length scale associated with this type of distribution, since a transformation like $x \rightarrow x/b$ would keep the functional form unchanged. Observables (e.g., magnetization, susceptibility, etc.) show power-law behavior near criticality. Therefore, it is often considered as a signature of critical behavior.

slow earthquakes: Fault slip events that produce little or no seismic-wave radiation. Rupture propagation velocities and slip velocities of slow earthquakes are much smaller than those of ordinary earthquakes. Slow earthquakes without seismic wave radiation are often called silent earthquakes.

quenched randomness: This is the randomness in a system that is not in thermal equilibrium with the same reservoir as the system and does not fluctuate.

rate- and-state rate-and state-dependent friction (RSF) law: An empirical constitutive law describing the dynamic friction coefficient in either steady or transient states.

self-organized criticality (SOC): When the dynamics of a system leads it to a state of criticality (where scale invariance in time and space is observed) without any need of a external tuning parameter, the system is said to have self-organized to a critical state. This phenomenon, where a critical point is an attractor of the dynamics, is called self-organized criticality.

self-similarity and self-affinity: Self-similarity refers to a property of an object that it is similar (exactly or approximately) to one or more of its own part(s). Self-affinity refers to the properties of those objects which, in order to be self-similar, are to be scaled by different factors in the x and y directions (for a 2D object).

Sierpinski gasket and Sierpinski carpet: A Sierpinski carpet is a fractal object embedded in a 2D surface. Its construction is as follows: First a square is taken and divided into nine equal squares. Then the square in the middle is removed and a similar operation is performed upon the eight remaining squares. This process is continued *ad infinitum* to obtain what is called a Sierpinski carpet. The Sierpinski gasket (also called the Sierpinski triangle) is again a fractal object. Its construction is as follows: First an equilateral triangle is taken and is divided into four equilateral triangles of the same sizes; the middle one is removed. Then the same operation is performed upon the three remaining triangles. When this process is continued *ad infinitum*, one is left with what is called the Sierpinski gasket.

universality class: Phase transitions are characterized by a set of critical exponent values. The values of these exponents are independent of the microscopic details of the system and depend only on the symmetry and dimensionality of the order parameter. Therefore, a large class of systems often have the same critical exponent values. A universality class is a group of systems having the same critical exponent values.

REFERENCES

Abe, S., and K. Mair, 2009, Geophys. Res. Lett. **36**, L23302.

Amar, J. G., and F. Family, 1990, Phys. Rev. A **41**, 3399.

Ampuero, J.-P., and A. Rubin, 2008, J. Geophys. Res. **113**, B01302.

Andrews, D., 2005, J. Geophys. Res. **110**, B01307.

Andrews, D. J., 1976, J. Geophys. Res. **81**, 5679.

Bach, M., F. Wissel, and B. Drossel, 2008, Phys. Rev. E **77**, 067101.

Bak, P., and C. Tang, 1989, J. Geophys. Res. **94**, 15635.

Bak, P., C. Tang, and K. Wiesenfeld, 1987, Phys. Rev. Lett. **59**, 381.

Barabaśi, A. L., and H. E. Stanley, 1995, *Fractal Concepts in Surface Growth* (Cambridge University Press, New York).

Ben-Zion, Y., 2008, Rev. Geophys. **46**, RG4006.

Ben-Zion, Y., and J. R. Rice, 1995, J. Geophys. Res. **100**, 12959.

Ben-Zion, Y., and J. R. Rice, 1997, J. Geophys. Res. **102**, 17771.

Bergman, D. J., and D. Stroud, 1992, in *Solid State Phys*, edited by H. Ehrenreich, and D. Turnbull (Academic press, New York), Vol. 46, p. 147.

Bhattacharya, P., B. K. Chakrabarti, and Kamal, 2011, J. Phys. Conf. Ser. **319**, 012004.

Bhattacharya, P., B. K. Chakrabarti, Kamal, and D. Samanta, 2009, in *Rev. Nonlin. Dyn. and Complexity*, edited by H. G. Schuster (Wiley-VCH, Berlin), Vol. 2, pp. 107–158.

Bhattacharyya, P., 2005, Physica A (Amsterdam) **348**, 199.

Bhattacharyya, P., and B. K. Chakrabarti, 2006, Eds., *Modelling Critical and Catastrophic Phenomena in Geoscience* (Springer-Verlag, Heidelberg).

Bhattacharyya, P., S. Pradhan, and B. K. Chakrabarti, 2003, Phys. Rev. E **67**, 046122.

Bhushan, B., J. N. Israelachvili, and U. Landman, 1995, Nature (London) **374**, 607.

Biswas, S., and B. K. Chakrabarti, 2011, arXiv:1108.1707.

Bizzarri, A., and M. Cocco, 2003, J. Geophys. Res. **108**, 2373.

Bizzarri, A., and M. Cocco, 2006a, J. Geophys. Res. **111**, B05303.

Bizzarri, A., and M. Cocco, 2006b, J. Geophys. Res. **111**, B05304.

Blanpied, M. L., D. A. Lockner, and J. D. Byerlee, 1995, J. Geophys. Res. **100**, 13045.

Bocquet, L., E. Charlaix, S. Ciliberto, and J. Crassous, 1998, Nature (London) **396**, 735.

Bonamy, D., and E. Bouchaud, 2011, Phys. Rep. **498**, 1.

Bosl, W. J., and A. Nur, 2002, J. Geophys. Res. **107**, 2366.

Bottani, S., and B. Delamotte, 1997, Physica D (Amsterdam) **103**, 430.

Boulter, C. J., and G. Miller, 2003, Phys. Rev. E **68**, 056108.

Bowden, F. P., and D. Tabor, 2001, *The Friction and Lubrication of Solids (Oxford Classic Texts in the Physical Sciences)* (Oxford University Press, New York).

Braun, O. M., and Y. S. Kivshar, 2004, *The Frenkel-Kontorova Model: Concepts, Methods, and Applications* (Springer-Verlag, Berlin).

Braun, O. M., and A. G. Naumovets, 2006, Surf. Sci. Rep. **60**, 79.

Brechet, Y., and Y. Estrin, 1994, Scr. Metall. Mater. **30**, 1449.

Brown, S. R., C. Scholz, and J. B. Rundle, 1991, Geophys. Res. Lett. **18**, 215.

Burridge, R., 2006, in *Modelling Critical and Catastrophic Phenomena in Geoscience*, edited by P. Bhattacharyya, and B. K. Chakrabarti (Springer-Verlag, Heidelberg), pp. 113–154.

Burridge, R., and L. Knopoff, 1967, Bull. Seismol. Soc. Am. **57**, 341.

Caldarelli, G., C. Castellano, and A. Petri, 1999, Physica A (Amsterdam) **270**, 15.

Cao, T., and K. Aki, 1986, Pure Appl. Geophys. **124**, 487.

Carlson, J. M., 1991a, J. Geophys. Res. **96**, 4255.

Carlson, J. M., 1991b, Phys. Rev. A **44**, 6226.

Carlson, J. M., and J. S. Langer, 1989a, Phys. Rev. Lett. **62**, 2632.

Carlson, J. M., and J. S. Langer, 1989b, Phys. Rev. A **40**, 6470.

Carlson, J. M., J. S. Langer, and B. E. Shaw, 1994, Rev. Mod. Phys. **66**, 657.

Carlson, J. M., J. S. Langer, B. E. Shaw, and C. Tang, 1991, Phys. Rev. A **44**, 884.

Cartwright, J. H., E. H. Garcia, and O. Piro, 1997, Phys. Rev. Lett. **79**, 527.

Ceva, H., 1995, Phys. Rev. E **52**, 154.

Chakrabarti, B. K., and L. G. Benguigui, 1997, *Statistical Physics of Breakdown and Fracture is Disorder Systems* (Oxford University Press, Oxford).

Chakrabarti, B. K., and R. B. Stinchcombe, 1999, Physica A (Amsterdam) **270**, 27.

Chauve, P., P. Le Doussal, and K. J. Wiese, 2001, Phys. Rev. Lett. **86**, 1785.

Chester, F., and J. Chester, 1998, Tectonophysics **295**, 199.

Chlieh, M., J. P. Avouac, K. Sieh, D. H. Natawidjaja, and J. Galetzka, 2008, J. Geophys. Res. **113**, B05305.

Clancy, I., and D. Corcoran, 2005, Phys. Rev. E **71**, 0461124.

Clancy, I., and D. Corcoran, 2006, Phys. Rev. E **73**, 046115.

Clancy, I., and D. Corcoran, 2009, Phys. Rev. E **80**, 016113.

Cochard, A., and R. Madariaga, 1996, J. Geophys. Res. **101**, 25321.

Corral, A., 2004, Phys. Rev. Lett. **92**, 108501.

Christensen, K., and Z. Olami, 1992, Phys. Rev. A **46**, 1829.

Csahok, Z., K. Honda, E. Somfai, M. Vicsek, and T. Vicsek, 1993, Physica A (Amsterdam) **200**, 136.

da Cruz, F., S. Emam, M. Prochnow, J.-N. Roux, and F. Chevoir, 2005, Phys. Rev. E **72**, 021309.

Daniels, H. E., 1945, Proc. R. Soc. A **183**, 405.

Daub, E., and J. Carlson, 2010, Annu. Rev. Condens. Matter Phys. **1**, 397.

De, R., and G. Ananthakrisna, 2004, Europhys. Lett. **66**, 715.

de Carvalho, J. X., and C. P. C. Prado, 2000, Phys. Rev. Lett. **84**, 4006.

De Rubeis, V., R. Hallgass, V. Loreto, G. Paladin, L. Pietronero, and P. Tosi, 1996, Phys. Rev. Lett. **76**, 2599.

De Rubies, V., V. Loreto, L. Pietronero, and P. Tosi, 2006, in *Modelling Critical and Catastrophic Phenomena in Geoscience*, edited by P. Bhattacharyya, and B. K. Chakrabarti (Springer-Verlag, Heidelberg), pp. 259–280.

Dieterich, J. H., 1979, J. Geophys. Res. **84**, 2161.

Dieterich, J. H., 1986, in *Earthquake Source Mechanics*, edited by S. Das, J. Boarwright, and C. H. Scholz (American Geophysical Union, Washington, DC), pp. 37–47.

Dieterich, J. H., 1992, Tectonophysics **211**, 115.

Dieterich, J. H., 1994, J. Geophys. Res. **99**, 2601.

Dieterich, J. H., 2009, in *Treatise on Geophysics*, edited by H. Kanamori (Elsevier, Amsterdam), Vol. 4, pp. 107–129.

Dieterich, J. H., and B. D. Kilgore, 1994, Pure Appl. Geophys. **143**, 283.

Dieterich, J. H., and B. D. Kilgore, 1996, Tectonophysics **256**, 219.

Di Toro, G., D. L. Goldsby, and T. E. Tullis, 2004, Nature (London) **427**, 436.

Duemmer, O., and W. Krauth, 2007, J. Stat. Mech., P01019.

Edwards, S. F., and D. R. Wilkinson, 1982, Proc. R. Soc. A **381**, 17.

Eriksen, J. A., S. Biswas, and B. K. Chakrabarti, 2010, Phys. Rev. E **82**, 041124.

Español, P., 1994, Phys. Rev. E **50**, 227.

Fialko, Y., and Y. Khazan, 2005, J. Geophys. Res. **110**, B12407.

Freed, A. M., 2007, Geophys. Res. Lett. **34**, L06312.

Frenkel, Y., and T. Kontorova, 1938, Zh. Eksp. Teor. Fiz. **8**, 1340.

Fukuda, J., K. M. Johnson, K. M. Larson, and S. Miyazaki, 2009, J. Geophys. Res. **114**, B04412.

GDRMidi, 2004, Eur. Phys. J. E **14**, 341.

Goldsby, D. L., and T. E. Tullis, 2002, Geophys. Res. Lett. **29**, 1844.

Grassberger, P., 1994, Phys. Rev. E **49**, 2436.

Gu, J.-C., J. R. Rice, A. L. Ruina, and S. T. Tse, 1984, J. Mech. Phys. Solids **32**, 167.

Guatteri, M., and P. Spudish, 2000, Bull. Seismol. Soc. Am. **90**, 98.

Hainzl, S., G. Zöllar, and J. Kurths, 1999, J. Geophys. Res. **104**, 7243.

Hainzl, S., G. Zöller, J. Kurths, and J. Zschau, 2000, Geophys. Res. Lett. **27**, 597.

Han, R., T. Hirose, T. Shimamoto, Y. Lee, and J. Ando, 2011, Geology **39**, 599.

Han, R., T. Shimamoto, T. Hirose, J. Ree, and J. Ando, 2007, Science **316**, 878.

Hashimoto, C., A. Noda, T. Sagiya, and M. Matsu'ura, 2009, Nature Geosci. **2**, 141.

Hatano, T., 2007, Phys. Rev. E **75**, 060301(R).

Hatano, T., 2009, Geophys. Res. Lett. **36**, L18304.

Hayashi, N., and A. Tsutsumi, 2010, Geophys. Res. Lett. **37**, L12305.

Helmstetter, A., S. Hergarten, and D. Sornette, 2004, Phys. Rev. E **70**, 046120.

Hemmer, P. C., and A. Hansen, 1992, J. Appl. Mech. **59**, 909.

Hergarten, S., 2002, *Self-Organized Criticality in Earth Systems* (Springer, Berlin).

Hergarten, S., and R. Krenn, 2011, Nonlinear Proc. Geophys. **18**, 635.

Hergarten, S., and H. Neugebauer, 2000, Phys. Rev. E **61**, 2382.

Hergarten, S., and H. Neugebauer, 2002, Phys. Rev. Lett. **88**, 238501.

Herrmann, H. J., and S. Roux, 1990, Eds., *Statistical Models for the Fracture of Disordered Media* (Elsevier, Amsterdam).

Heslot, F., T. Baumberger, B. Perrin, B. Caroli, and C. Caroli, 1994, Phys. Rev. E **49**, 4973.

Hillers, G., P. M. Mai, Y. Ben-Zion, and J.-P. Ampuero, 2007, Geophys. J. Int. **169**, 515.

Hillers, G., and S. A. Miller, 2007, Geophys. J. Int. **168**, 431.

Hirose, H., K. Hirahara, F. Kimata, N. Fujii, and S. Miyazaki, 1999, Geophys. Res. Lett. **26**, 3237.

Hirose, H., and K. Obara, 2006, Geophys. Res. Lett. **33**, L17311.

Hirose, T., and T. Shimamoto, 2005, J. Geophys. Res. **110**, B05202.

Hölscher, H., A. Schirmeisen, and U. D. Schwarz, 2008, Phil. Trans. R. Soc. A **366**, 1383.

Hori, T., N. Kato, K. Hirahara, T. Baba, and Y. Kaneda, 2004, Earth Planet. Sci. Lett. **228**, 215.

Horowitz, F., and A. Ruina, 1989, J. Geophys. Res. **94**, 10279.

Hyun, S., L. Pei, J.-F. Molinari, and M. Robbins, 2004, Phys. Rev. E **70**, 026117.

Ida, Y., 1972, J. Geophys. Res. **77**, 3796.

Ide, S., and M. Takeo, 1997, J. Geophys. Res. **102**, 27379.

Igarashi, T., T. Matsuzawa, and A. Hasegawa, 2003, J. Geophys. Res. **108**, 2249.

Ishibe, T., and K. Shimazaki, 2009, Earth Planets Space **61**, 1041, http://www.terrapub.co.jp/journals/EPS/pdf/2009/6109/61091041.pdf.

Ito, K., and M. Matsuzaki, 1990, J. Geophys. Res. **95**, 6853.

Jagla, E. A., 2010, Phys. Rev. E **81**, 046117.

Jánosi, I. M., and J. Kertész, 1993, Physica A (Amsterdam) **200**, 179.

Jaume, S. C., and L. R. Sykes, 1999, Pure Appl. Geophys. **155**, 279.

Johnson, K. M., R. Bürgmann, and K. Larson, 2006, Bull. Seismol. Soc. Am. **96**, S321.

Kagan, Y. Y., 2006, in *Modelling Critical and Catastrophic Phenomena in Geoscience*, edited by P. Bhattacharyya, and B. K. Chakrabarti (Springer-Verlag, Heidelberg), pp. 303–361.

Kakui, S., and H. Kawamura, 2011, (unpublished).

Kanamori, H., 1981, in *Earthquake Prediction: an International Review*, edited by D. W. Simpson, and P. G. Richards (American Geophysical Union, Washington, DC), pp. 1–19.

Kanamori, H., 2009, Ed., *Earthquake Seismology, Treatise on Geophysics* (Elsevier, Amsterdam), Vol. 4.

Kanamori, H., and J. J. Cipar, 1974, Phys. Earth Planet. Inter. **9**, 128.

Kanamori, H., and K. C. McNally, 1982, Bull. Seismol. Soc. Am. **72**, 1241.

Kanamori, H., and G. S. Stewart, 1979, Phys. Earth Planet. Inter. **18**, 167.

Kaneko, Y., J.-P. Avouac, and N. Lapusta, 2010, Nature Geosci. **3**, 363.

Kardar, M., G. Parisi, and Y. C. Zhang, 1986, Phys. Rev. Lett. **56**, 889.

Kato, N., 2003a, Earth Planet. Sci. Lett. **216**, 17.

Kato, N., 2003b, Bulletin of the Earthquake Research Institute, University of Tokyo **78**, 151.

Kato, N., 2004, J. Geophys. Res. **109**, B12306.

Kato, N., 2007, Geophys. J. Int. **168**, 797.

Kato, N., 2008, J. Geophys. Res. **113**, B06302.

Kato, N., and T. Hirasawa, 1999a, Bull. Seismol. Soc. Am. **89**, 1401.

Kato, N., and T. Hirasawa, 1999b, Pure Appl. Geophys. **155**, 93.

Kato, N., M. Ohatake, and T. Hirasawa, 1997, Pure Appl. Geophys. **150**, 249.

Kato, N., and T. E. Tullis, 2001, Geophys. Res. Lett. **28**, 1103.

Kawamura, H., 2006, in *Modelling Critical and Catastrophic Phenomena in Geoscience*, edited by P. Bhattacharyya, and B. K. Chakrabarti (Springer-Verlag, Heidelberg), pp. 223–257.

Kawamura, H., T. Yamamoto, T. Kotani, and H. Yoshino, 2010, Phys. Rev. E **81**, 031119.

King, C.-Y., R. D. Nason, and D. Tocher, 1973, Phil. Trans. R. Soc. A **274**, 355.

Koivisto, J., J. Rosti, and M. J. Alava, 2007, Phys. Rev. Lett. **99**, 145504.

Koketsu, K., Y. Yokota, N. Nishimura, Y. Yagi, S. Miyazaki, K. Satake, Y. Fujii, H. Miyake, S. Sakai, Y. Yamanaka, and T. Okada, 2011, Earth Planet. Sci. Lett. **310**, 480.

Kossobokov, V. G., and J. M. Carlson, 1995, J. Geophys. Res. **100**, 6431.

Kotani, T., H. Yoshino, and H. Kawamura, 2008, Phys. Rev. E **77**, R010102.

Kumagai, H., Y. Fukao, S. Watanabe, and Y. Baba, 1999, Geophys. Res. Lett. **26**, 2817.

Kuroki, H., H. M. Ito, and A. Yoshida, 2002, Phys. Earth Planet. Inter. **132**, 39.

Kuwano, O., and T. Hatano, 2011, Geophys. Res. Lett. **38**, L17305.

Lachenbruch, A. H., 1980, J. Geophys. Res. **85**, 6097.

Lapusta, N., and Y. Liu, 2009, J. Geophys. Res. **114**, B09303.

Lawn, B., 1993, *Fracture of Brittle Solids* (Cambridge University Press, Cambridge).

Lay, T., H. Kanamori, and L. Ruff, 1982, Earthq. Predict. Res. **1**, 3.

Leschhorn, H., 1992, J. Phys. A **25**, L555.

Linde, A. T., M. T. Gladwin, M. J. S. Johnston, R. L. Gwyther, and R. G. Bilham, 1996, Nature (London) **383**, 65.

Linde, A. T., and I. S. Sacks, 2002, Earth Planet. Sci. Lett. **203**, 265.

Lise, S., and M. Paczuski, 2001, Phys. Rev. E **63**, 036111.

Liu, Y., and J. R. Rice, 2007, J. Geophys. Res. **112**, B09404.

Marone, C., 1998, Annu. Rev. Earth Planet Sci. **26**, 643.

Marone, C., C. Scholtz, and R. Bilham, 1991, J. Geophys. Res. **96**, 14635.

Marone, C., and C. H. Scholz, 1989, J. Struct. Geol. **11**, 799.

Mase, C., and L. Smith, 1987, J. Geophys. Res. **92**, 6249.

Matsukawa, H., and H. Fukuyama, 1994, Phys. Rev. B **49**, 17286.

Matsumura, S., 1997, Tectonophysics **273**, 271.

Matsuzawa, T., H. Hirose, B. Shibazaki, and K. Obara, 2010, J. Geophys. Res. **115**, B12301.

Matsuzawa, T., T. Igarashi, and A. Hasegawa, 2002, Geophys. Res. Lett. **29**, 1543.

Matthews, M. V., W. L. Ellsworth, and P. A. Reasenberg, 2002, Bull. Seismol. Soc. Am. **92**, 2233.

Middleton, A. A., and C. Tang, 1995, Phys. Rev. Lett. **74**, 742.

Miller, G., and C. J. Boulter, 2002, Phys. Rev. E **66**, 016123.

Miyazaki, S., P. Segall, J. Fukuda, and T. Kato, 2004, Geophys. Res. Lett. **31**, L06623.

Miyazaki, S., P. Segall, J. J. McGuire, T. Kato, and Y. Hatanaka, 2006, J. Geophys. Res. **111**, B03409.

Mizoguchi, K., T. Hirose, T. Shimamoto, and E. Fukuyama, 2006, Geophys. Res. Lett. **33**, L16319.

Mogi, K., 1969, Bulletin of the Earthquake Research Institute, University of Tokyo **47**, 395.

Mogi, K., 1979, Pure Appl. Geophys. **117**, 1172.

Moore, D. E., D. A. Lockner, M. Shengli, R. Summers, and J. D. Byerlee, 1997, J. Geophys. Res. **102**, 14787.

Morgan, J. K., 1999, J. Geophys. Res. **104**, 2721.

Mori, T., and H. Kawamura, 2005, Phys. Rev. Lett. **94**, 058501.

Mori, T., and H. Kawamura, 2006, J. Geophys. Res. **111**, B07302.

Mori, T., and H. Kawamura, 2008a, J. Geophys. Res. **113**, B06301.

Mori, T., and H. Kawamura, 2008b, Phys. Rev. E **77**, 051123.

Mori, T., and H. Kawamura, 2008c, J. Geophys. Res. **113**, B11305.

Morimoto, S., and H. Kawamura, 2011, (unpublished).

Moser, K., J. Kertész, and D. E. Wolf, 1991, Physica A (Amsterdam) **178**, 215.

Mousseau, N., 1996, Phys. Rev. Lett. **77**, 968.

Myers, C. R., and J. S. Langer, 1993, Phys. Rev. E **47**, 3048.

Myers, C. R., B. E. Shaw, and J. S. Langer, 1996, Phys. Rev. Lett. **77**, 972.

Nadeau, R. M., and L. R. Johnson, 1998, Bull. Seismol. Soc. Am. **88**, 790.

Nakanishi, H., 1990, Phys. Rev. A **41**, 7086.

Nakatani, M., 2001, J. Geophys. Res. **106**, 13347.

Nielsen, S., G. Di Toro, T. Hirose, and T. Shimamoto, 2008, J. Geophys. Res. **113**, B01308.

Nishenko, S. P., and R. Buland, 1987, Bull. Seismol. Soc. Am. **77**, 1382.

Obara, K., H. Hirose, F. Yamamizu, and K. Kasahara, 2004, Geophys. Res. Lett. **31**, L23602.

Ogata, Y., 2005, J. Geophys. Res. **110**, B05S06.

Ohmura, A., and H. Kawamura, 2007, Europhys. Lett. **77**, 69001.

Ohnaka, M., and L. Shen, 1999, J. Geophys. Res. **104**, 817.

Okada, T., T. Matsuzawa, and A. Hasegawa, 2003, Earth Planet. Sci. Lett. **213**, 361.

Olami, Z., H. Feder, and K. Christensen, 1992, Phys. Rev. Lett. **68**, 1244.

Ozawa, S., M. Murakami, M. Kaidzu, T. Tada, T. Sagiya, Y. Hatanaka, H. Yarai, and T. Nishimura, 2002, Science **298**, 1009.

Pacheco, J. F., L. R. Sykes, and C. H. Scholz, 1993, J. Geophys. Res. **98**, 14133.

Park, S.-C., and J. Mori, 2007, J. Geophys. Res. **112**, B03302.

Peirce, F. T., 1926, J. Text. Ind. **17**, 355.

Peixoto, T. P., and C. P. C. Prado, 2004, Phys. Rev. E **69**, R025101.

Peixoto, T. P., and C. P. C. Prado, 2006, Phys. Rev. E **74**, 016126.

Pelletier, J. D., 2000, Geophysical monograph **120**, 27.

Peng, Z. G., and P. Zhao, 2009, Nature Geosci. **2**, 877.

Pepke, S. L., J. M. Carlson, and B. E. Shaw, 1994, J. Geophys. Res. **99**, 6769.

Perfettini, H., and J.-P. Avouac, 2004, J. Geophys. Res. **109**, B02304.

Perfettini, H., J.-P. Avouac, H. Tavera, A. Kositsky, J.-M. Nocquet, F. Bondoux, M. Chlieh, A. Sladen, L. Audin, D. L. Farber, and P. Soler, 2010, Nature (London) **465**, 78.

Petri, A., A. Vespignani, A. Alippi, and M. Constantini, 1994, Phys. Rev. Lett. **73**, 3423.

Peyrard, M., and S. Aubry, 1983, J. Phys. C **16**, 1593.

Phoenix, S. L., 1978, SIAM J. Appl. Math. **34**, 227.

Phoenix, S. L., 1979, Adv. Appl. Probab. **11**, 153.

Pinho, S. T. R., and C. P. C. Prado, 2000, Eur. Phys. J. B **18**, 479.

Politi, A., S. Ciliberto, and R. Scorretti, 2002, Phys. Rev. E **66**, 026107.

Ponson, L., 2009, Phys. Rev. Lett. **103**, 055501.

Ponson, L., and D. Bonamy, 2010, Int. J. Fract. **162**, 21.

Popov, V. L., B. Grzemba, J. Starcevic, and M. Popov, 2012, Tectonophysics **532535**, 291.

Pradhan, S., P. Bhattacharyya, and B. K. Chakrabarti, 2002, Phys. Rev. E **66**, 016116.

Pradhan, S., and B. K. Chakrabarti, 2001, Phys. Rev. E **65**, 016113.

Pradhan, S., and B. K. Chakrabarti, 2003a, Phys. Rev. E **67**, 046124.

Pradhan, S., and B. K. Chakrabarti, 2003b, Int. J. Mod. Phys. B **17**, 5565.

Pradhan, S., B. K. Chakrabarti, P. Ray, and M. K. Dey, 2003, Phys. Scr. **T106**, 77.

Pradhan, S., A. Hansen, and B. K. Chakrabarti, 2010, Rev. Mod. Phys. **82**, 499.

Pradhan, S., A. Hansen, and P. C. Hemmer, 2005, Phys. Rev. Lett. **95**, 125501.

Pradhan, S., A. Hansen, and P. C. Hemmer, 2006, Phys. Rev. E **74**, 016122.

Pradhan, S., and P. C. Hemmer, 2009, Phys. Rev. E **79**, 041148.

Pradhan, S., and P. C. Hemmer, 2011, Phys. Rev. E **83**, 041116.

Rabinowicz, E., 1965, *Friction and Wear of Materials* (Wiley, New York).

Ramos, O., E. Altshuler, and K. J. Maloy, 2006, Phys. Rev. Lett. **96**, 098501.

Ray, P., and B. K. Chakrabarti, 1985, Solid State Commun. **53**, 477.

Rice, J. R., 1993, J. Geophys. Res. **98**, 9885.

Rice, J. R., 2006, J. Geophys. Res. **111**, B05311.

Rice, J. R., N. Lapusta, and K. Ranjith, 2001, J. Mech. Phys. Solids **49**, 1865.

Rogers, G., and H. Dragert, 2003, Science **300**, 1942.

Rubin, A. M., 2008, J. Geophys. Res. **113**, B11414.

Rubin, A. M., and J.-P. Ampuero, 2005, J. Geophys. Res. **110**, B11312.

Ruina, A. L., 1983, J. Geophys. Res. **88**, 10359.

Rundle, D. L., J. B. Turcotte, R. Shcherbakov, W. Klein, and C. Sammis, 2003, Rev. Geophys. **41**, 1019.

Rundle, J. B., D. L. Turcotte, and W. Klein, 2000, *GeoComplexity and the Physics of Earthquakes, Geophysical Monograph 120* (American Geophysical Union, Washington DC), pp. 127146.

Rundle, J. B., W. Klein, S. Gross, and D. L. Turcotte, 1995, Phys. Rev. Lett. **75**, 1658.

Sahimi, M., 2003, *Heterogeneous Materials* (Springer, New York), Vol. 2.

Santucci, S., K. J. Måløy, A. Delaplace, J. Mathiesen, A. Hansen, J. O. Haavig Bakke, J. Schmittbuhl, L. Vanel, and P. Ray, 2007, Phys. Rev. E **75**, 016104.

Sasamoto, T., and H. Spohn, 2010, Phys. Rev. Lett. **104**, 230602.

Schmittbuhl, J., J.-P. Vilotte, and S. Roux, 1996, J. Geophys. Res. **101**, 27741.

Scholz, C., 1998, Nature (London) **391**, 37.

Scholz, C. H., 2002, *The Mechanics of Earthquakes and Faulting* (Cambridge University Press, New York), 2nd ed..

Schwartz, S. Y., and J. M. Rokosky, 2007, Rev. Geophys. **45**, RG3004.

Segall, P., and J. L. Davis, 1997, Annu. Rev. Earth Planet Sci. **25**, 301.

Shaw, B. E., 1994, Geophys. Res. Lett. **21**, 1983.

Shaw, B. E., 1995, J. Geophys. Res. **100**, 18239.

Shaw, B. E., J. M. Carlson, and J. S. Langer, 1992, J. Geophys. Res. **97**, 479.

Shelly, D. R., 2009, Geophys. Res. Lett. **36**, L17318.

Shibazaki, B., and Y. Iio, 2003, Geophys. Res. Lett. **30**, 1489.

Shibazaki, B., and T. Shimamoto, 2007, Geophys. J. Int. **171**, 191.

Shimamoto, T., 1986, Science **231**, 711.

Sibson, R., 1973, Nature (London) **243**, 66.

Sornette, D., 2004, *Critical Phenomena in Natural Sciences* (Springer Heidelberg, Berlin), 2nd ed..

Stauffer, D., and A. Aharony, 1992, *Introduction to Percolation Theory* (Taylor & Francis, London).

Stirling, M. W., S. G. Wesnousky, and K. Shimazaki, 1996, Geophys. J. Int. **124**, 833.

Stuart, W. D., 1988, Pure Appl. Geophys. **126**, 619.

Stuart, W. D., and T. E. Tullis, 1995, J. Geophys. Res. **100**, 24079.

Suyehiro, S., T. Asada, and M. Ohtake, 1964, Papers in meteorology and geophysics **15**, 71.

Suzuki, T., and T. Yamashita, 2010, J. Geophys. Res. **115**, B02303.

Sykes, L. R., and W. Menke, 2006, Bull. Seismol. Soc. Am. **96**, 1569.

Tajima, F., and H. Kanamori, 1985, Phys. Earth Planet. Inter. **40**, 77.

Thatcher, W., 1990, J. Geophys. Res. **95**, 2609.

Thompson, P. A., G. S. Grest, and M. O. Robbins, 1992, Phys. Rev. Lett. **68**, 3448.

Toda, S., R. S. Stein, P. A. Reasenberg, J. H. Dieterich, and A. Yoshida, 1998, J. Geophys. Res. **103**, 24543.

Tomlinson, G. A., 1929, Philos. Mag. **7**, 905.

Torvund, F., and J. Froyland, 1995, Phys. Scr. **52**, 624.

Tse, S. T., and J. R. Rice, 1986, J. Geophys. Res. **91**, 9452.

Tsutsumi, A., and T. Shimamoto, 1997, Geophys. Res. Lett. **24**, 699.

Tullis, T. E., 2009, in *Earthquake Seismology, Treatise on Geophysics*, edited by H. Kanamori (Elsevier, Amsterdam), Vol. 4, p. 131.

Turcotte, D. L., 1997, *Fractals and Chaos in Geology and Geophysics* (Cambridge University Press, New York), 2nd ed..

Turcotte, D. L., R. Shcherbakov, and J. B. Rundle, 2009, in *Treatise on Geophysics*, edited by H. Kanamori (Elsevier, Amsterdam), Vol. 4, pp. 675–700.

Uchida, N., T. Matsuzawaa, A. Hasegawaa, and T. Igarashi, 2005, Earth Planet. Sci. Lett. **233**, 155.

Utsu, T., Y. Ogata, and R. S. Matsuura, 1995, J. Phys. Earth **43**, 1.

Vannimenus, J., 2002, Physica A (Amsterdam) **314**, 264.

Vannimenus, J., and B. Derrida, 2001, J. Stat. Phys. **105**, 1.

Vasconcelos, G. L., 1996, Phys. Rev. Lett. **76**, 4865.

Vieira, M. S., 1992, Phys. Rev. A **46**, 6288.

Vieira, M. S., 1996, Phys. Rev. E **54**, 5925.

Vieira, M. S., and A. J. Lichtenberg, 1996, Phys. Rev. E **53**, 1441.

Vieira, M. S., G. L. Vasconcelos, and S. R. Nagel, 1993, Phys. Rev. E **47**, R2221.

Wallace, L. M., and J. Beavan, 2006, Geophys. Res. Lett. **33**, L10301.

Wissel, F., and B. Drossel, 2006, Phys. Rev. E **74**, 066109.

Working Group on California Earthquake Probabilities, 1995, Bull. Seismol. Soc. Am. **85**, 379.

Wyss, M., 1997, Pure Appl. Geophys. **149**, 3.

Wyss, M., F. W. Klein, and A. C. Johnston, 1981, J. Geophys. Res. **86**, 3881.

Xia, J., H. Gould, W. Klein, and J. B. Rundle, 2005, Phys. Rev. Lett. **95**, 248501.

Xia, J., H. Gould, W. Klein, and J. B. Rundle, 2008, Phys. Rev. E **77**, 031132.

Yagi, Y., M. Kikuchi, and T. Nishimura, 2003, Geophys. Res. Lett. **30**, 2177.

Yamamoto, T., and H. Kawamura, 2011, (unpublished).

Yamamoto, T., H. Yoshino, and H. Kawamura, 2010, Eur. Phys. J. B **77**, 559.

Yamanaka, Y., and M. Kikuchi, 2004, J. Geophys. Res. **109**, B07307.

Yamashita, T., and L. Knopoff, 1987, Geophys. J. R. Astron. Soc. **91**, 13.

Yoshida, S., and N. Kato, 2003, Geophys. Res. Lett. **30**, 1681.

Yoshioka, N., 1997, Tectonophysics **277**, 29.

Zapperi, S., P. Ray, H. E. Stanley, and A. Vespignani, 1997, Phys. Rev. Lett. **78**, 1408.